USING A BAYESIAN NETWORK FRAMEWORK TO PREDICT PERMAFROST THAW IN THE ARCTIC

A Thesis

by

KATHERINE ELIZABETH BEALL

Submitted to the Office of Graduate and Professional Studies of
Texas A&M University
in partial fulfillment of the requirements for the degree of

MASTER OF SCIENCE

Chair of Committee,	Julie Loisel
Co-Chair of Committee,	Zenon Medina-Cetina
Committee Members,	David Cairns
	Oliver Frauenfeld
Head of Department,	David Cairns

May 2021

Major Subject: Geography

ABSTRACT

Rising global temperatures are a threat to Arctic ecosystems. Thawing permafrost is expected to expose previously frozen carbon to microbial decomposition, an action that will promote further warming and have consequences for both the natural environment and human communities. However, there is a critical gap in the ability of current permafrost models to simulate permafrost thaw under future projected climate conditions. A model based on Bayesian methods may help address existing limitations in the representation of physically complex processes and availability of observational data. A particular strength of Bayesian methods over more traditional methods is the ability to integrate various types of evidence (e.g., observations, model outputs, or expert assessments) into a single model through probability and statistics. This ability is particularly helpful in regions such as the Arctic that have sparse or no data. Here, I outline a new modeling framework using a Bayesian network (PermaBN) to simulate permafrost thaw in the continuous permafrost region of the Arctic. The PermaBN model development process involves: (1) identifying variables relevant to permafrost thaw via extensive literature review and collaboration with experts at Texas A&M University, (2) pre-validating and validating the model via expert assessment, and (3) evaluating the model with physical observations from a local case study. Pre-validation and expert assessment validation results show that, as expected, increases in thaw depth are expected to be low under initial conditions favoring lower temperatures, increased soil moisture conditions, and high active layer ice content while changes are expected to be

high under initial conditions favoring higher temperatures, decreased soil moisture conditions, and low active layer ice content. Model evaluation shows that performance of PermaBN is enhanced when system conditions are known. Future work includes refining the model probabilities, calibrating the model, and evaluating the model performance using a pan-Arctic case study. Results from this study are expected to provide better predictions of permafrost thaw that can then be applied to carbon modeling studies, infrastructure hazard assessments, and policy decisions aimed at mitigation of and adaptation to permafrost thaw.

ACKNOWLEDGEMENTS

I would like to thank my committee chair, Dr. Loisel, for her dedication and support throughout my undergraduate and graduate education at Texas A&M University. If not for her undergraduate Planet Earth course and undergraduate research opportunities, I may not have pursued my interests in the earth sciences. I am truly grateful of all of the opportunities that have arisen from her mentorship, including this graduate opportunity and the opportunity to experience the Arctic firsthand.

I would also like to thank my committee co-chair, Dr. Medina-Cetina, for his guidance and support on the technical aspects of this work, and my committee members Dr. Cairns and Dr. Frauenfeld for their guidance and support throughout the course of this research, as well as for teaching some of my favorite geography courses. Thanks also goes to my colleagues Yichuan Zhu and Guillermo Duran Sierra in the Zachry Department of Civil and Environmental Engineering for their help and collaboration in the early stages of this research.

Even though my time spent on-campus was limited, thank you to my officemates who made the graduate experience more enjoyable.

Finally, I would like to thank my family for always encouraging me to pursue my goals and for their patience and support throughout the years. Most of all, thank you to Rocky Ribaudo – you have been my biggest supporter, and I truly would not have accomplished all that I have these last few years if not for you.

CONTRIBUTORS AND FUNDING SOURCES

Contributors

This work was supervised by a thesis committee consisting of Drs. Julie Loisel (advisor), David Cairns, and Oliver Frauenfeld of the Department of Geography and Dr. Zenon Medina-Cetina (co-advisor) of the Zachry Department of Civil and Environmental Engineering.

The expert assessments in Sections 3 and 4 were provided by the thesis committee members. All other work conducted for the thesis was completed by the student independently.

Funding Sources

Graduate study was supported by a fellowship and assistantship from Texas A&M University as well as an X-Grant award to Dr. Julie Loisel.

NOMENCLATURE

ALT	Active Layer Thickness
BBN	Bayesian Belief Network
BN	Bayesian Network
CPT	Conditional Probability Table
ERA	Environmental Risk Assessment
ESM	Earth System Model

TABLE OF CONTENTS

Page

LIST OF FIGURES

Page

LIST OF TABLES

Page

1. INTRODUCTION

1.1. Context and Problem Statement

In the face of warming global temperatures, the Arctic is undergoing rapid change, with important effects on the cryosphere, ocean, and terrestrial ecosystems (IPCC, 2013, Schuur and Mack, 2018, Serreze and Barry, 2014). The cryosphere, which encapsulates all portions of Earth's surface that are covered in frozen water, is particularly vulnerable to current and future warming. Decreasing trends and record lows in sea ice extents and thicknesses have been observed in recent decades, in addition to prolonged summer melt seasons and ice sheet loss (Comiso et al., 2008, Hanna et al., 2020, Kwok et al., 2009, Serreze et al., 2007, Serreze and Meier, 2019, Stroeve et al., 2014). In marine ecosystems, the consequences of sea ice loss include increased sea surface temperatures (Stroeve et al., 2014), habitat loss for marine mammals (Laidre et al., 2008), and the amplification of Arctic temperatures (Pistone et al., 2014, Screen and Simmonds, 2010, Serreze et al., 2009). On land, permafrost is increasingly vulnerable to thaw (Biskaborn et al., 2019, Jorgenson et al., 2010, Koven et al., 2013). Permafrost thaw has direct consequences for both the natural environment and human communities (Schuur and Mack, 2018), including damage to built infrastructure (Hjort et al., 2018, Karjalainen et al., 2019), landscape change through the creation of thermokarst terrain (Kokelj and Jorgenson, 2013, Olefeldt et al., 2016), and release of previously frozen soil carbon (Schuur et al., 2015, Schuur et al., 2009).

Permafrost soils are an important and dynamic component of the global climate system. Permafrost is perennially frozen ground (soil, rock, or sediment) that remains at or below 0°C for at least two years (Permafrost Subcommittee, 1988). Permafrost, which covers almost a quarter of the Northern Hemisphere's land surface at 22.79×10^6 km^2 (excluding permafrost under glaciers and ice sheets) (Zhang et al., 2003), occurs both on land and beneath arctic continental shelves and is classified as continuous (90-100% area), discontinuous (50-90% area), sporadic (10-50% area), or isolated (0-10% area) (Brown et al., 1997). This frozen ground can be further characterized by the percent by volume of its ground ice content (Brown et al., 1997). An important component of permafrost is its active layer, which is the top layer of the frozen ground subject to annual thawing and freezing (Permafrost Subcommittee, 1988). Northern peatlands, which have accumulated large stocks of carbon and nitrogen over time, are estimated to occupy $1.7 \pm 0.5 \times 10^6$ km^2 of the permafrost region (Hugelius et al., 2020).

In recent decades, the temperatures of circumpolar permafrost have increased by 2 – 4°C (Kokelj and Jorgenson, 2013) as a result of Earth's northernmost latitudes warming at a rate twice as fast as the global average (IPCC, 2013). Warming temperatures are often associated with permafrost thaw and degradation, but permafrost is not directly connected to the atmosphere. Instead, the ground thermal regime, along with soil properties, snow, surface and subsurface hydrology, vegetation, and topography, mediate permafrost stability (Gockede et al., 2019, Jorgenson et al., 2010, Stiegler et al., 2016, Zhang et al., 2018). Likewise, just as these factors control permafrost stability, permafrost also controls these properties and processes. Despite

decades of observations and modeling efforts (e.g., Biskaborn et al. (2015), Jafarov et al. (2012), and Nelson and Outcalt (1987)), there is much that remains unknown about Arctic permafrost systems and processes. For instance, the total northern permafrost soil organic carbon (SOC) pool remains uncertain, with estimates ranging from 1140 – 1476 Pg (Hugelius et al., 2014) to 1672 Pg (Tarnocai et al., 2009). In permafrost-affected peatlands alone, the organic carbon stock is estimated at 185 ± 66 Pg (Hugelius et al., 2020). The range in uncertainty is a result of difficulties with estimating organic soil area, thickness, and carbon density (Loisel et al., 2017). Estimates are further limited by the lack of observations in the northern latitudes due to their remoteness and harsh climate (Serreze and Barry, 2014); there are also limitations pertaining to soil carbon stock and flux representations in Earth system models (ESMs) (Tian et al., 2015).

The exposure of previously frozen carbon to microbial decomposition via permafrost thaw is expected to promote further warming, and subsequently further thaw, through a positive feedback loop between carbon emissions and the atmosphere (Schuur et al., 2015). Depending on the thaw conditions, the previously frozen ground – and the soil organic matter (SOM) it contains – could be exposed to either aerobic or anaerobic conditions (Parmentier et al., 2017, Schuur et al., 2015). In the case of the former, carbon dioxide (CO_2) would be released to the atmosphere through intensive microbial decomposition of that SOM under drier conditions, while the latter would allow for methane (CH_4) to be produced and released to the atmosphere under saturated conditions (Parmentier et al., 2017, Schuur et al., 2015). CH_4 has a global warming potential 34 times greater than CO_2 on a century time scale (Myhre et al., 2013), which would allow

for warming to be further enhanced. At the same time, recent shrub expansion trends in the Arctic (Myers-Smith et al., 2011) may help offset some of this carbon release through a negative feedback loop involving increased carbon uptake by vascular plants (Sweet et al., 2015) and shading of ground underlain by permafrost in the summer (Blok et al., 2010). However, the warming that is driving the Arctic greening trends is ultimately expected to increase rather than decrease the vulnerability of carbon release from terrestrial ecosystems due to surface albedo changes related to the protrusion of shrub stems above the spring snowpack that lead to warmer soil temperatures and deeper active layers (Lawrence and Swenson, 2011). Other predicted Arctic changes with indirect impacts on carbon cycling include changes in precipitation patterns (Bintanja and Andry, 2017, Bintanja et al., 2020, Screen and Simmonds, 2012), shifts in vegetation and ecoregion patterns (Feng et al., 2012, Myers-Smith et al., 2011, Myers-Smith et al., 2020), intensification of the hydrological cycle (Box et al., 2019), increased occurrence of fires (Hu et al., 2015), and insect outbreaks (Barrio et al., 2017).

To gain a better understanding of how the Arctic will change in a warming world and assess the consequences of permafrost degradation, many researchers and stakeholders rely on models to inform their studies or decisions (Flynn et al., 2019, Koven et al., 2013). While there is a general understanding of how permafrost thaw is impacted by various feedbacks and surface properties (Gockede et al., 2019, Jorgenson et al., 2010, Schuur and Mack, 2018, Stiegler et al., 2016, Zhang et al., 2018), current research emphasizes the need to further improve permafrost modeling and address model shortcomings (Lawrence et al., 2008, Riseborough, 2007, Tao et al., 2017). Often-cited

shortcomings include difficulties with (or lack of) the representation of the ground thermal regime and vegetation dynamics, limitations inherent to the modeling approach adopted (e.g., fixed temporal domain in equilibrium models or requirement of spatial data for numerical models), and heterogeneity in variable conditions (Lawrence et al., 2008, Riseborough, 2007, Tao et al., 2017). Many studies aim at addressing these known issues and improving existing models or modeling approaches (e.g., Jafarov et al. (2012), Tao et al. (2017), Westermann et al. (2016)). While these advancements are essential, alternative modeling methods that allow for the integration of different data types should be further explored.

To address the difficulty in simulating permafrost thaw under future projected climate conditions with current models, this paper presents a new modeling technique based on Bayesian methods. This approach allows explicit representation of the variables related to permafrost thaw and simulation of changes in permafrost thaw depth with quantification of uncertainty. Based on cause-effect relationships and the integration of multiple types of evidence (here, observational data and expert assessments), the method links four major components of the Arctic ecosystem to permafrost thaw depth: geological, atmospheric, surface insulation, and soil characteristics.

1.2. Research Questions and Associated Objectives

The purpose of this research is to develop a new modeling framework (PermaBN) in the form of a Bayesian Network (BN) to simulate permafrost thaw in the Arctic and evaluate how the BN performs relative to an existing observational case

study. A BN framework combines physics- and empirically-based modeling approaches with statistics and probability in order to link various components of a system (e.g., the Arctic) together and make predictions (e.g., permafrost thaw depth). The framework allows for the integration of multiple types of evidence, such as model outputs, observations, and expert assessments. This integration of evidence is significant in that it may help address the limitations and gaps of current permafrost models. It also reduces uncertainty in simulations of future permafrost thaw by quantifying uncertainties pertaining to each variable on those predictions. Further, this modeling approach is transparent in that the interactions between variables in the BN are explicitly represented. Few studies have utilized Bayesian methods to assess environmental changes in the Arctic (e.g., Qin et al. (2018) and Wainwright et al. (2017)), and the most comprehensive Arctic BN study only includes evidence in the form of expert assessment (Webster and McLaughlin, 2014). This research will expand upon these studies and include comparison of the PermaBN results to *in situ* observations.

The primary objective of this research is to develop a new method for assessing permafrost thaw in the Arctic. The secondary objective is to evaluate the performance of this new method in relation to an observational case study. The outcome of the primary objective is a BN model validated through expert assessment that produces estimations of permafrost thaw depth that are consistent with current research. The outcome of the secondary objective is that the BN model output agrees with physical observations of permafrost thaw depth from a local case study. Results from this study could be applied

to future carbon modeling studies, infrastructure hazard assessments, and policy decisions aimed at mitigation of and adaptation to permafrost thaw.

2. BACKGROUND AND LITERATURE REVIEW

2.1. Geomorphic and Ecological Processes that Influence Permafrost Thaw

The Arctic, defined here as the land area north of the Arctic Circle (approximately 66.5°N) (McGuire et al., 2006), is a complex, interconnected system. Permafrost soils are an important and dynamic component of this system and a distinctive feature of the northern polar region. For instance, permafrost acts as a structural component for regulating ecosystems through its impact on temperature, water, and nutrients. Active layer depth controls the temperature regime of soil layers, with soil near the bottom of the active layer remaining only a degree or two above freezing when thawed; temperature also affects SOM decomposition and plant and animal physiology (Schuur and Mack, 2018). The presence of permafrost, especially ice-rich permafrost, affects water flowpaths and water availability by decreasing infiltration and increasing evaporation and runoff when water sits on the surface of the upper thaw layer; this has implications for plant access to water and whether heterotrophic organisms are exposed to aerobic or anaerobic conditions (Schuur and Mack, 2018). Permafrost also controls nutrient availability, primarily of nitrogen, through seasonal thaw depth and permafrost temperature; near-freezing temperatures inhibit nitrogen release by microorganisms (Schuur and Mack, 2018).

The distribution of permafrost is strongly latitudinal (Figure 2.1), with continuous permafrost (> 90% of area underlain by permafrost) in the north followed by

discontinuous permafrost, sporadic permafrost, and isolated patches (< 10% of area underlain by permafrost) as one moves farther south (Brown et al., 1997).

Figure 2.1 Continuous, discontinuous, sporadic, and isolated permafrost distribution across the Northern Hemisphere. Reprinted from Rekacewicz (2005).

Continuous permafrost occupies ~84.5% of the northern permafrost region while discontinuous permafrost occupies ~15% (Brown et al., 2002). Aside from differences in percent of frozen ground, these two permafrost types also primarily occupy different ecoregions. Continuous permafrost is commonly found in the tundra while discontinuous permafrost is more characteristic of the boreal region (Brown et al., 2002, The Nature Conservancy, 2009). The extent of permafrost alters water movement, surface topography, and the distribution of vegetation communities across landscapes. For example, in the tundra, water infiltration is limited due to the frozen ground, which restricts plant growth from both water availability and rooting perspectives; as such, vegetation is primarily limited to nonvascular mosses and lichens that lack root systems (Schuur and Mack, 2018). In the boreal region, conditions are more favorable for water infiltration, contributing to taller vegetation coverage; ground subsidence due to thawing of ice-rich ground is also less common than in the tundra (Jorgenson and Osterkamp, 2005). Along those lines, factors that control permafrost thaw may differ between these two regions. For instance, taller vegetation can contribute to higher snow depths, thereby altering the ground thermal regime and accelerating permafrost degradation; increased surface water coverage can also accelerate permafrost degradation through surface energy fluxes (Burn and Kokelj, 2009).

In my research, the emphasis is on the geomorphic and ecological processes that influence permafrost thaw in the continuous permafrost region. While I recognize that hydrological processes such as river dynamics and the presence of surface water (e.g., lakes) also exert an important control on permafrost thaw (Burn and Kokelj, 2009,

Kokelj and Jorgenson, 2013, Zheng et al., 2019), my model, along with the majority of existing permafrost models (e.g., Kudryavtsev model by Anisimov et al. (1997), GIPL2-MPI by Jafarov et al. (2012), and Catchment Land Surface Model (CLSM) by Tao et al. (2017)), implicitly include hydrological processes through the representation of ground heat fluxes and thermal conductivity. The following subsections define and review key processes that influence continuous permafrost thaw:

(1) Topography: landscape-scale geologic and topographic characteristics and processes typically remain consistent, at the human timescale, in their influence on other system components such as vegetation communities, snow depth, and soil moisture. As such, local topography can influence snow distribution, incident radiation, and wind exposure, which can impact soil moisture and soil temperature (Aalto et al., 2013, Serreze and Barry, 2014, Young et al., 1997). In the northern hemisphere, northerly aspects tend to be snowier, cooler, and receive less intense incoming radiation than southerly aspects (Evans et al., 1989, Petzold and Mulhern, 1987, Wilcox et al., 2019). The effects of aspect on radiation are lessened at higher latitudes, particularly for east and west aspects (Holland and Steyn, 1975). Nonetheless, the differences between north and south slopes can still be significant. In the Brooks Range northern foothills of Alaska, Evans et al. (1989) found that dry-type vegetation communities (e.g., dry dwarf-shrubs and fruticose-lichen tundra such as *Dryas octopetala*, *Arctous alpina*, *Vaccinium uliginosum*, and *Cassiope tetragona*) dominate south- and southwest-facing slopes, while dry-type moist vegetation assemblages (e.g., moist dwarf-shrub, moss, fruticose-lichen tundra such as *Cassiope tetragnoa* or *Salix rotundifolia*) dominate north- and

northwest-facing slopes. Similarly, Myers-Smith et al. (2020) found that shrub cover throughout the Arctic has been noticeably increasing on south-facing slopes.

(2) Soil texture and density: the effects of soil particle size and density on soil moisture and soil temperature are considered. Soil particle size, also referred to as soil texture, influences soil moisture by controlling the moisture retention rate and thermal conductivity of the soil (Arya and Paris, 1981, Young et al., 1997). For instance, finer particles such as clay can retain more moisture than coarser particles such as sand (Meentemeyer and Zippin, 1981). Meentemeyer and Zippin (1981) found that higher net moisture was required to produce needle ice when the percentage of fine soil particles decreased. However, too high of a fine particle content can also inhibit ice growth, indicating that a mixture of fine and coarse particles is optimal for ice growth. Soil texture can also be considered from the perspective of soil bulk (dry) density, which is the measure of the amount of dry solid particles per unit volume. In this case, a sandy soil has a higher dry density than a silty or clayey soil; organic soils generally have very low dry densities (Abu-Hamdeh and Reeder, 2000). Dry bulk density influences soil thermal conductivity, such that an increase in density at a given soil moisture content increases the thermal conductivity of that soil (Abu-Hamdeh and Reeder, 2000). Thermal conductivity therefore tends to be highest in sandy (i.e., high bulk density) soils and lowest in organic (i.e., low bulk density) soils. A study by Xu et al. (2020) noted that the effect of density on thermal conductivity is weaker when temperatures are positive as opposed to negative. It should also be noted that sandy soils have a high infiltration rate,

but low available water content, while clayey and organic soils have the highest volumetric water contents (Abu-Hamdeh and Reeder, 2000).

(3) Surface air temperature and precipitation regimes: surface air temperature and precipitation exert direct and important influences on soil and vegetation properties. For instance, warmer surface air temperatures are expected to increase the length of the growing season, which may contribute to shrub expansion and increased photosynthetic activity across the tundra (Myers-Smith et al., 2011, Myers-Smith et al., 2020). Increased air temperatures have also been linked to changes in soil temperature, soil moisture, and precipitation. The relationship between increased surface air temperatures and increased soil temperatures is well documented (Boike et al., 2003, Oelke and Zhang, 2004, Park et al., 2014, Zhang et al., 2018). Many studies have also identified surface characteristics that work to modulate the relationship between air and soil temperatures, such as snow and water cover (Kokelj and Jorgenson, 2013, Zhang et al., 2018). As for precipitation, atmospheric air temperatures affect the ratio of precipitation that falls as rain vs. snow, and as temperatures continue to warm, a higher ratio of precipitation falling as rain is expected (Bintanja and Andry, 2017). A higher ratio of rainfall would impact snow depths by not only reducing snowfall amounts but also by melting existing snow cover (Boike et al., 2003, Screen and Simmonds, 2012). As for precipitation regimes, the Arctic is expected to experience increased precipitation totals throughout the 21st century (Bintanja and Andry, 2017). This may be due to reduced sea ice cover, which allows for increased evaporation, cloud formation, and precipitation (Bintanja and Andry, 2017), and/or changes in poleward moisture transport (Bintanja et

al., 2020). Despite the projected increase in Arctic precipitation, however, decreased amounts of snow are also expected, primarily as a result of warming temperatures (Bintanja and Andry, 2017). Precipitation also contributes directly and indirectly to soil moisture, primarily through snowmelt and rainfall, with air temperature moderating the moisture content via evaporative processes (Rouse et al., 1997, Young et al., 1997).

(4) Biota: vegetation properties considered here include vegetation cover and height. Height has known influences on ground insulation via shading in the summer and increased snow depth in the winter (Grunberg et al., 2020, Myers-Smith et al., 2011, Wilcox et al., 2019), which has implications for soil temperatures and permafrost thaw depths. More is known about winter vegetation influences on active layer thickness (ALT) than summer vegetation influences. In winter, increased vegetation density and height have been shown to locally increase snow depths by trapping snow in branches (Gockede et al., 2019, Grunberg et al., 2020, Myers-Smith et al., 2011, Wilcox et al., 2019), and the insulative properties of snow contribute to warmer winter soil temperatures (Gockede et al., 2019, Myers-Smith et al., 2011, Park et al., 2014, Zhang et al., 2018). This slows down, or prevents, the active layer from refreezing during the cold season (Jan and Painter, 2020, Zhang et al., 1996). In the summer, vegetation cover shades the ground and reduces the thermal gradient into the ground, thereby leading to cooler summer soil temperatures and reduced active layer depths (Aalto et al., 2013, Blok et al., 2010, Grunberg et al., 2020, Myers-Smith et al., 2011, Young et al., 1997). Some studies, such as the field observation study by Blok et al. (2010), have suggested that vegetation shading may help protect permafrost from thaw by offsetting some of the

influences of increased air temperatures. However, other studies, such as another field observation study by Lawrence and Swenson (2011), argue that the warming-induced increase in shrub cover will ultimately offset the local cooling influence due to surface albedo changes related to the protrusion of shrub stems above the spring snowpack that lead to warmer soil temperatures and deeper active layers. In this latter case, the vulnerability of permafrost to thaw could be increased.

(5) Soil temperature and moisture: soil moisture content influences soil temperature, as it alters the thermal dynamics of the soil (Oelke and Zhang, 2004, Zwieback et al., 2019). Increased soil moisture, which would be more characteristic of lower bulk density (i.e., organic or clayey) soils than high bulk density (i.e., sandy) soils, typically leads to decreased soil temperatures since it increases the heat capacity of the soil, and evaporation consumes a large amount of energy. However, soil moisture and high bulk density also increase the thermal conductivity of soil, allowing heat to penetrate the ground more effectively and increase active layer depths (Frauenfeld et al., 2004). Many recent studies suggest that the influence of soil moisture is stronger on thermal conductivity than on conductive heat transfers, though it is also noted that this influence may not hold at deeper soil depths and in continuous permafrost areas that have a higher concentration of mineral soils (Douglas et al., 2020, Fisher et al., 2016, Loranty et al., 2018). The relationship between soil temperature and permafrost thaw is well established. Increased soil temperatures lead to increased ALT through increases in the ground heat flux (Frauenfeld et al., 2004, Liljedahl et al., 2016, Loranty et al., 2018, Schuur and Mack, 2018).

(6) Ground ice content within the active layer: another important aspect of Arctic sub-surface processes. Similar to permafrost, ground ice is vulnerable to degradation as a result of increased soil temperatures (Jorgenson et al., 2015, Liljedahl et al., 2016). While soil moisture is a critical variable in ground ice growth, with wet sites more likely to have high ice concentrations than dry sites (Meentemeyer and Zippin, 1981, O'Neill and Burn, 2012), the presence of ground ice can help delay active layer thickening due to the large amount of latent heat required to melt the ice (Jorgenson et al., 2015, Lee et al., 2014, Loranty et al., 2018, Schuur and Mack, 2018). Conversely, high ground ice content can lead to pronounced ground subsidence when that ice melts, further promoting permafrost thaw (Jorgenson et al., 2015, Kokelj and Jorgenson, 2013).

2.2. Permafrost Modeling and Observational Data

There is a substantial research interest in gaining a greater understanding of how the Arctic will change in a warming world. As permafrost is a key component of the terrestrial Arctic system, there is a long history of observations, experiments, and models that have been made to better understand its spatial and temporal dynamics. It is well known that consequences of permafrost thaw include soil carbon emissions (Schuur et al., 2015, Schuur et al., 2009), landscape transformation through lake formation and drainage (Haynes et al., 2018, Nitze et al., 2018), and infrastructure damage (Hjort et al., 2018, Karjalainen et al., 2019). While Arctic observational networks have improved over the years, many regions remain undersampled and understudied (Biskaborn et al., 2015, Gruber, 2012, Serreze and Barry, 2014); models are often relied on to fill these data and knowledge gaps and to make future estimations and predictions. In general, models

allow for an approximate physical, conceptual, or mathematical representation of a phenomenon that is difficult to observe directly, whether that is due to the remote nature of a region or the time scale over which the phenomena of interest operate. As such, models can allow researchers to untangle the different cross-scale interactions between climate, topography, hydrology, biota, and permafrost dynamics. That said, observational data are still necessary for validation of these permafrost models and are an important component of the model development process (Gruber, 2012, Rykiel, 1996).

Non-modeling methods for monitoring permafrost changes include field measurements and remote sensing data. Field measurements vary greatly across studies. They can consist, for example, of highly localized, repeated frost table depth measurements as seen in Wilcox et al. (2019), or of boreholes from which permafrost temperatures can be measured at various ground depths. Prior to the establishment of the Global Terrestrial Network for Permafrost (GTN-P) (Biskaborn et al., 2015), boreholes were scattered across permafrost regions with no globally organized permafrost data network or reference baseline to compare temperatures to (Biskaborn et al., 2019). Russia has the most boreholes, followed by the United States (Alaska) and Canada (Biskaborn et al., 2015). As for remote sensing, a relatively new application of interferometric synthetic aperture radar (InSAR) measurements allows for the detection of ground subsidence related to the seasonal thaw of the active layer; this method provides the benefit of being able to capture a wider area of measurement than traditional *in situ* methods (Dutta and Barnhart, 2020, Liu et al., 2010, Zhao et al., 2016).

The breadth and complexity of existing permafrost models varies. Some of the first permafrost models used empirical, analytical, and/or equilibrium modeling approaches. Empirical models are developed using observations and focused on describing data, such as relationships that can be used for forecasting; they can be either deterministic or probabilistic. Empirical models include N Factors (Lunardini, 1978), the Frost Index (Nelson and Outcalt, 1987), and the statistical-empirical model PERMAKART (Keller, 1992). In contrast, analytical models are based on mathematical formulations (analytic functions) that have a closed-form solution; these models describe changes in a system, such as the thermal behavior of the ground when freezing or thawing occurs. There are few purely analytic permafrost models, although a commonly used analytic equation is the Stefan model (Lunardini, 1981). Analytic equations can be validated with empirical observations, as seen in the Kudryavtsev model that serves as an alternative to the Stefan model (Kudryavtsev et al., 1974); an analytical-empirical variation of the Kudryavtsev solution was used by Anisimov et al. (1997) where they combined the Kudryavtsev predictions of thaw depth with climatic data from general circulation models (GCMs) to provide ALT estimates for a variety of soil conditions. Meanwhile, equilibrium models are process- and physics-based models that define equilibrium permafrost conditions for a given annual regime by assuming a stationary temperature and snow cover climate; variations in either of these assumptions produce a range of mean annual ground temperatures (MAGTs) that cause permafrost conditions to deviate from equilibrium (Riseborough et al., 2008, Riseborough, 2007). Examples of equilibrium models include the Frost Number model (Nelson, 1986), TTOP model

(Smith and Riseborough, 1996), and variations of the Kudryavtsev model (Anisimov et al., 1997).

More recent modeling efforts have adopted numerical and statistical approaches. Similar to equilibrium models, numerical models are also physics-based and are a type of mathematical model that relies on computational techniques to represent the behavior of a process over time. For example, numerical models can simulate the evolution of permafrost and ground thermal regimes over continental and decadal scales (Riseborough et al., 2008). They differ from the closed-form solutions of analytical models in that they are flexible enough to accommodate highly variable materials, geometries, and boundary conditions (Riseborough et al., 2008). Examples of numerical models include a one-dimensional finite-difference model (Goodrich, 1982, Goodrich, 1978), the Northern Ecosystem Soil Temperature (NEST) model (Zhang et al., 2006), the GIPL2-MPI model (Jafarov et al., 2012), the NASA CLSM (Tao et al., 2017), and the work of Nicolsky and Romanovsky (2018). Lastly, statistical models are mathematical models based on a set of statistical assumptions that were made on a particular dataset. Statistical modeling studies tend to include a limited number of variables. Examples of statistical models include an analysis of the relationship between MAGT and ALT developed by Aalto et al. (2018), a permafrost infrastructure hazard assessment developed by Hjort et al. (2018), and an evaluation of the spatial and temporal influence of shrub expansion on frost table depth developed by Wilcox et al. (2019). A table comparing the input and output parameters of the models listed above can be seen in Table 2.1.

Table 2.1 Table of select permafrost models detailing their model type classification, select input parameters, and outputs. Ten of the most common input parameters were selected for comparison, with an "X" denoting if a model includes that input parameter. Type abbreviations: EQ (equilibrium), A (analytical), N (numerical), EM (empirical), S (statistical). Refer to text for references.

Name	Type	Inputs										Outputs
		Air Temperature	Aspect	Ground Temperature	Precipitation	Snow Depth	Soil Density	Soil Water Content	Solar Radiation	Thermal Conductivity	Vegetation Height	
Frost Number	EQ	X			X	X		X		X		Depth of frost; surface frost number
TTOP	EQ	X		X						X		Mean annual temp. at base of active layer
Kudryavtsev	EQ; A - EM	X		X		X	X	X		X	X	Depth of seasonal freezing/ thawing
One-dimensional finite-difference model	N					X	X	X		X		Position of freezing/ thawing interface
Northern Ecosystem Soil Temperature (NEST)	N	X			X		X		X	X	X	ALT; depth to permafrost table
GIPL2-MPI	N	X		X	X	X		X		X		MAGT; ALT
Catchment Land Surface Model (CLSM)	N	X		X	X				X	X	X	ALT; soil temp. profile

Table 2.1 Continued.

Name	Type	Inputs										Outputs
		Air Temperature	Aspect	Ground Temperature	Precipitation	Snow Depth	Soil Density	Soil Water Content	Solar Radiation	Thermal Conductivity	Vegetation Height	
Numerical Experiments by Nicolsky and Romanovsky (2018)	N			X			X	X		X		Rate of permafrost thaw
Stefan model	A	X								X		Phase change boundary
N Factors	EM	X		X								n-factor
Frost Index	EQ; EM	X		X	X	X	X	X		X		Stefan frost number
PERMAKART	S - EM	X	X	X		X			X			Map of permafrost distribution
Aalto et al. (2018)	S	X			X				X			MAGT; ALT
Hjort et al. (2018)	S			X			X					Geohazard indices
Wilcox et al. (2019)	S		X			X					X	Quantifica-tion of micro-scale variables on frost table depth

Models can also be coupled or uncoupled. ESMs are coupled, which means that different subsystems (e.g., ocean, atmosphere, biosphere) are represented by sub-models that communicate with each other to represent feedbacks and fluxes in all directions. In contrast, uncoupled or standalone models do not exchange information between models. In the Arctic, an example of a coupled model would include a set of sub-models that dynamically link changes in atmospheric conditions with sea ice conditions and vegetation dynamics. One of the most commonly used coupled land surface models (LSMs) in permafrost modeling studies is the Community Land Model version 4 (CLM4) (Oleson et al., 2010). This LSM is used within the Community Earth System Model (CESM) and reflects the philosophy that terrestrial ecosystems are key determinants of climate (Bonan, 2008). Conversely, an uncoupled atmospheric model may be initialized with sea surface temperature or sea ice extent information, but the ocean itself is not modeled. In the Permafrost Modeling Toolbox by the Community Surface Dynamics Modeling System (CSDMS), the Frost Index (Nelson and Outcalt, 1987) and Kudryavtsev (Anisimov et al., 1997) models can be coupled to other CSDMS models, while the GIPL2-MPI (Jafarov et al., 2012) model is currently standalone (Overeem et al., 2018). Serreze and Barry (2014) discuss other uncoupled land surface, global climate, regional climate, and ecosystem models used in the study of the Arctic climate system. As for coupled models, a thorough review of models participating in the Coupled Model Intercomparison Project Phase 5 (CMIP5) and their performance in regards to permafrost modeling can be found in Koven et al. (2013). A table of the models used in their analysis is shown in Table 2.2, and a table of the modeled current

and future permafrost extent in the upper 3 meters of soil for each model is shown in Table 2.3. This modeling study concluded that the models included in CMIP5 differ in their degree of warming and the response of permafrost to warming (Koven et al., 2013). While all models showed a loss of permafrost, the percentage of loss ranged from 6 – 29% (Koven et al., 2013). Many of the differences in the model results can be attributed to the representation of ground thermal relationships between surface air temperature and the land surface, particularly in regards to snow cover (Koven et al., 2013).

Table 2.2 Some key models relevant to soil physics at high latitudes (e.g., snow properties, differing frozen- and unfrozen-soil thermal conductivity); model attributes and model references used are also presented. Reprinted from Koven et al. (2013).

Model name	Modeling group	Land model	Multiple snow layers	Snow between soil and atmosphere	Latent heat of soil water	Differing frozen/unfrozen soil thermal conductivity	Organic matter	Reference
BCC-CSM1–1	BCC	BCC Atmosphere-Vegetation Interaction Model (BCC_AVIM1.0)	Yes	Yes	Yes	Yes	No	Ji (1995)
CCSM4.0	NCAR	CLM4	Yes	Yes	Yes	Yes	Yes	Lawrence et al. (2011)
CESM1-CAM5	NCAR	CLM4	Yes	Yes	Yes	Yes	Yes	Lawrence et al. (2011)
CanESM2	Canadian Centre for Climate Modelling and Analysis (CCCMA)	Canadian Land Surface Scheme (CLASS)	No	Yes	Yes	Yes	No	Verseghy (1991)
GFDL-ESM with GOLD ocean component (2G)	GFDL	GFDL Land Model 3.0 (LM3.0)	Yes	Yes	Yes	Yes	No	Dunnea et al. (2012)
GFDL-ESM with MOM4 ocean component (2M)	GFDL	GFDL LM3.0	Yes	Yes	Yes	Yes	No	Dunnea et al. (2012)
GISS Model E coupled with Russell ocean model (E2-R)	Goddard Institute for Space Studies (GISS)	GISS Land Surface Model	Yes	Yes	Yes	Yes	Yes	Rosenzweig and Abramopoulos (1997)
HadCM3	Met Office Hadley Centre (MOHC)	MOSES	No	No	Yes	Yes	No	Cox et al. (1999)
HadGEM2-CC	MOHC	MOSES2	No	No	Yes	Yes	No	Essery et al. (2003)
HadGEM2 Earth System (ES)	MOHC	MOSES2	No	No	Yes	Yes	No	Essery et al. (2003)
INM-CM4	INM	INM-CM4	Yes	Yes	Yes	Yes	Yes	Volodin et al. (2010)
IPSL-CM5 Coupled with NEMO (A) Low Resolution (LR)	IPSL	ORCHIDEE	Yes	No	No	No	No	Krinner et al. (2005)
IPSL-CM5A Medium Resolution (MR)	IPSL	ORCHIDEE	Yes	No	No	No	No	Krinner et al. (2005)
MIROC-ESM Chemistry Coupled (CHEM)	Japan Agency for Marine-Earth Science and Technology (JAMSTEC)	Minimal Advanced Treatments of Surface Interaction and Runoff (MATSIRO)	Yes	Yes	Yes	No	No	Takata et al. (2003)
MIROC-ESM	JAMSTEC	MATSIRO	Yes	Yes	Yes	No	No	Takata et al. (2003)
MIROC5	JAMSTEC	MATSIRO	Yes	Yes	Yes	No	No	Takata et al. (2003)
MPI-ESM-LR	Max Planck Institute for Meteorology	JSBACH	Yes	No	No	No	Yes	Raddatz et al. (2007)
MRI-CGCM3	MRI	Hydrology, Atmosphere and Land (HAL)	Yes	Yes	Yes	Yes	No	Yukimoto et al. (2012)
NorESM1-M	Norwegian Climate Centre (NCC)	CLM3	Yes	Yes	Yes	Yes	Yes	Lawrence et al. (2011)

Table 2.3 Modeled current and future permafrost extent in the upper 3 m of soil. For qualitative comparison, the 50% of models with the least bias for the present time period are noted in boldface type. Reprinted from Koven et al. (2013).

		Historical		RCP4.5				
Model name	PF area 2005 ($\times 10^6$ km^2)	PF area 1850 ($\times 10^6$ km^2)	Fraction PF lost 1850–2005 (unitless)	PF area 2050 ($\times 10^6$ km^2)	Fraction PF remaining 2005–50 (unitless)	PF area 2100 ($\times 10^6$ km^2)	Fraction PF remaining 2005–2100 (unitless)	Global warming 2005–2100 (°C)
BCC-CSM1–1	1.4	2.7	0.47	0.9	0.66	0.8	0.58	1.2
CCSM4.0	**10.5**	13.1	0.20	8.0	0.76	5.7	0.54	1.2
CESM1-CAM5	**12.3**	13.8	0.11	9.1	0.74	6.1	0.49	2.0
CanESM2	3.2	5.7	0.43	0.9	0.29	0.5	0.14	1.9
GFDL-ESM2G	25.6	27.3	0.06	23.5	0.92	22.0	0.86	0.7
GFDL-ESM2M	24.3	27.0	0.10	21.1	0.87	20.0	0.82	0.8
GISS-E2-R	4.5	8.2	0.45	2.6	0.58	2.5	0.57	0.9
HadCM3	27.3	28.6	0.05	—	—	—	—	—
HadGEM2-CC	25.1	24.6	−0.02	20.6	0.82	17.1	0.68	2.0
HadGEM2-ES	22.3	23.4	0.05	17.8	0.80	14.5	0.65	2.1
INM-CM4	**14.0**	15.6	0.11	12.8	0.92	11.5	0.82	1.1
IPSL-CM5A-LR	**12.6**	18.5	0.32	8.5	0.68	7.0	0.56	1.8
IPSL-CM5A-MR	**10.1**	14.9	0.32	6.5	0.64	4.6	0.46	1.8
MIROC-ESM	**11.5**	12.6	0.08	7.3	0.63	4.7	0.40	2.1
MIROC5	**17.4**	19.0	0.08	14.5	0.83	12.3	0.70	1.3
MPI-ESM-LR	8.6	13.7	0.37	6.2	0.72	4.0	0.46	1.3
MRI-CGCM3	**15.5**	16.7	0.08	13.2	0.86	10.9	0.70	1.5
NorESM1-M	**13.3**	15.1	0.11	10.2	0.77	7.3	0.55	1.5
Observations	15.0	—	—	—	—	—	—	—

		RCP4.5		RCP2.6		RCP8.5	
High-latitude warming 2005–2100 (°C)	Arctic amplification (unitless)	Total loss PF/degree high-latitude warming ($\times 10^6$ km^2 °C^{-1})	Fractional loss PF/degree high-latitude warming (% °C^{-1})	PF area 2100 RCP2.6 ($\times 10^6$ km^2)	Fraction PF remaining 2005–2100 (unitless)	PF area 2100 ($\times 10^6$ km^2)	Fraction PF remaining 2005–2100 (unitless)
2.7	2.3	0.2	15.4	—	—	0.5	0.36
2.1	1.7	2.3	21.8	7.7	0.73	2.7	0.26
4.2	2.1	1.5	12.1	7.9	0.64	2.4	0.19
4.1	2.2	0.7	20.8	1.1	0.34	0.0	0.01
1.5	2.2	2.3	9.1	25.1	0.98	15.3	0.60
1.2	1.5	3.5	14.3	22.1	0.91	14.8	0.61
1.4	1.5	1.4	31.0	4.4	0.98	1.0	0.23
—	—	—	—	—	—	—	—
5.2	2.6	1.5	6.2	—	—	9.4	0.38
5.3	2.6	1.5	6.5	17.5	0.78	7.0	0.31
2.3	2.2	1.1	7.7	—	—	9.8	0.70
3.4	1.9	1.7	13.2	9.8	0.78	2.0	0.16
3.5	1.9	1.6	15.7	8.1	0.80	1.4	0.14
5.0	2.4	1.4	11.8	6.4	0.55	0.6	0.05
3.3	2.5	1.5	8.9	14.2	0.81	6.5	0.37
2.6	2.0	1.7	20.3	6.9	0.80	0.5	0.06
3.0	2.0	1.5	9.8	12.7	0.82	7.7	0.50
4.1	2.8	1.5	11.1	9.7	0.73	3.5	0.27
—	—	—	—	—	—	—	—

There are advantages and disadvantages to every model development approach. For instance, while analytical models can provide closed-form solutions based on mathematical representations, they cannot integrate site-specific, real-world conditions such as snow cover time series (Riseborough et al., 2008). Conversely, numerical models can address this limitation, but they require the input of spatial data to set up initial conditions and subsequent model spin up; this can be an issue, as data are not always readily available to initialize every model component (Biskaborn et al., 2015, Gruber, 2012, Serreze and Barry, 2014). In these cases, modelers revert to alternative mathematical representations or parameterizations and/or do not fully validate their models (Gruber, 2012, Riseborough et al., 2008). In the permafrost modeling realm, the representation of ground thermal regime and/or vegetation dynamics can be very limited. Other key limitations include those inherent to the chosen modeling approach adopted and data variability (Lawrence et al., 2008, Riseborough et al., 2008, Tao et al., 2017). Along those lines, the models can only be as good as the data available; in the case of permafrost, there remains large uncertainties that pertain to permafrost distribution, thickness, and ice content, among many more (Gruber, 2012).

Permafrost models commonly include the following input parameters (Table 2.1): air temperature, precipitation (particularly snow cover and/or depth), soil temperature, and soil moisture. Vegetation cover, topography, and soil texture are less common, albeit important additions. A difficulty in assessing permafrost model performance and representation is that most model simulations are conducted in Alaska, as that is where there are the most and highest quality observations that allow for model

calibration. By limiting the spatial domain for model development and/or testing, it is possible that the model may not be as applicable to other regions, such as Canada or Siberia. As a result, current research emphasizes the need to further improve permafrost modeling, and many studies are aimed at improving existing models or modeling approaches to fill the aforementioned gaps and limitations (e.g., Jafarov et al. (2012), Tao et al. (2017), Westermann et al. (2016)). While this is important work, it is possible that an alternative type of model – one that would allow for the integration of different data types and a novel representation of permafrost thaw dynamics – would provide the community with new benchmarks against which to compare and contrast model outputs.

2.3. Bayesian Methods

BNs are probabilistic, cause-effect frameworks and mathematical tools; they are constructed to represent variables ("nodes") and the relationships ("arcs") between these variables. Variables may be classified as "parent" (cause) or "child" (effect) nodes. Variables can also be further classified by their "type," such as "decision" or "chance" nodes. Decision nodes are those that are non-random or non-variable (e.g., topographic aspect), while chance nodes are those that have a random component to them (e.g., air temperature). A number of "states" are then attributed to each node; these states are typically represented as categories that capture the current state the variable is in and the states that the variable can shift to. For instance, a variable may exist in a low, medium, or high state. Decision nodes do not have probabilities associated with them, and the user sets the states. The inclusion of decision nodes aids in the exploratory analysis of different scenarios. For chance nodes, on the other hand, a probability is assigned to each

one of these states based on existing evidence, such as physical observations, model outputs, or expert assessment.

BNs are based on a specific case of Bayes' theorem that describes the probability of an event given prior conditions and how beliefs change to account for new evidence (Korb and Nicholson, 2004). The concept of Bayesian inference is formalized in the equation:

$$P(H|E) = \frac{P(E|H)P(H)}{P(E)}$$

where the probability of a hypothesis *H* given some evidence *E* is equal to its likelihood *P(E|H)* times its probability prior to any evidence *P(H)*, normalized by the probability of the evidence *P(E)* being true (Korb and Nicholson, 2004). A graphical representation of the causal relationship between *H* and *E* is seen in Figure 2.2.

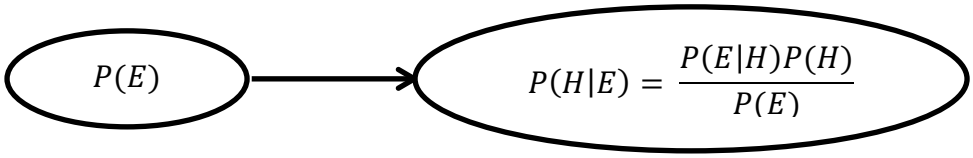

Figure 2.2 Graphical (BN) representation of the casual relationship between the hypothesis (*H*) and evidence (*E*). Note that there could be multiple parent nodes. Adapted from Varela Gonzalez (2017).

A BN with a synthetic case containing three chance nodes (air temperature, soil temperature, and thaw depth) is seen in Figure 2.3. Parentless nodes, such as air temperature, are quantified by marginal probabilities. Assume that it is known that air temperature has a 75% marginal probability of being low, 15% probability of being medium, and 10% probability of being high. Arcs represent the causal dependencies

between nodes; they help build the conditional probability table (CPT) that links a parent node to a child node. In a BN with *n* nodes, $X_1 \ldots X_n$, the joint distribution is represented by $P(X_1 = x_1, X_2 = x_2, \ldots, X_n = x_n)$, or $P(x_1, x_2, \ldots, x_n)$. Using the chain rule of probability theory, this factorizes to $P(x_1, x_2, \ldots, x_n) = P(x_1) \times P(x_2|x_1) \ldots, \times P(x_n|x_1, \ldots, x_{n-1}) = \prod_i P(x_i|x_1, \ldots, x_{i-1})$; when the value of a particular node is conditional only on the values of the parent nodes, this reduces to $P(x_1, x_2, \ldots, x_n) = \prod_i P(x_i|Parents(X_i))$ (Korb and Nicholson, 2004).

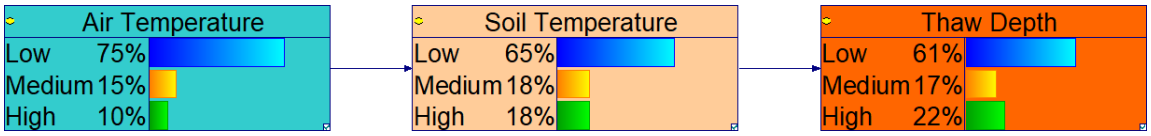

Air Temperature P(E)	
Low	0.75
Medium	0.15
High	0.10

$P(H_1\|E)$		Air Temperature P(E)		
		Low	Medium	High
Soil Temperature $P(H_1)$	Low	0.80	0.25	0.10
	Medium	0.10	0.60	0.10
	High	0.10	0.15	0.80

$$[0.75 \quad 0.15 \quad 0.10]^T \begin{bmatrix} 0.80 & 0.25 & 0.10 \\ 0.10 & 0.60 & 0.10 \\ 0.10 & 0.15 & 0.80 \end{bmatrix}$$

$$= \begin{bmatrix} (0.75 * 0.80) + (0.15 * .25) + (0.10 * 0.10) \\ (0.75 * 0.10) + (0.15 * 0.60) + (0.10 * 0.10) \\ (0.75 * 0.10) + (0.15 * 0.15) + (0.10 * 0.80) \end{bmatrix} = \begin{bmatrix} 0.6475 \\ 0.175 \\ 0.1775 \end{bmatrix}$$

Soil Temperature $P(H_1)$	
Low	0.65
Medium	0.18
High	0.18

$P(H_2\|H_1)$		Soil Temperature $P(H_1)$		
		Low	Medium	High
Thaw Depth $P(H_2)$	Low	0.85	0.25	0.10
	Medium	0.10	0.50	0.10
	High	0.05	0.25	0.80

$$[0.65 \quad 0.18 \quad 0.18]^T \begin{bmatrix} 0.85 & 0.25 & 0.10 \\ 0.10 & 0.50 & 0.10 \\ 0.05 & 0.25 & 0.80 \end{bmatrix}$$

$$= \begin{bmatrix} (0.65 * 0.85) + (0.18 * 0.25) + (0.18 * 0.10) \\ (0.65 * 0.10) + (0.18 * 0.50) + (0.18 * 0.10) \\ (0.65 * 0.05) + (0.18 * 0.25) + (0.18 * 0.80) \end{bmatrix} = \begin{bmatrix} 0.6155 \\ 0.173 \\ 0.2215 \end{bmatrix}$$

Figure 2.3 Example of a BN with three chance nodes: air temperature, soil temperature, and thaw depth. Probabilities represent synthetic cases of the marginal (air temperature) and joint (soil temperature and thaw depth) probabilities. Tables show the marginal or conditional probabilities followed by the equations calculating the joint probabilities.

In this example, the arc between air temperature and soil temperature builds the soil temperature CPT, and the arc between soil temperature and thaw depth builds the thaw depth CPT. The topology of the network captures qualitative relationships between the variables, while the probabilities provide a quantification of the relationships (Aguilera et al., 2011, Korb and Nicholson, 2004). It is important to note that BNs are directed acyclic graphs, meaning that nodes and arcs cannot be connected in a directly cyclic manner. As such, the relationships between nodes and arcs represent the causal evidence for a process that cascades through the model, from parent to children, in a cause-effect manner, within a given "step" in space and time (Varela Gonzalez, 2017). Within each model step, feedbacks are not allowed between nodes. For instance, if high thaw depth is considered a proxy for carbon release, an arc from thaw depth to air temperature cannot be made to represent the effects of increased carbon release on air temperature. Instead, the BN model would have to be run again with updated marginal probabilities for air temperature to reflect the new increased carbon conditions. Alternatively, a dynamic BN could be used to represent feedbacks (Chen and Pollino, 2012, Kjaerulff, 1995).

A primary advantage to using a BN approach is the ability to incorporate three types of evidence (i.e., observational data, model outputs, and expert assessments) into a single model. This is particularly helpful to represent the Arctic system, as data observations or model outputs may be regionally limited, incomplete, or inexistent. The BN approach also tends to be more transparent than traditional modeling methods by reducing the black-box aspect commonly seen in traditional models through explicit

representation of the interaction between variables in the BN (Chen and Pollino, 2012). In addition, the BN approach allows for quantification of uncertainties; uncertainties in the model and the system are expressed through the distribution of probabilities assigned to each node state, and the uncertainties are propagated through the network to the final model endpoint (Chen and Pollino, 2012). Lastly, by employing the principle of Occam's Razor, which here means aiming for the simplest model that still accurately represents the process being modeled, BNs may be more suitable than other modeling approaches for scenarios where it is important to engage stakeholders in the modeling process of a system (Chen and Pollino, 2012). Keeping the BN as simple as possible is also necessary for maintaining sensitivity of outputs to inputs and for avoiding additional uncertainty propagation in the model (Chen and Pollino, 2012). Despite appearing simpler than other models, BNs are well suited for modeling complex systems with a large number of variables (Getoor et al., 2004) or being integrated into larger models as sub-models (Chen and Pollino, 2012).

Another unique advantage to BNs is their capability for both forward (prognosis/cause to effect) and inverse (diagnosis/effect to cause) modeling. The synthetic case in Figure 2.3 can be used as a basis for explaining examples of prognosis (Figure 2.4) and diagnosis (Figure 2.5). In prognosis, the state of the parent node is set to the model scenario of interest. In Figure 2.4, the scenario being modeled is low air temperature. The 100% chance of low air temperature determines which probabilities are used in the soil temperature CPT, and the joint probabilities of soil temperature are then propagated to thaw depth. Conversely, the 100% chance of high thaw depth in the

diagnosis scenario in Figure 2.5 back propagates through the model, first determining the soil temperature probabilities and then those of air temperature.

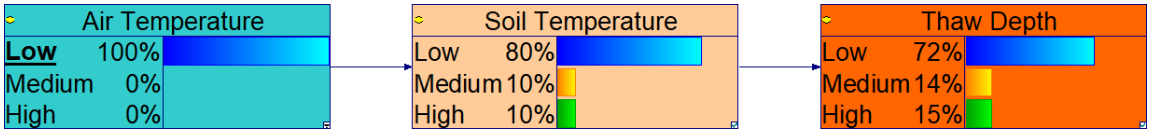

Air Temperature P(E)	
Low	0.75
Medium	0.15
High	0.10

$P(H_1\|E)$		Air Temperature P(E)		
		Low	Medium	High
Soil Temperature $P(H_1)$	Low	**0.80**	0.25	0.10
	Medium	**0.10**	0.60	0.10
	High	**0.10**	0.15	0.80

Soil Temperature $P(H_1)$	
Low	0.80
Medium	0.10
High	0.10

$P(H_2\|H_1)$		Soil Temperature $P(H_1)$		
		Low	Medium	High
Thaw Depth $P(H_2)$	Low	0.85	0.25	0.10
	Medium	0.10	0.50	0.10
	High	0.05	0.25	0.80

$$[0.80 \quad 0.10 \quad 0.10]^T \begin{bmatrix} 0.85 & 0.25 & 0.10 \\ 0.10 & 0.50 & 0.10 \\ 0.05 & 0.25 & 0.80 \end{bmatrix}$$

$$= \begin{bmatrix} (0.80 * 0.85) + (0.10 * 0.25) + (0.10 * 0.10) \\ (0.80 * 0.10) + (0.10 * 0.50) + (0.10 * 0.10) \\ (0.80 * 0.05) + (0.10 * 0.25) + (0.10 * 0.80) \end{bmatrix} = \begin{bmatrix} 0.715 \\ 0.14 \\ 0.145 \end{bmatrix}$$

Figure 2.4 Synthetic prognosis case exploring likely thaw depth states under low air temperature. Low air temperature contributes to predominately low soil temperature, which then contributes to predominately low thaw depth. The bolded values in the tables show which air temperature state and soil temperature probabilities are being propagated through the BN to thaw depth.

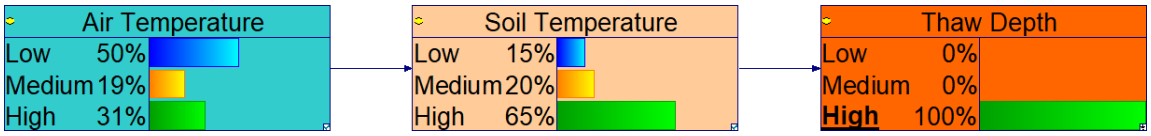

Soil Temperature $P(H_1)$	
Low	0.15
Medium	0.20
High	0.65

$P(H_2\|H_1)$		Soil Temperature $P(H_1)$		
		Low	Medium	High
Thaw Depth $P(H_2)$	Low	0.85	0.25	0.10
	Medium	0.10	0.50	0.10
	High	**0.05**	**0.25**	**0.80**

Air Temperature P(E)	
Low	0.50
Medium	0.19
High	0.31

$P(H_1\|E)$		Air Temperature P(E)		
		Low	Medium	High
Soil Temperature $P(H_1)$	Low	0.80	0.25	0.10
	Medium	0.10	0.60	0.10
	High	**0.10**	**0.15**	**0.80**

$$P\left(H_{1_{High}} \middle| H_{2_{High}}\right)$$

$$= \frac{P\left(H_{2_{High}} \middle| H_{1_{High}}\right) * P(H_{1_{High}})}{P\left(H_{2_{High}} \middle| H_{1_{Low}}\right) * P(H_{1_{Low}}) + P\left(H_{2_{High}} \middle| H_{1_{Med}}\right) * P(H_{1_{Med}}) + P\left(H_{2_{High}} \middle| H_{1_{High}}\right) * P(H_{1_{High}})}$$

$$P\left(H_{1_{High}} \middle| H_{2_{High}}\right) = \frac{0.80 * 0.18}{(0.05 * 0.65) + (0.25 * 0.18) + (0.80 * 0.18)} = \frac{0.144}{0.2215} = 0.65$$

Figure 2.5 Synthetic diagnosis case exploring likely soil and air temperature states under high thaw depth. High thaw depth is conditional on predominately high soil temperatures, which can occur under warmer air temperature conditions. Equations demonstrate an example of calculating high soil temperature given high thaw depth. Probabilities for low and medium soil temperature given high thaw depth, and low, medium, and high air temperature given low, medium, and high soil temperature can be calculated similarly.

As with all methodologies, there are a number of limitations to the BN approach. One such limitation is that non-dynamic BNs are not strong at representing processes at varying temporal scales (i.e., feedbacks) due to their acyclic nature (Chen

and Pollino, 2012, Uusitalo, 2007). Instead, processes are represented at a single moment in time, unless the time steps are directly integrated into the model itself. BNs are also not well suited for non-discrete data, as discretization of continuous variables may lead to a loss of statistical power (Chen and Pollino, 2012, Uusitalo, 2007). Development of BNs is also hindered by the lack of a universally accepted methodology and use of terminology (Weber et al., 2012), and reliable expert elicitation is a known challenge (Kaikkonen et al., 2021, Uusitalo, 2007). Another limitation arises when experts must validate the model; the size of a node's CPT increases $S\prod_{i=1}^{n} P_i$ where $S =$ the number of states and $P_i =$ the number of states in the *i*th parent node (Marcot et al., 2006), meaning that limiting the size of the node's CPT is especially important in BNs where CPTs are defined through expert assessment since the CPT can quickly become too large for the human brain to adequately comprehend. Despite these limitations, the unique advantages of this approach hold great potential for application to the environmental sciences.

Recent reviews by Aguilera et al. (2011) and Kaikkonen et al. (2021) show that few BN studies have been applied to environmental modeling and environmental risk assessment (ERA), respectively. Aguilera et al. (2011)'s review found that only 4.2% of papers published about the applications of BNs fell under the environmental modeling category. BNs are most commonly applied to problems in the computer sciences, mathematics, and engineering (Aguilera et al., 2011). While an exact percentage was not given, Kaikkonen et al. (2021)'s review also concluded that the methodology is not commonly used in ERA. In ERA, BNs were used in the fields of ecology, environmental

chemistry, environmental toxicology, hydrology, and more to assess (1) the risk of a specific stressor to the environment in general, (2) the risk from various stressors to specific species or areas, or (3) both; most ERAs focused on freshwater and marine environments (Kaikkonen et al., 2021). Reflecting these trends, the use of BNs in Arctic studies appears to be rather limited. Several studies have applied BNs to Arctic shipping, transportation, and aquatic life (Afenyo et al., 2017, Fahd et al., 2020, Zhang et al., 2020), but most terrestrial studies that used Bayesian statistics did not use a BN framework. For instance, a Bayesian model was developed to predict the maximum thickness of seasonally frozen ground in the Yellow River source region of northwestern China using historical air temperature and precipitation observations (Qin et al., 2018). Likewise, a Bayesian approach was recently used to integrate LiDAR digital elevation model (DEM) and multiscale snow depth and ground penetrating radar (GPR) probe datasets to estimate snow depth in the tundra of Arctic Alaska (Wainwright et al., 2017). The former study found that the results of their stochastic approach was consistent with results obtained from traditional deterministic methods, while the latter study allowed for consistent integration of three disparate datasets as well as estimation of uncertainty.

So far, the most comprehensive use of a BN in the context of the Arctic and permafrost is a study by Webster and McLaughlin (2014) that assesses the vulnerability of permafrost to thaw and estimates the impacts of permafrost thaw on greenhouse gas (GHG) emissions and climate feedbacks in the Canadian Arctic and Hudson Plain regions using a Bayesian belief network (BBN). The objective of the study was to create a tool that aids policy makers in understanding the vulnerability of permafrost to thaw

and resulting carbon emissions (Webster and McLaughlin, 2014). The BBN is arranged in a hierarchical manner to reflect the vulnerability assessment components of sensitivity, exposure, and adaptive capacity; however, the adaptive capacity component is not explicitly represented in the version of the model presented in the study. Nodes in the BBN represent the themes of future and current mean annual air temperature and ground conditions, heat transfer, carbon susceptibility, permafrost thaw, GHGs, and feedback to climate change. Although Bayesian networks are capable of integrating various types of evidence, the study by Webster and McLaughlin (2014) only included evidence from expert assessment. It is arguable that their findings could have been augmented by the integration of observational data and/or model outputs, as the authors recognize that the expert assessment approach can lead to accurate, but not precise, predictions. That said, their study is a convincing example of how observational data are not necessarily required in order to generate useful predictions of permafrost thaw and demonstrated the usefulness of BBNs as potential policy tools, as the model allows for various future scenarios and consequences to be analyzed.

3. PERMABN DEVELOPMENT AND METHODS

The PermaBN is a Bayesian network designed to assess permafrost thaw in the continuous permafrost region of the Arctic. It provides an alternative modeling technique for assessing permafrost thaw in the Arctic, and expands upon the work of Webster and McLaughlin (2014) by supplementing their expert assessments with physical observations. Following the best practices in BN modeling outlined by Chen and Pollino (2012), the model development process (Figure 3.1) entails:

1. Defining model objectives and scope
2. Creating a conceptual model of the system to form the structure of the BN
3. Defining states and conditional probabilities of all variables
4. Evaluating the BN using a suite of both quantitative and qualitative model evaluation methods
5. Documenting assumptions, uncertainties, descriptions and reasoning for each node and linkage, data and information sources, and evaluation results

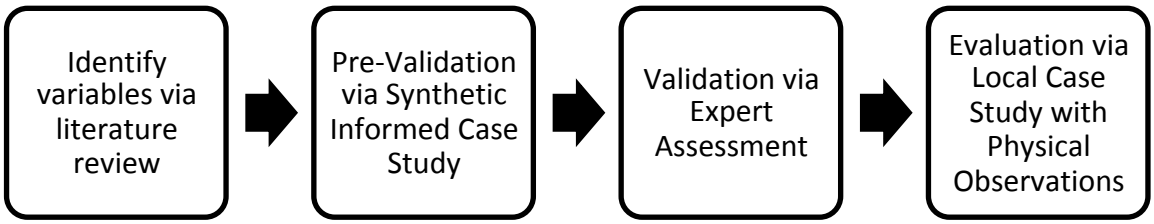

Figure 3.1 Workflow diagram of the PermaBN model development process.

The objectives of PermaBN are to:

1. Provide an alternative permafrost modeling framework that improves understanding and prediction of permafrost dynamics under various climate or ecosystem conditions (i.e., provide a method that allows for exploratory and scenario analysis)

2. Identify knowledge and data gaps that hinder our understanding (and modeling capabilities) of permafrost dynamics

3. Facilitate participatory modeling amongst researchers and/or stakeholders

In this proof-of-concept stage, the scope of PermaBN is limited to the prediction of permafrost thaw depth in the continuous permafrost region as a result of a handful of key terrestrial factors. The initial conceptual models were designed with the assumption of a multiyear time scale. While hydrological influences on permafrost thaw are important at this temporal scale, the emphasis here is on the geomorphic and ecological processes that influence continuous permafrost thaw in order to better compare PermaBN results to existing modeling efforts. That said, future development of PermaBN could introduce hydrological factors. Another limiting assumption that was made in the model developmental phase was that the variable selection was limited to a few key terrestrial processes. This was done to reduce the size of the BN and the CPTs, which are desirable features (Chen and Pollino, 2012, Marcot et al., 2006). In its current form, PermaBN is not meant to be viewed as a true environmental risk assessment model since it lacks the quantification of utility associated with the consequences of permafrost thaw. Instead, it should be viewed as a model aimed at predicting environmental

impacts. Future development could use PermaBN as a sub-module that would be included into a comprehensive Arctic ecosystem risk framework. It should also be noted that, in its current form, PermaBN might not be applicable to non-continuous permafrost regions or transitional permafrost regions due to differing drainage patterns, vegetation types, and ground temperature/permafrost relationships (Burn and Kokelj, 2009).

3.1. Pre-Validation

After defining the objectives and scope of the PermaBN model, a conceptual model of the Arctic terrestrial system was created to form the structure of the BN. The "nodes" and "arcs" of BNs are easy to represent graphically in a BN software program; these graphical networks provide a means to visualize hypotheses in the form of conceptual models. Here, the conceptual model was created using the software program GeNIe (BayesFusion, 2019). In the case of PermaBN, the network represents a hypothesis about the terrestrial variables that control permafrost thaw depth. Multiple BNs could be created to reflect different hypotheses or spatiotemporal domains, if desired. In other words, PermaBN is by no means a unique or "be-all and end-all" representation; rather, it is the best initial attempt at representing the key terrestrial processes at play in permafrost thaw. Ultimately, the goals of the conceptual model are to provide a structure for the BN and identify the causal relationships across the system. In environmental BNs, node and arc selection and definition are typically determined through literature review or expert judgment (Kaikkonen et al., 2021). For this reason, the variables included in my conceptual model were determined primarily through extensive review of peer-reviewed scientific literature and collaboration with other

researchers and scientists during two workshops that took place in 2019 at Texas A&M University.

Following the background and review in Section 2.1, the following variables were selected for the PermaBN model because they are thought to be most impactful on permafrost thaw: (1) geological setting (aspect and soil particle size) (Arya and Paris, 1981, Wilcox et al., 2019), (2) atmospheric conditions (air temperature, rain, snow, and season) (Bintanja and Andry, 2017, Bintanja and Selten, 2014, IPCC, 2013), (3) surface insulation (vegetation density/height, snow depth, and insulation) (Gockede et al., 2019, Wilcox et al., 2019), and (4) soil properties (soil moisture, soil water input, soil temperature, and ground ice volume) (Gockede et al., 2019, Jorgenson et al., 2015, Oelke and Zhang, 2004, Schuur and Mack, 2018, Westermann et al., 2011, Zhang et al., 2018, Zwieback et al., 2019). ALT is the final variable in the network and is the response, or endpoint, of the system. The influencing variables were identified explicitly for their known impacts on permafrost thaw. Other variables, such as soil thermal conductivity, are implicit to the model through the causal relationships between nodes. For instance, soil particle size influences soil moisture and insulation, which are known to influence thermal conductivity, and hence, soil temperatures. Similarly, some hydrological processes could be considered implicit to the soil moisture node (Woodard et al., 2021). For example, snow melt contributes to soil water input, and soil particle size controls infiltration rates, and hence, soil moisture content.

Variables in the model are classified as either “decision” or “chance” nodes. As discussed in Section 2.3, decision nodes are those that are non-random or non-variable.

For instance, topographic aspect and season only exist in set states, such as north/east/south/west or snow-free/snow, respectively. These decision nodes are set by the user; they do not have probabilities associated with them. The inclusion of decision nodes aids in the exploratory analysis of different scenarios. In the case of PermaBN, each decision node is determined by a set of two to four states. Conversely, chance nodes are those that have a random component to them. Variations in air temperature or amount of precipitation are examples of these chance nodes, which contain probabilities; a set of three states is determined for each chance node. These possible states (low, medium, and high) capture the current state the variable is in and the states that the variable can shift to. When incorporating physical observations or modeling results, low, medium, and high could correspond to 0 - 33%, 33 - 66%, and 66 - 100% cumulative probabilities, respectively, from the empirical cumulative density function for the variable; states could alternatively be defined by average conditions identified in the literature.

Determination of the CPTs followed characterization of each node and associated possible states; the maximum number of parent nodes for any node was limited to five in order to limit the size of the CPTs while still allowing for as many causal relationships to be explicitly represented as possible. It is ideal to include as much evidence as possible when creating the CPTs (Medina-Cetina and Nadim, 2008), but evidence can sometimes be sparse in environmental studies. In that case, the CPTs can be derived through expert judgment. One method for initially determining the CPTs for any given node is to assign a uniform distribution; this is commonly the case if the variable conditions are unknown.

CPT values can then be adjusted as necessary when evidence becomes available for the variable, whether it is from physical observations, model outputs, or expert assessments (Marcot et al., 2006). It is also common to initially determine the CPTs in a symmetric manner when using expert assessments as the evidence source (McLaughlin and Packalen, In Review). In a symmetric CPT, the probability of the "lowest" scenario would be equal to the probability of the "highest" scenario. In the pre-validation version of the PermaBN model, probability values were selected to represent trends rather than true probabilities of what may occur in reality. For example, a high probability (60%) was given to the medium air temperature scenario, indicating the state of knowledge that it is more likely that a moderate amount of warming will occur in the Arctic over the coming decades as opposed to no/little warming or extreme warming; similarly, extreme warming is more likely than no/little warming (Meredith et al., 2019).

To test the accuracy or representativeness of the CPTs (Appendix A), 46 prognostic experiments (Appendix B) were designed to illustrate how the incorporation of evidence affected children nodes in the model, particularly the model endpoint (prediction of ALT). The first set of experiments was conducted on a model where all the nodes were set to a uniform distribution. Then, informed nodes at varying levels of the model were introduced. The final set of experiments was conducted on a model where all the nodes were informed. In each of the experiment sets, a combination of the primary parent nodes (i.e., those nodes with no preceding nodes or incoming arcs) were set to the extreme scenarios that could be encountered in the system (e.g., low air temperatures, solar radiation, and soil particle size or high air temperatures, solar

radiation, and soil particle size). A set of 13 diagnostic experiments (Appendix B) was also designed to check for consistency in the model. In contrast to the prognosis experiments, these effect-to-cause experiments focused on setting the response variable (ALT) to each of its states in a fully informed model to see if the parent node distributions responded as expected. Some of the diagnostic experiments also set intermediate parent nodes to different states to assess whether a node seems to be a primary driver of change in the model.

Collectively, these prognostic and diagnostic experiments represent the process of pre-validation. Pre-validation, or pre-reliability analysis, is the process of assessing the extreme or likely scenarios that could be experienced in the system (Medina-Cetina and Nadim, 2008). It allows for a check on the consistency of the model at the lower and upper bounds; for instance, if thaw depth does not respond as expected given the state of the parent nodes in the prognostic experiments, it is possible that: (1) the CPTs may not be well defined, and/or (2) the variables and connections between them may not sufficiently represent the process of permafrost thaw. In the event of the former, the CPTs simply need to be adjusted through further expert judgment, or ideally, through the incorporation of physical observations or model outputs. In the event of the latter, the model may need to be redesigned. When the system responds as expected per the modeler's judgment, the model can be considered pre-validated, and the results can be used for further validation of the model.

3.2. Validation – Expert Assessment

With the model pre-validated, the model moved into the validation stage. Here, validation first entailed meeting with a group of four experts at Texas A&M University to review the conceptual model and the results of the prognostic and diagnostic experiments. This validation stage is a fairly unique attribute of the PermaBN model development process, as most BN studies exclude validation from the development process (Aguilera et al., 2011, Kaikkonen et al., 2021). Of the studies that do conduct validation, the most common method for doing so is through expert assessment (Kaikkonen et al., 2021). Since the experts were familiar with both Arctic climates and introductory Bayesian modeling principles, only a brief overview of the current state of permafrost modeling research and of the statistical methods behind the two types of experiments was provided. The feedback and suggestions from the validation session were then used to refine the BN conceptual model. Refinements included: (1) renaming or redefining of nodes in the pre-validation conceptual model, (2) considering differing soil moisture and soil temperature relationships dependent on location and/or season, (3) correcting known errors in the soil moisture CPT, and (4) implementing a qualitative threshold for passing the CPTs defined in the pre-validation prognosis and diagnosis experiments.

The nodes that were renamed and redefined are: (1) “soil particle size” to “soil density,” (2) “vegetation density/height” to “vegetation height,” (3) “ground ice volume” to “active layer ice content,” and (4) “active layer thickness” to “thaw depth.” An additional arc from “soil density” to “insulation” was added following the redefinition of

state names from clay, silt, and sand to low, medium, and high; the air temperature nodes was also redefined from the RCP scenarios to the corresponding low, medium, and high states (e.g., the RCP 2.6 scenario was redefined to low). As for the relationship between soil moisture and soil temperature on annual and seasonal time scales, it was further investigated to establish whether those variables are positively correlated. Statistical analyses revealed a positive relationship in the snow season (i.e., higher moisture leads to warmer temperatures), indicating the dominance of thermal conductivity over evaporative processes, but a negative correlation between the two soil variables in the snow free season (i.e., higher moisture leads to cooler temperatures); see Appendix C for details. While modifying the soil moisture and soil temperature CPTs to reflect these findings, errors were resolved in the soil moisture CPT where soil moisture conditions for certain aspects under low soil water input conditions were swapped. Lastly, a qualitative assessment of the experiments was introduced, where at least 75% (i.e., 9 out of the 12) chance nodes had to respond as expected to the prognosis and diagnosis experiments prior to informing the model with physical observations.

Before testing PermaBN with physical observations, the prognostic and diagnostic synthetic informed case study experiments were repeated with the updated conceptual model. The number of prognostic experiments was increased to 50, and the number of diagnostic experiments was increased to 32 in order to capture additional test cases (Appendix B). Similar to the pre-validation experiments, the trend in the node responses was given higher priority than the magnitude of the response for determining whether the model responds as expected. If the extreme, fully informed prognosis and

diagnosis experiments fail the qualitative validation method, then the nodes, their CPTs, and connections should be closely evaluated prior to informing the model with physical observations.

3.3. Evaluation – Case Study with Physical Observations

Integrating physical observations from a local case study was the final step in the PermaBN development process. The criteria for determining which local case study to use were: (1) high spatiotemporal density of thaw depth observations, and (2) availability of additional variables at the same spatial and temporal scales. One site that meets these criteria is the Siksik Creek Basin in Trail Valley Creek, Northwest Territories, Canada (Figure 3.2) where Wilcox et al. (2019) collected 1528 aspect, vegetation height, and frost table depth (i.e., thaw depth) measurements over the time period 2015-06-11 to 2015-08-20 across 10 transects.

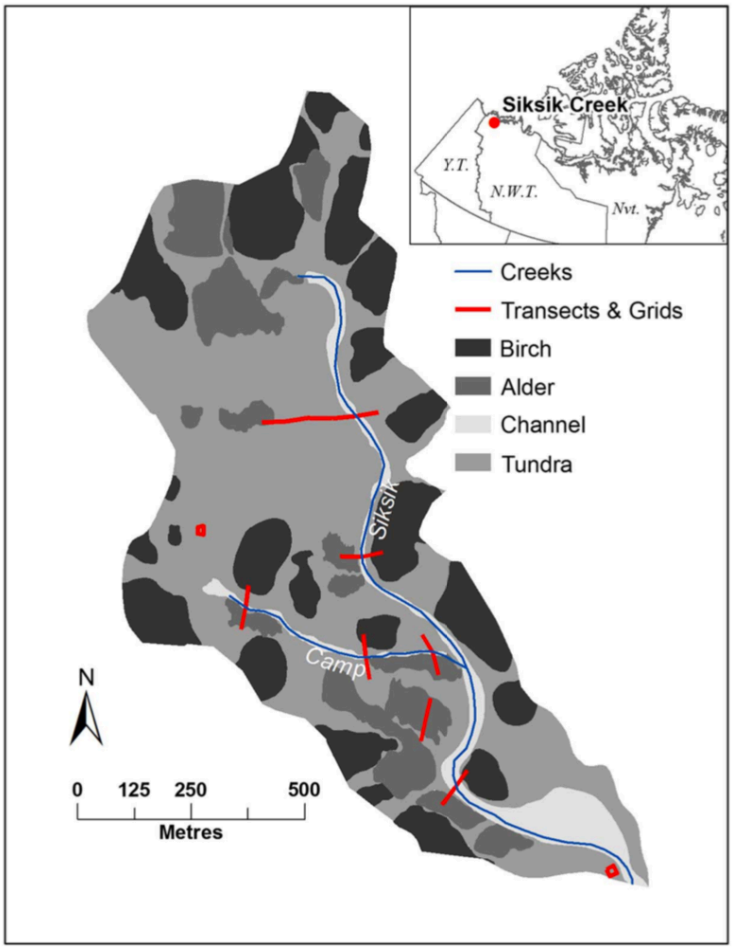

Figure 3.2 Siksik Creek Basin study area detailing the observational transect and grid locations in addition to creek locations and spatial distribution of the vegetation classes. Reprinted from Wilcox et al. (2019).

The general Trail Valley Creek area is described in detail by Wilcox et al. (2019) and Grunberg et al. (2020). In summary, it is located approximately 45 km north of Inuvik (or 80 km south of Tuktoyaktuk) and characterized by an 8-month-long snow cover period. The mean annual air temperature is about -7.9°C to -10°C, and mean annual precipitation is ~266 mm, of which ~66% falls as snow. Vegetation ranges from 0.5 – 3 m in height, with the primary vegetation classes being tundra, birch, alder, and channel. The "tundra" plant community is characterized by low-lying vegetation such as

reindeer lichen (*Cladonia rangiferina* L.), *Sphagnum* moss (*Sphagnum* L.), and tussock and non-tussock sedges (*Carex* L.) that range from 5 – 25 cm in height. As for the "channel" community, it is dominated by alder and willow (*Salix* L.) that range from 150 – 250 cm in height. The "birch" community primarily consists of dwarf birch (*Betula glandulosa* Michx.) ranging from 40 – 60 cm in height, and the "alder" community is comprised of alder (*Alnus alnobetula* (Ehrh.) K. Koch.) ranging from 80 – 150 cm in height. The total thickness of ice-rich permafrost in the region is between 350 – 500 m, with the ALT varying between 0.5 – 0.8 m (Burn and Kokelj, 2009).

Wilcox et al. (2019) took environmental measurements along 10 transects and grids. These transects are several hundred meters apart (Figure 3.2) and observation dates for each sampling campaign range by 2 – 3 days. Therefore, descriptive statistics were calculated for each transect separately (see Appendix D for examples). The probability distribution of thaw depth from each transect was then compared to see which transects could be grouped together for use in PermaBN. Only two transects (ss1 and ss1lys) had similar frost table depth (i.e., thaw depth) probability distributions (Figure 3.3) for the entire June – August 2015 time period; these two transects also had their thaw depth measurements collected on the same days (Julian days 168, 173, 190, 194, 208, 222, and 232). A total of 146 observations were made along transect ss1, whereas 216 observations were made along transect ss1lys. It should be noted that aspect and vegetation height remained constant at this time scale; in other words, frost table depth is the only value to change throughout the study period. It should also be noted that the observations only represent the snow-free season in PermaBN, as observations

were all made during the summer season. Therefore, physical observations that would be used to refine the snow season probabilities are not available.

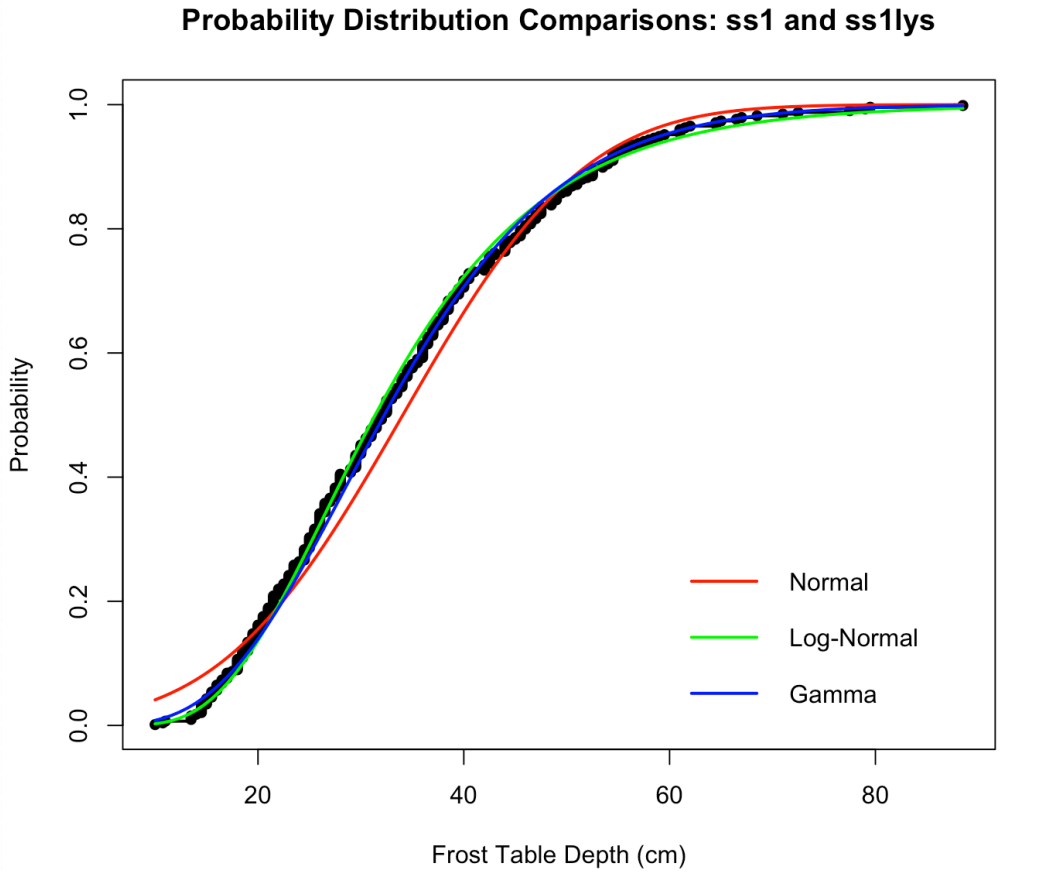

Figure 3.3 Empirical cumulative density function (eCDF) for the combined ss1 and ss1lys transects with best-fit distributions. Best-fits were determined with curve fitting and AIC analysis in the programming language R. At a seasonal (June – August) time scale, both transects exhibit a log-normal distribution (green line), with a gamma distribution (blue line) as the next best fit. A normal distribution (red) line is provided for comparison.

The datasets for aspect and vegetation height were binned for direct use with the model as evidence for the vegetation height node. In the case of aspect, which is a

decision node, observations were simply categorized as north, east, south, or west based on their degree value, where 0° – 45° and 315° – 360° is north, 45° – 135° is east, 135° – 225° is south, and 225° – 315° is west. As for vegetation height, since only three of the four vegetation classes were present in the ss1 and ss1lys transects, "tundra" (5 – 25 cm in height) was considered low, "alder" (80 – 150 cm) was considered medium, and "channel" (150 – 200 cm) was considered high. Probabilities for the vegetation height node were determined by counting how many low, medium, and high vegetation height values coincided with north, east, south, or west aspects, and then dividing by the total number within each aspect state. For example, if 25 of the 29 vegetation observations that were made on eastern aspects were classified as "tundra" (i.e., low vegetation height), then the probability of there being low vegetation on an east aspect is 25/29, or 86%. While air temperature data are not available for the Siksik Creek Basin, I argue that they would not affect vegetation growth enough on this temporal scale (i.e., June – August 2015) to change the vegetation class of a particular observation; likewise, air temperature is not expected to vary substantially along transects. Therefore, the vegetation height probabilities are only dependent on aspect in this stage of the PermaBN model.

Since physical observations are not available for the frost table depth variable's parent nodes of soil moisture, soil temperature, and active layer ice content, the frost table depth measurements could not be used to directly inform the model. Instead, the measurements for both the ss1 and ss1lys transects were binned according to the average Trail Valley Creek ALT range of 50 – 80 cm cited in Wilcox et al. (2019), where low

thaw depth was less than 50 cm, medium thaw depth was between 50 – 80 cm, and high thaw depth was greater than 80 cm; this yielded a distribution of 87% low, 13% medium, and 0% high thaw depths to be used as a benchmark for evaluating the performance of PermaBN. A set of 20 prognosis experiments (Appendix B) testing the effects of aspect/vegetation height, the extreme low and high scenarios, and the most likely Siksik Creek Basin aspect, soil density, air temperature, and soil temperature conditions were conducted to evaluate the ability of PermaBN to match the expected thaw depth distributions. A set of 15 diagnosis experiments (Appendix B) were also defined simply for exploratory purposes, as there is no way to conclusively evaluate the diagnosis performance given the limited parent node evidence available.

4. RESULTS

4.1. Pre-Validation

The pre-validation conceptual model is shown in Figure 4.1. Table 4.1 provides a description of each node and possible states, while Table 4.2 provides a summary of and references for the causal relationships used to build the conceptual model; the CPTs for each node can be found in Appendix A. Arcs appear grey when the corresponding nodes are non-informed and dark blue when the corresponding nodes are informed. A node is considered non-informed when its CPT is set to a uniform distribution. In other words, each state of the node has an equal probability of occurring. Likewise, a node is considered informed when its CPT is not uniform due to the introduction of evidence. In an informative case, each state of a node may have a different probability of occurring.

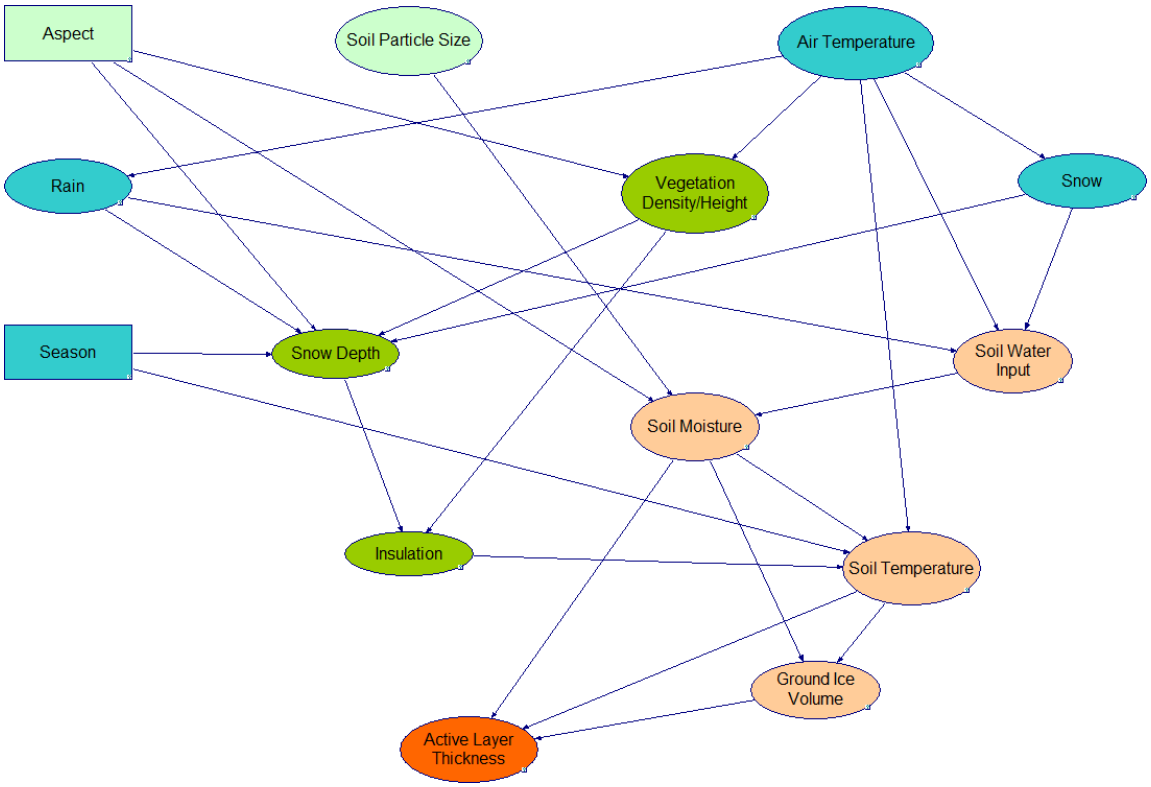

Figure 4.1 Pre-validation conceptual model, which includes 14 nodes, 26 arcs, and 43 states. Geological variables are represented in light green, atmospheric variables in teal, surface insulation variables in dark green, soil variables in light orange, and ALT in dark orange. Decision nodes are represented as boxes; chance nodes are ovals.

Table 4.1 Definition of nodes and associated possible states included in the pre-validation version of PermaBN.

Node	Type	Definition	States
Active Layer Thickness	Chance	The depth/thickness of the layer of ground subject to annual thawing and freezing in areas underlain by permafrost	Low, Medium, High
Air Temperature	Chance	Temperature of the air near the surface of the Earth based on 2081-2100 RCP future warming projections	RCP 2.6, RCP 4.5, RCP 8.5
Aspect	Decision	The arrangement of the natural and artificial physical features of an area, or more particularly, the aspect, or positioning of a feature in a specified direction	North, East, South, West
Ground Ice Volume	Chance	Volume of all types of ice contained in freezing and frozen ground, which includes bedrock, sediment, organic matter, and water	Low, Medium, High
Insulation	Chance	The state of something being insulated, or protection of something by interposing material that prevents the loss of heat	Low, Medium, High
Rain	Chance	Moisture condensed from the atmosphere that falls visibly in separate drops	Low, Medium, High
Season	Decision	Division of the year marked by the presence or absence of snow	Snow Free, Snow
Snow	Chance	Atmospheric water vapor frozen into ice crystals and falling in light white flakes or lying on the ground as a white layer	Low, Medium, High
Snow Depth	Chance	Measurement of snow that has fallen during previous weather events	Low, Medium, High
Soil Moisture	Chance	Water that is held in the pore spaces between soil particles	Low, Medium, High
Soil Particle Size	Chance	Composition of mineral soil by relative soil particle size	Clay, Silt, Sand
Soil Temperature	Chance	Measurement of the warmth of the soil	Low, Medium, High
Soil Water Input	Chance	The ratio of precipitation to evaporation	Low, Medium, High
Vegetation Density/Height	Chance	Percentage of soil which is covered by green vegetation, or height of the dominant vegetation classes	Low, Medium, High

Table 4.2 List of causal relationships (i.e., arcs) in the pre-validation version of PermaBN with select references. Refer to Section 2.1 for additional references.

Parent Node	Child Node	Reference
Air Temperature	Rain	Bintanja and Andry (2017)
	Snow	Bintanja and Andry (2017)
	Soil Temperature	Park et al. (2014)
	Soil Water Input	Young et al. (1997)
	Vegetation Height/Density	Myers-Smith et al. (2020)
Aspect	Snow Depth	Evans et al. (1989)
	Soil Moisture	Young et al. (1997)
	Vegetation Height/Density	Evans et al. (1989)
Ground Ice Volume	Active Layer Thickness	Schuur and Mack (2018)
Insulation	Soil Temperature	Zhang et al. (2018)
Rain	Snow Depth	Screen and Simmonds (2012)
	Soil Water Input	Rouse et al. (1997)
Season	Snow Depth	N/A – node used to control CPT
	Soil Temperature	N/A – node used to control CPT
Snow	Snow Depth	Bintanja and Andry (2017)
	Soil Water Input	Rouse et al. (1997)
Snow Depth	Insulation	Zhang et al. (2018)
Soil Moisture	Active Layer Thickness	Lee et al. (2014)
	Ground Ice Volume	O'Neill and Burn (2012)
	Soil Temperature	Frauenfeld et al. (2004)
Soil Particle Size	Soil Moisture	Abu-Hamdeh and Reeder (2000)
Soil Temperature	Active Layer Thickness	Frauenfeld et al. (2004)
	Ground Ice Volume	Jorgenson et al. (2015)
Soil Water Input	Soil Moisture	N/A – aggregate node
Vegetation Density/Height	Insulation	Lawrence and Swenson (2011)
	Snow Depth	Wilcox et al. (2019)

A total of 46 prognosis experiments (Appendix B) were conducted in the pre-validation stage to assess the response of the model to the introduction of evidence. Experiments started with a completely non-informed model and gradually incorporated evidence, starting with the parent nodes until the model was completely informed. In every experiment, both of the decision nodes (i.e., aspect and season) and one or both of the chance parent nodes (i.e., soil particle size and air temperature) were set to a state. State combinations were meant to reflect scenarios where changes in ALT (i.e., thaw depth) were expected to be low or high. In the following paragraphs, some of the key prognosis runs are presented.

In the completely non-informed, or uniform, model run, changing the states of any of the nodes did not result in a change in any of the other nodes (Figure 4.2). This is an illustration of the Bayesian principle of Markov conditions. The principle states that a node does not influence nodes that do not descend from it. Another way of stating this is that each node relies on what its prior nodes know. This principle is also illustrated in the experiments where only the four parent nodes are informed and, in many of the experiments, where only the uppermost children nodes are informed. For example, when only the air temperature and rain nodes are informed, rain will respond to changes in air temperature, but any children of rain will not exhibit any responses.

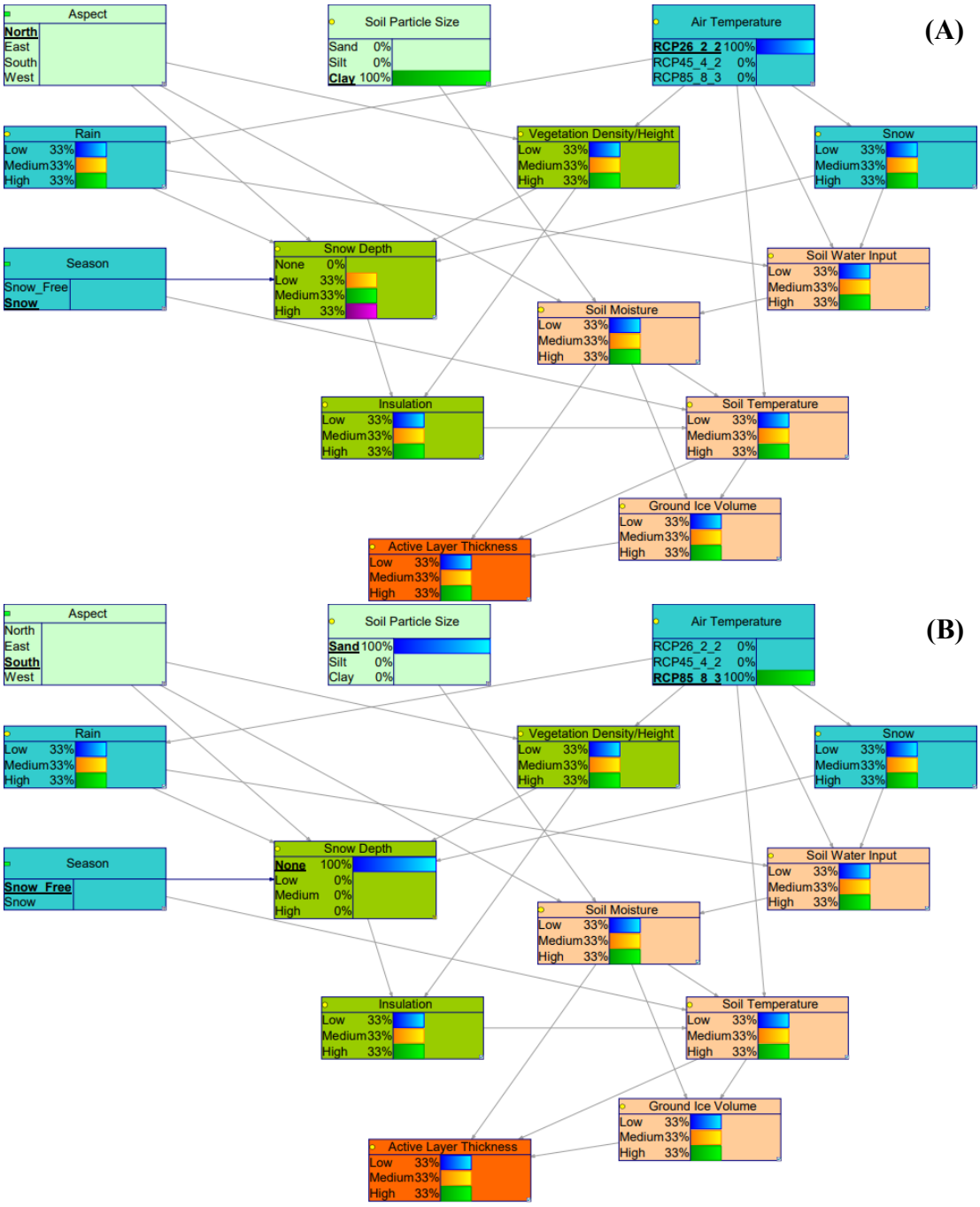

Figure 4.2 Non-informative prognosis experiments using the (A) extreme low (i.e., north aspect, clay soil particle size, RCP 2.6 scenario for air temperature, and snow season) and (B) extreme high (i.e., south aspect, sand soil particle size, RCP 8.5 scenario for air temperature, and snow free season) scenarios.

Similarly, if every node is informed except for ALT, the ALT node will not respond to changes in the parent nodes until it has been informed (Figure 4.3). That said, it is possible for children nodes to respond if the child node and one or more of its prior nodes are informed. For instance, if the air and soil temperature nodes are informed, soil temperature will respond to changes in air temperature. However, if the insulation node is informed, it will still show a uniform conditional distribution since its parent nodes of vegetation density/height and snow depth are not informed. Thus, insulation will not affect soil temperature.

Increasing the number of informed nodes decreases the uncertainty in thaw depth (i.e., ALT) predictions. Uncertainties in the model and the system are expressed through the distribution of probabilities assigned to each node state, and the uncertainties are propagated through the network to the final model endpoint (Chen and Pollino, 2012). In the experiments where all nodes except for soil temperature and snow depth were informed, ALT responded very little to changes in the primary parent nodes (Figure 4.4).

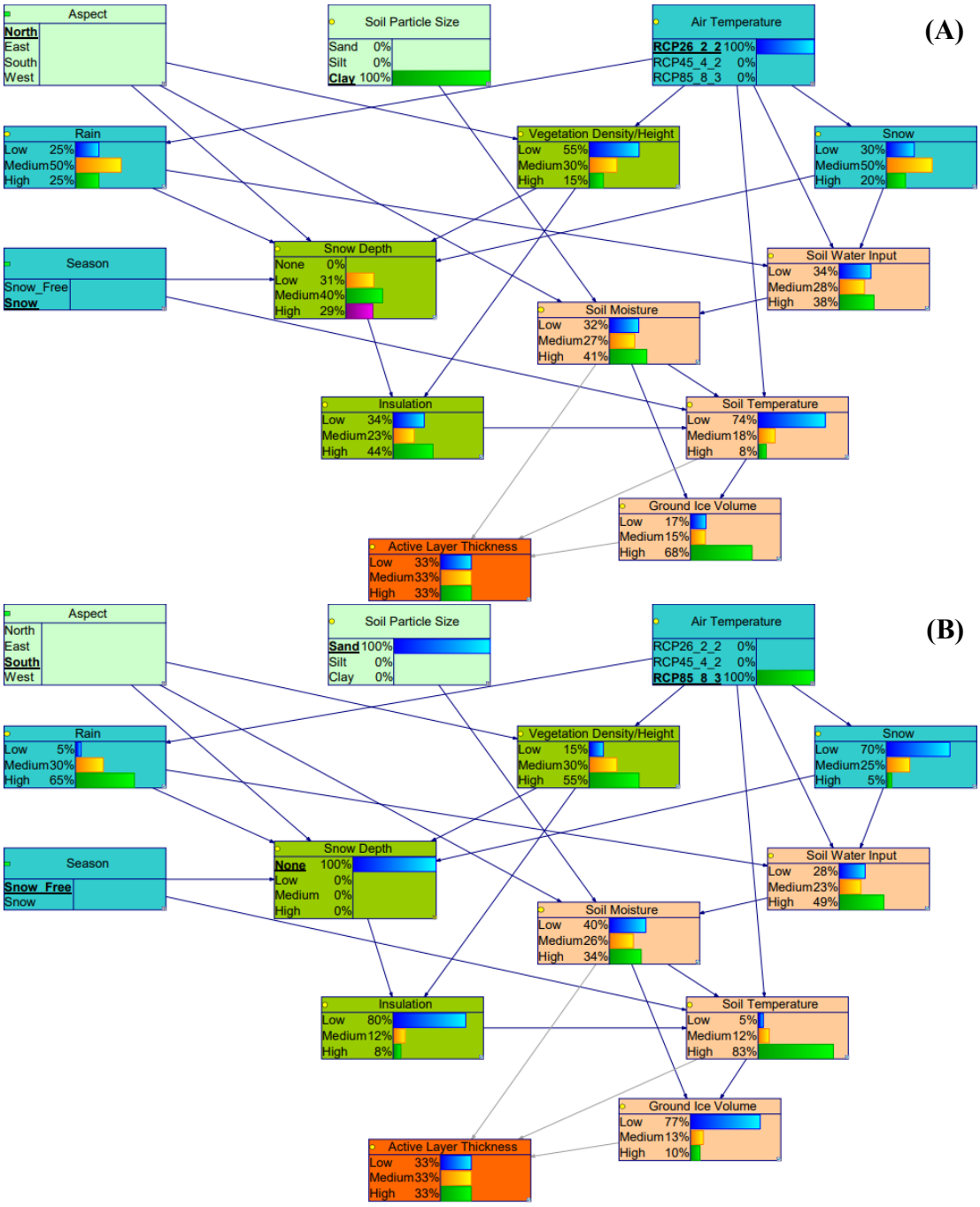

Figure 4.3 Prognosis experiments where every node except ALT is informed using the (A) extreme low (i.e., north aspect, clay soil particle size, RCP 2.6 scenario for air temperature, and snow season) and (B) extreme high (i.e., south aspect, sand soil particle size, RCP 8.5 scenario for air temperature, and snow free season) scenarios.

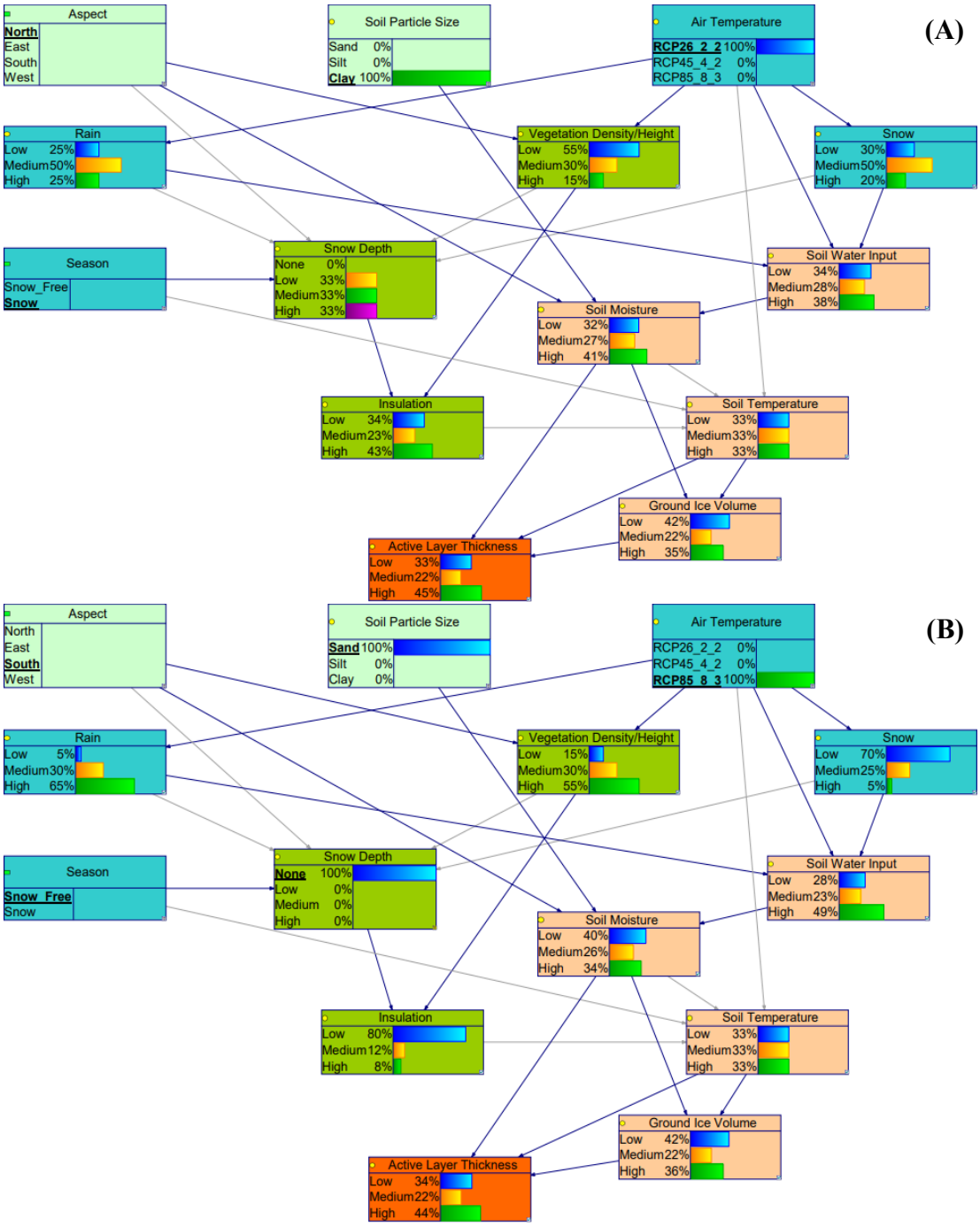

Figure 4.4 Prognosis experiments where every node except snow depth and soil temperature are informed using the (A) extreme low (i.e., north aspect, clay soil particle size, RCP 2.6 scenario for air temperature, and snow season) and (B) extreme high (i.e., south aspect, sand soil particle size, RCP 8.5 scenario for air temperature, and snow free season) scenarios.

However, when soil temperature and snow depth were informed, ALT responded as expected to the low and high scenarios of the parent nodes. Figure 4.5 shows the prognosis results for the low and high "extreme" scenarios of changes in ALT. In the case where aspect was set to north, soil particle size to clay, air temperature to the RCP 2.6 scenario, and season to snow, there was a high probability that ALT would be in a low state. This indicates a high probability that permafrost thaw would be low in scenarios promoting cooler temperatures and increased soil moisture. Similarly, in the case where aspect was set to south, soil particle size to sand, air temperature to the RCP 8.5 scenario, and the season to snow-free, there was a high probability that ALT would be in a high state. This indicated a high probability that permafrost thaw would be high in scenarios promoting warmer temperatures and decreased soil moisture. While the model responds as expected at this stage in the context of trends (e.g., cooler temperatures promote less thaw while warmer temperatures promote more thaw), further adjustments of the CPTs, especially for snow depth, vegetation height/density, insulation, and soil moisture, are needed for the magnitudes of the probabilities to reflect reality.

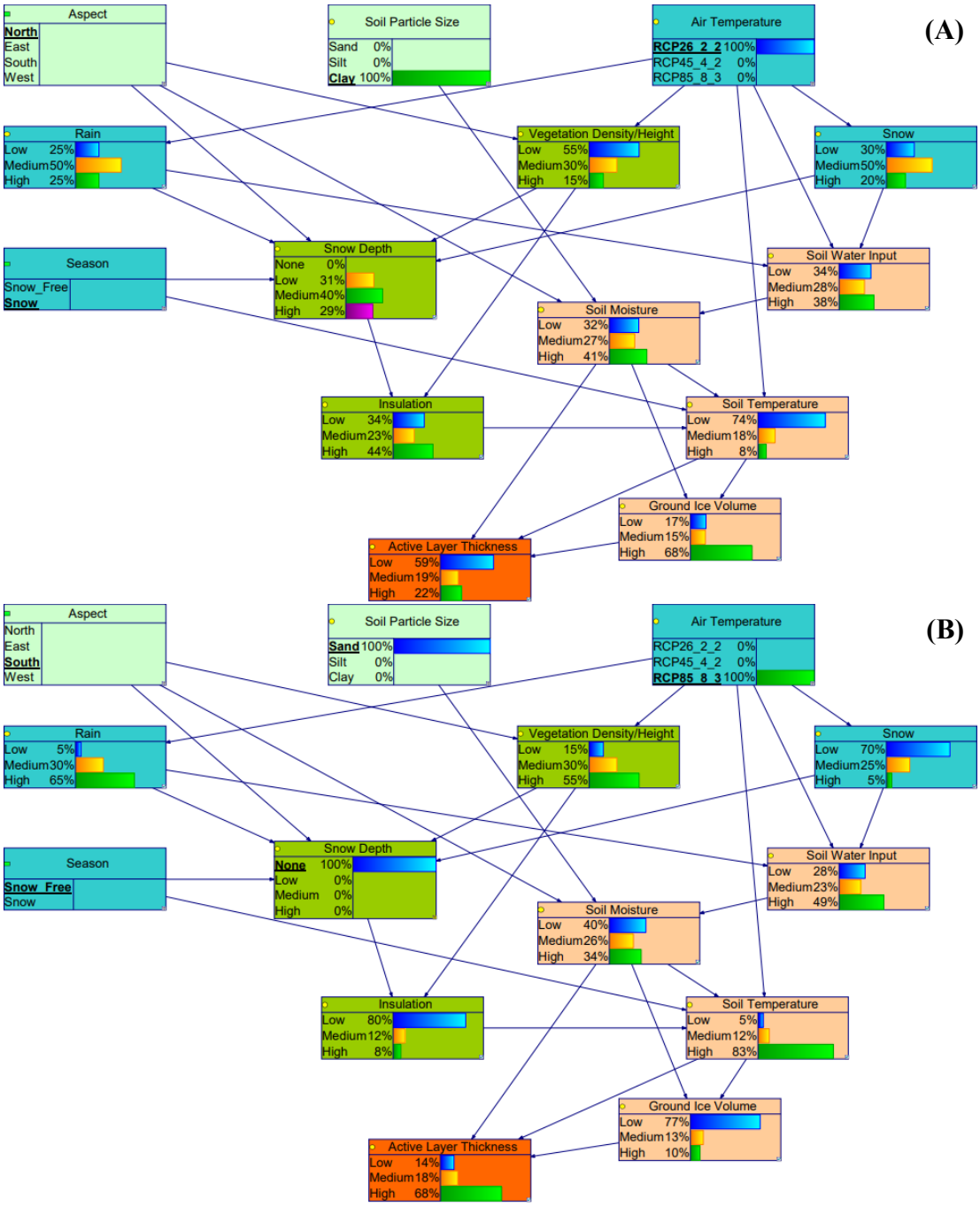

Figure 4.5 Prognosis experiments where all nodes are informed using the (A) extreme low (i.e., north aspect, clay soil particle size, RCP 2.6 scenario for air temperature, and snow season) and (B) extreme high (i.e., south aspect, sand soil particle size, RCP 8.5 scenario for air temperature, and snow free season) scenarios.

Next, 13 diagnosis experiments (Appendix B) were conducted in the pre-validation stage to assess the response of the model to changes in ALT. Experiments started with simply setting ALT (i.e., the response of the system) to low, medium, and high. Then, different combinations of aspect, season, and ALT were used to further assess the model response. Key diagnosis runs are described in the following paragraphs.

Overall, the system responds as expected. When changes to thaw depth (i.e., ALT) are low, ground ice volume and soil moisture are high while soil temperature is low (Figure 4.6). Conversely, when changes to ALT are high, ground ice volume and soil moisture are low while soil temperature is high (Figure 4.7).

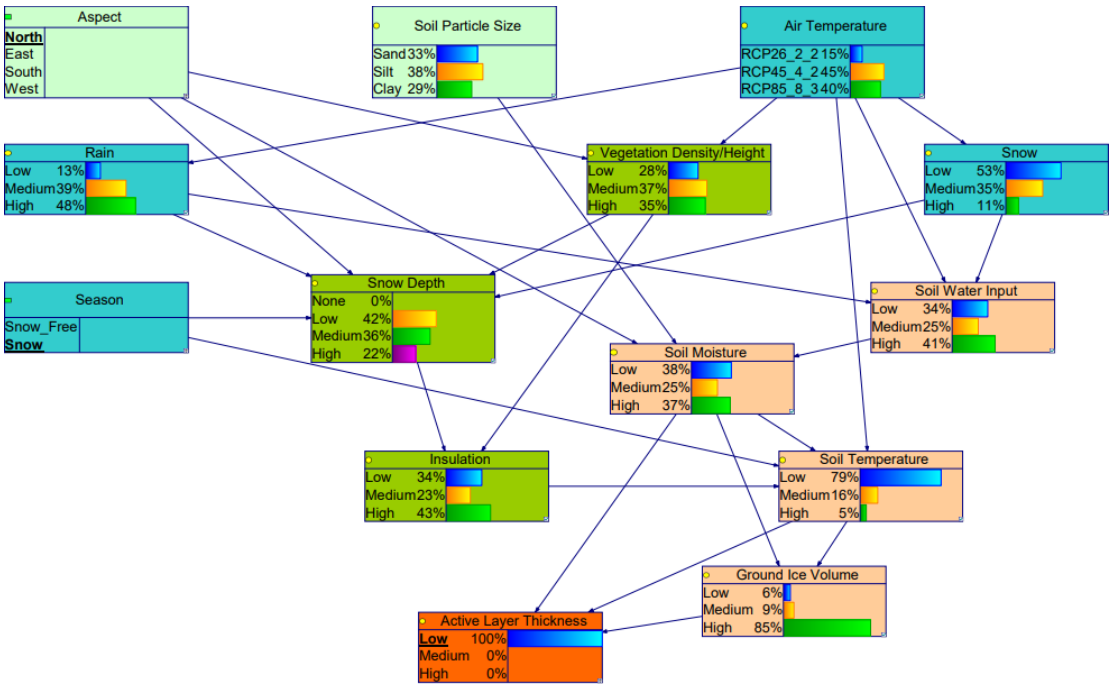

Figure 4.6 Diagnosis experiment testing the extreme low scenario where the response of the system (i.e., ALT) is low, aspect is north, and season is snow.

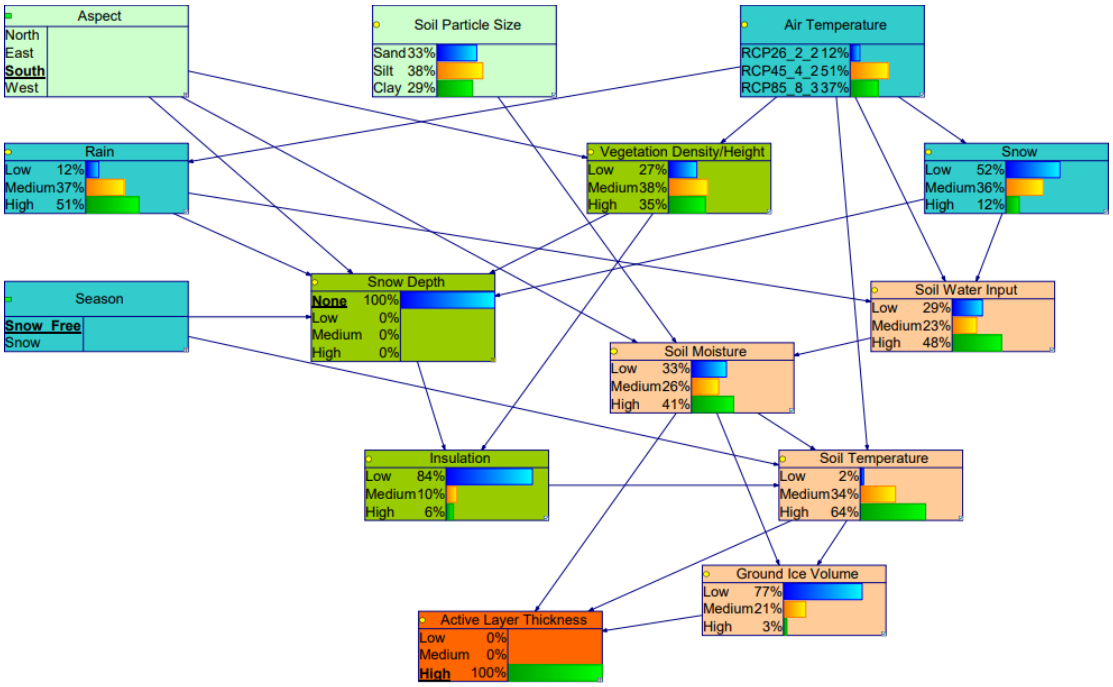

Figure 4.7 Diagnosis experiment testing the extreme high scenario where the response of the system (i.e., ALT) is high, aspect is south, and season is snow free.

Even though the probability distributions for high changes to ALT are more uniform than in the low case, the general trend upholds. However, in both cases, air temperature is predicted to fall within the RCP 4.5 scenario. While it is unsurprising that the RCP 4.5 scenario is considered the most likely air temperature scenario to occur given the air temperature CPT, higher probabilities for the RCP 2.6 and 8.5 were expected for the low and high ALT scenarios respectively. Air temperature appears to respond better when the node is set to a uniform distribution (Figure 4.8). This indicates that CPTs in the middle nodes of the model may need further refinement. Additional testing revealed that soil temperature and snow depth seem to be driving many of the responses in the model. Improving these distributions may improve the model response as a whole.

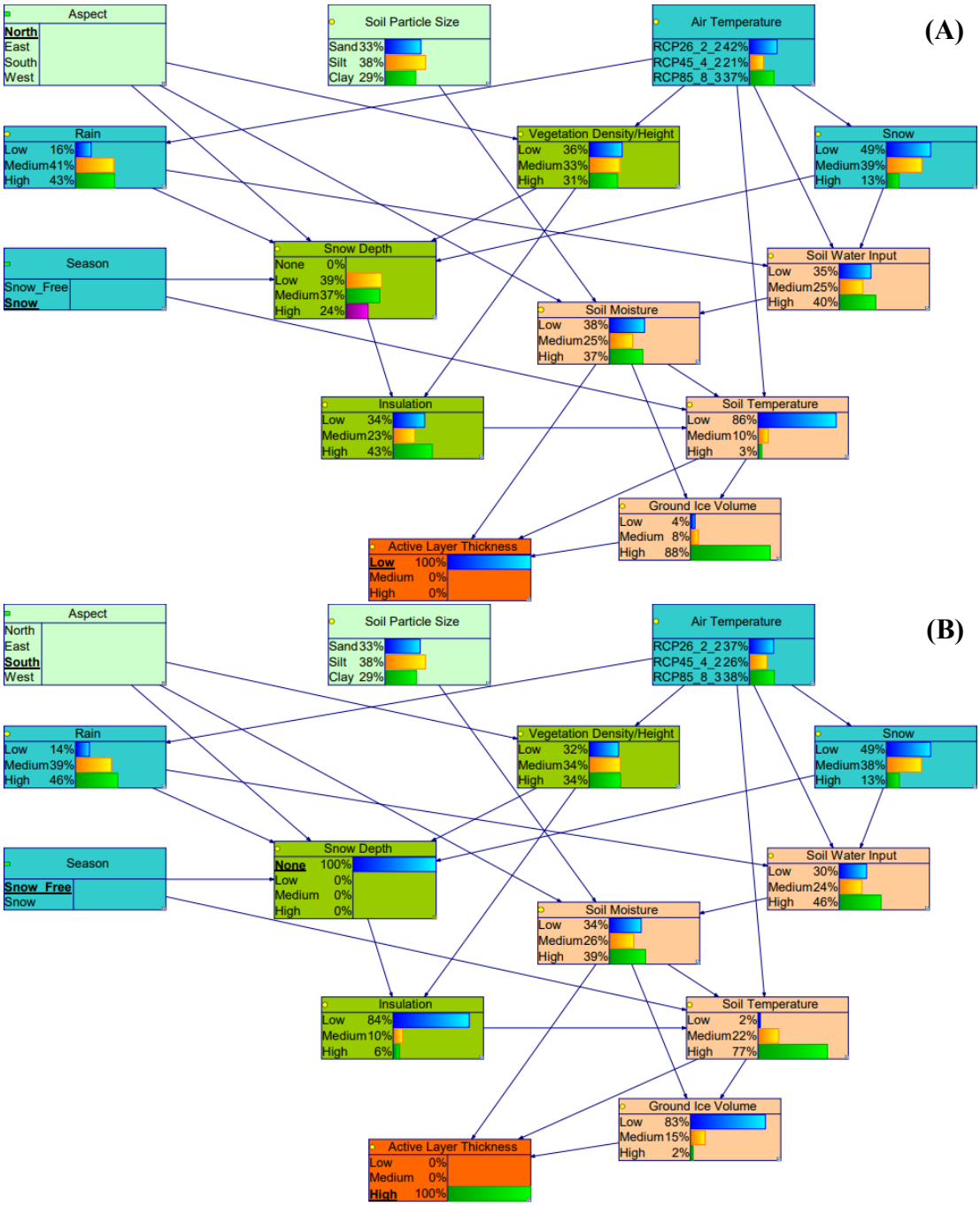

Figure 4.8 Diagnosis experiment testing air temperature with a uniform distribution for the (A) extreme low scenario where the response of the system (i.e., ALT) is low, aspect is north, and the season is snow and (B) extreme high scenario where the response of the system (i.e., ALT) is high, aspect is south, and season is snow free.

4.2. Validation – Expert Assessment

An updated version of the PermaBN conceptual model using the feedback from the experts is seen in Figure 4.9. Key changes to the pre-validation conceptual model include: (1) re-characterizing the "soil particle size" node into "soil density," (2) adding an additional arc from "soil density" to "insulation," (3) renaming the "vegetation density/height" node to "vegetation height," (4) renaming the "ground ice volume" node to "active layer ice content", (5) renaming the "active layer thickness" node to "thaw depth," (6) redefining the air temperature state names, and (7) reorganizing the graphical structure of the model.

Figure 4.9 PermaBN conceptual model after validation via expert assessment. In comparison to the pre-validation conceptual model, several nodes have been renamed, and an additional causal relationship has been added. There are now 27 arcs connecting the 14 nodes.

In the pre-validation conceptual model, "soil particle size" only accounted for the mineral soil states of sand, silt, or clay and their respective moisture retention properties. With the revised "soil density" definition and additional arc to "insulation," the effects of soil organic content on moisture retention, thermal conductivity, and insulation can be accounted for. The vegetation node was renamed to "vegetation height" in order to reflect the variable that is more often reported in physical observation datasets or in the literature, while the renaming of ground ice volume to "active layer ice content" better

reflects the assumption of ground ice limited to the upper layer of the soil column. Finally, renaming the endpoint node to “thaw depth” allows for a more accurate interpretation of the node in the context of seasonal dynamics represented in the model. Redefining the air temperature from using three RCP scenarios (2.6, 4.5, and 8.5) to only low, medium, and high was done to enhance the consistency of terminology in the model as well as to generalize the node for use with physical observations. Finally, the graphical structure of the nodes and arcs was re-organized to emphasize the cause-effect nature of the model. For instance, it is now easier to see the distinct tiers (parents at the top, intermediate children in the middle, and the response of the system at the bottom) in the model. It should be noted, however, that even though thaw depth is in the seventh row of the model, it is only a minimum of two or three arcs away from any of the parent nodes. Table 4.3 provides a revised description of each node and possible states; as there is only one additional arc (i.e., soil density to insulation from Abu-Hamdeh and Reeder (2000)) in the expert assessment validation model, an updated table for the causal relationships is not provided.

Table 4.3 Definition of nodes and associated possible states included in the expert assessment validation version of PermaBN. Changes from the pre-validation version are bolded.

Node	Type	Definition	States
Thaw Depth	Chance	**The depth/thickness of the layer of ground subject to annual thawing and freezing in areas underlain by permafrost**	Low, Medium, High
Air Temperature	Chance	**Temperature of the air near the surface of the Earth**	**Low, Medium, High**
Aspect	Decision	The arrangement of the natural and artificial physical features of an area, or more particularly, the aspect, or positioning of a feature in a specified direction	North, East, South, West
Active Layer Ice Content	Chance	**Volume of all types of ice contained in the upper portion of the soil column that is subject to annual thawing and freezing**	Low, Medium, High
Insulation	Chance	The state of something being insulated, or protection of something by interposing material that prevents the loss of heat	Low, Medium, High
Rain	Chance	Moisture condensed from the atmosphere that falls visibly in separate drops	Low, Medium, High
Season	Decision	Division of the year marked by the presence or absence of snow	Snow Free, Snow
Snow	Chance	Atmospheric water vapor frozen into ice crystals and falling in light white flakes or lying on the ground as a white layer	Low, Medium, High
Snow Depth	Chance	Measurement of snow that has fallen during previous weather events	Low, Medium, High
Soil Moisture	Chance	Water that is held in the pore spaces between soil particles	Low, Medium, High
Soil Density	Chance	**Organic and mineral composition of soil per the measure of the amount of dry solid particles per unit volume**	**Low, Medium, High**
Soil Temperature	Chance	Measurement of the warmth of the soil	Low, Medium, High
Soil Water Input	Chance	The ratio of precipitation to evaporation	Low, Medium, High
Vegetation Height	Chance	**Height of the dominant vegetation classes**	Low, Medium, High

CPTs for the conceptual model in Figure 4.9 are the same as those for the pre-validation conceptual model, with the exception of: (1) the revised CPT for insulation to accommodate its relationship with soil density, (2) the revised CPT for soil moisture to

reflect the re-characterization of soil particle size to soil density and a few updates to the relationships, and (3) modification to the CPT for soil temperature based on additional analysis into the annual and seasonal trends between soil moisture and soil temperature at two continuous permafrost sites in addition to better definition of the cases given medium air temperature (Appendix A). Values were updated in the insulation CPT to accommodate the new arc with soil density. In this revised table, insulation is low when vegetation height is low, snow depth is low, and soil density is high (i.e., has a low soil organic content); insulation is high when vegetation height and snow depth are high and soil density is low (i.e., has a high soil organic content). Also, to reflect the modified soil density node, low and high values in the CPT for soil moisture were flipped such that the soil particle size state of "sand" was redefined as "high" soil density and the soil particle size state of "clay" was redefined as "low" soil density. Additional updates in the soil moisture and soil temperature CPTs were made: (1) north aspects now contribute to higher rather than lower soil moisture under low soil water input conditions, and (2) soil temperature is now low when there is low air temperature, high insulation, and high soil moisture in the snow free season, and low when there is low air temperature, low insulation, and low soil moisture in the snow season.

A total of 50 prognosis experiments (Appendix B) were conducted in the expert assessment validation stage to assess the response of the model to the introduction of evidence. These 50 experiments reflect the 46 pre-validation prognosis experiments that start with a completely non-informed model and gradually incorporate evidence, with the addition of 4 experiments that test thaw depth as the only informed variable at

extreme low/high conditions and setting only the decision nodes to extreme low/high conditions when every variable is informed. The following paragraphs describe the key expert assessment validation experiments.

As with the pre-validation experiments, the Bayesian principle of Markov conditions is illustrated in the non-informed, or uniform, experiments, and increasing the number of informed nodes decreases the uncertainty in thaw depth predictions. Since the changes made to the conceptual model in response to the expert assessment validation were largely related to terminology, results are similar to those of the pre-validation prognosis experiments. Key differences include the modification of the soil moisture and soil temperature CPTs to reflect a positive correlation in the snow season and negative correlation in the snow free season and re-interpretation of the soil density and air temperature states. Results from the additional experiments show that informing only the endpoint node (i.e., thaw depth) results in a fairly uniform distribution that is slightly skewed towards high thaw depth in both the extreme low and high scenarios (Figure 4.10) and that only setting the decision parent nodes to the low and high scenarios results in distinctly low and high thaw depth, respectively (Figure 4.11).

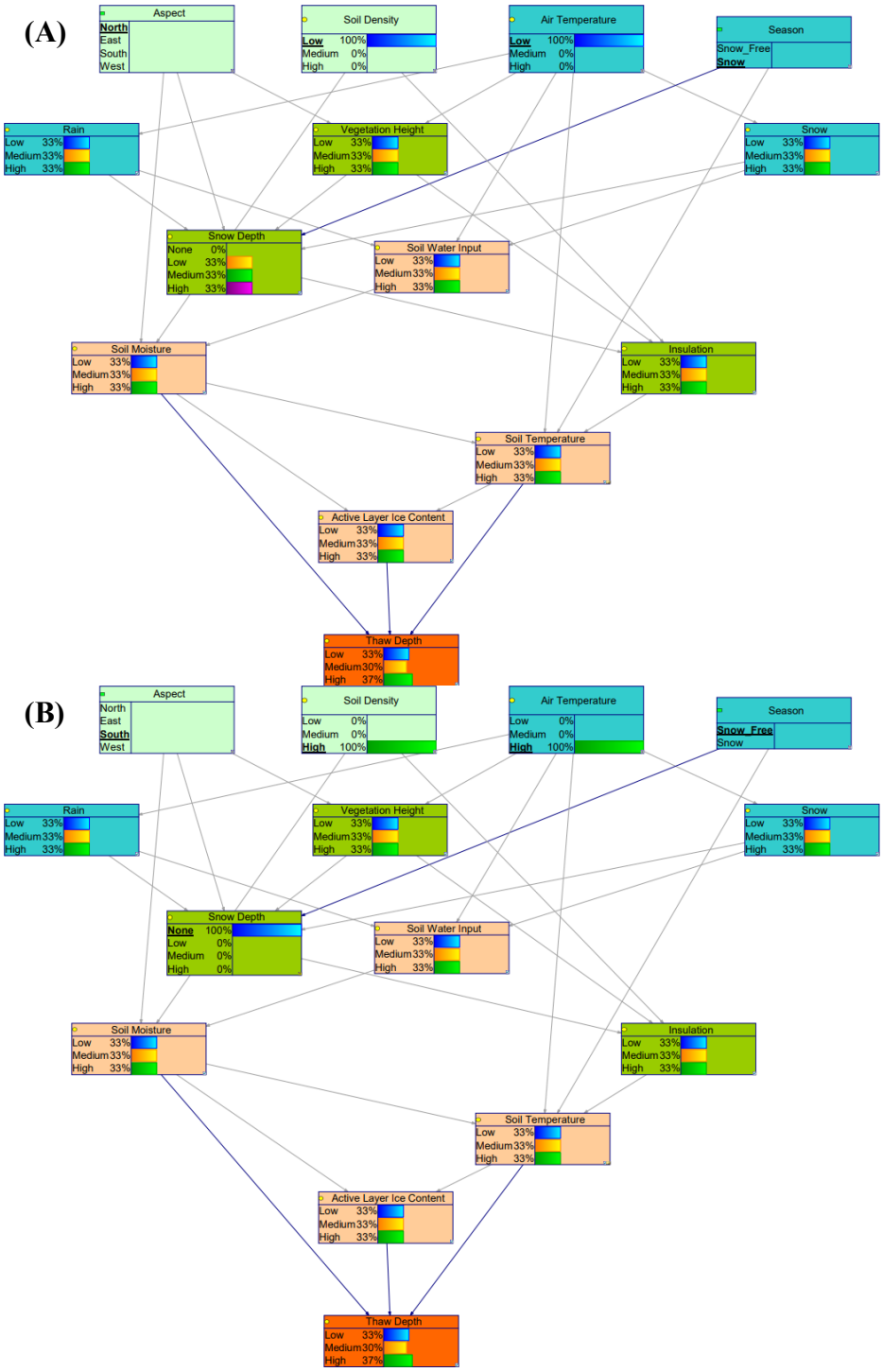

Figure 4.10 Prognosis experiments where thaw depth is the only informed node for the (A) extreme low (i.e., north aspect, low soil density, low air temperature, and snow season) and (B) extreme high (i.e., south aspect, high soil density, high air temperature, and snow free season) scenarios.

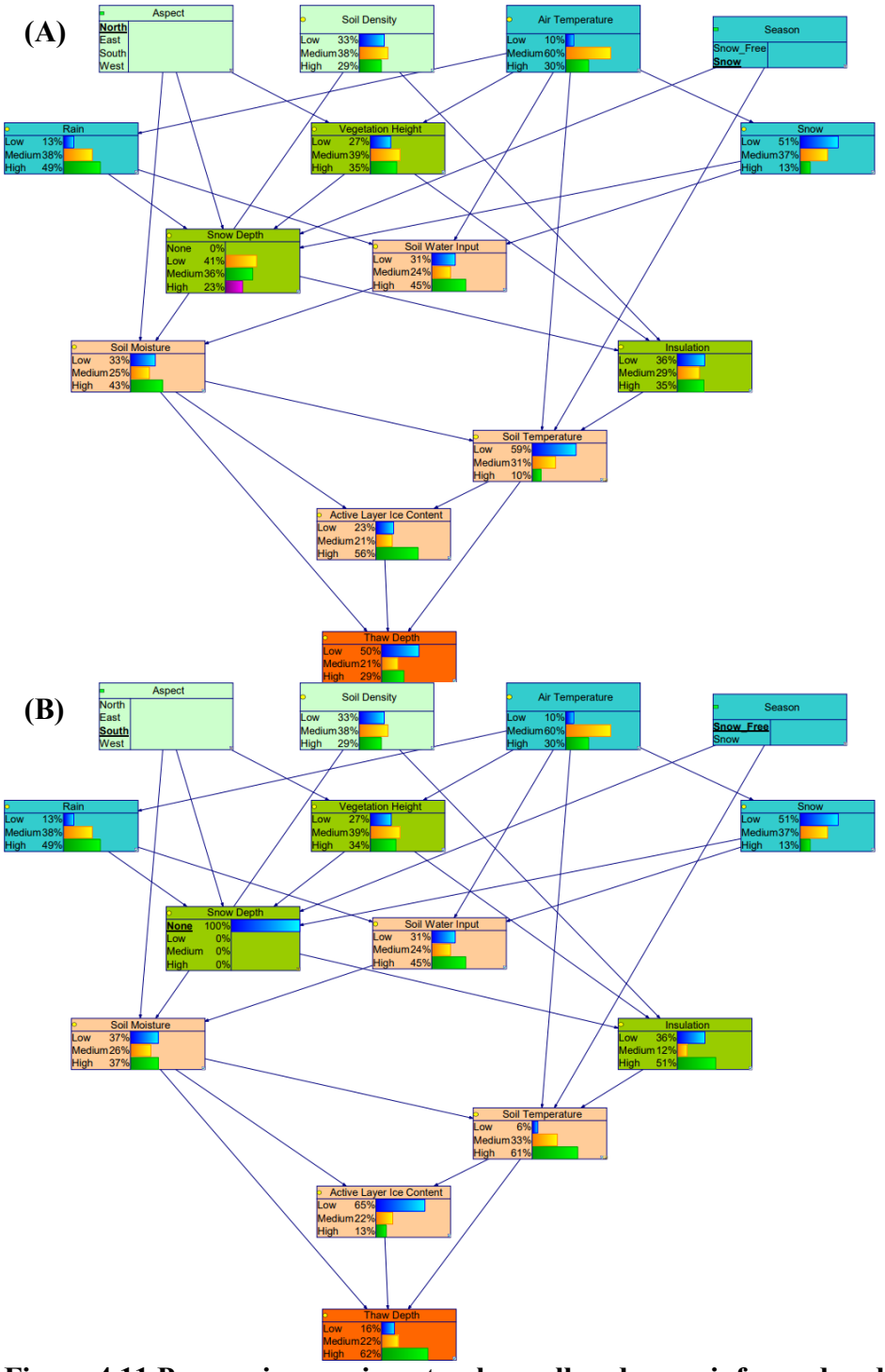

Figure 4.11 Prognosis experiments where all nodes are informed and only the decision parent nodes are set to (A) north aspect and snow season and (B) south aspect and snow free season.

Setting soil density and air temperature to their respective low and high states further increases the magnitude of these expected trends (Figure 4.12). Flipping the season of each extreme scenario (i.e., snow free instead of snow season for the north aspect, low soil density, and low air temperature scenario and vice versa) also responds as expected by having a lower percentage of high thaw in the north/snow free scenario as compared to the south/snow free scenario, and a lower percentage of low thaw in the south/snow scenario as compared to the north/snow scenario (Figure 4.13).

As with the pre-validation prognosis experiments, results show high probability that permafrost thaw would be low in scenarios promoting cooler temperatures and increased soil moisture and high in scenarios promoting warmer temperatures and decreased soil moisture. The results also indicate that even further adjustments of the CPTs are needed for the magnitudes of the probabilities to reflect reality.

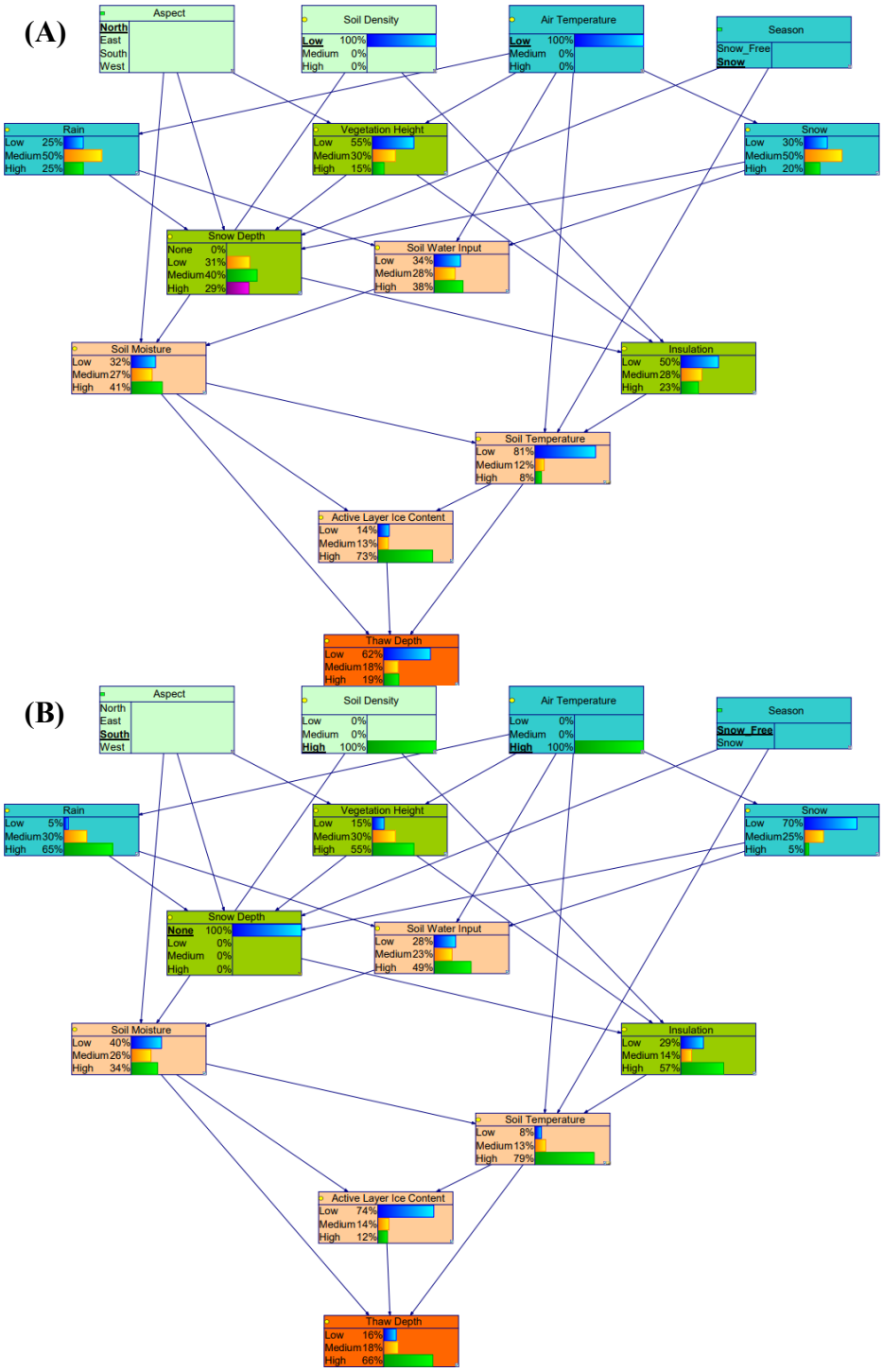

Figure 4.12 Prognosis experiments where all nodes are informed and all parents are set to the (A) extreme low (i.e., north aspect, low soil density, low air temperature, and snow season) and (B) extreme high (i.e., south aspect, high soil density, high air temperature, and snow free season) scenarios.

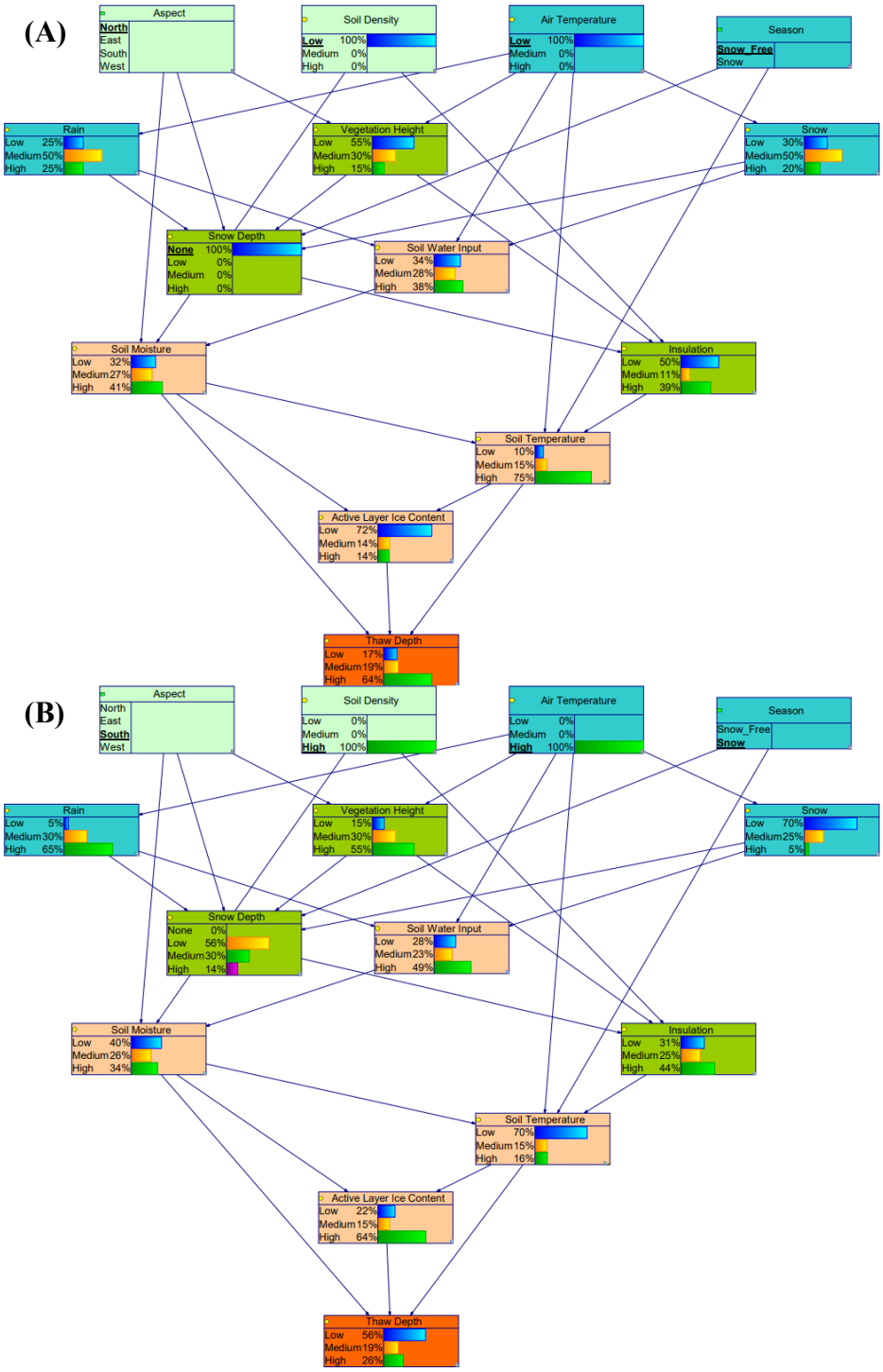

Figure 4.13 Prognosis experiments where all nodes are informed and all parents are set to the (A) extreme low (i.e., north aspect, low soil density, and low air temperature) with (opposite) snow free season and (B) extreme high (i.e., south aspect, high soil density, and high air temperature) with (opposite) snow season scenarios.

Next, 32 diagnosis experiments (Appendix B) were conducted in the expert assessment validation stage to assess the response of the model to changes in ALT. These 32 diagnosis experiments reflect the 13 pre-validation prognosis experiments while greatly expanding the initial experiments to include more robust testing of differing seasons and the effects of only informing the endpoint node. The key diagnosis experiment results are described in the following paragraphs.

The first set of experiments tested various combinations of north aspect during the snow season at low, medium, and high thaw depth, with thaw depth as the only informed node; the opposite combination (south aspect during the snow free season) was also tested (Figure 4.14). In each case, soil moisture, soil temperature, and ground ice volume nodes reflected non-uniform probabilities. Soil temperatures are lower for low thaw depths and higher for high thaw depths; conversely, ground ice volumes are higher for low thaw depths and lower for high thaw depths. In the all-informative cases, there is still a strong favoring of medium or high air temperature, regardless of aspect, season, or thaw depth state. Soil temperature and ground ice volume distributions are as expected (i.e., low soil temperature and high ground ice volume for low thaw depth and vice versa) with fairly uniform soil moisture distributions in each case.

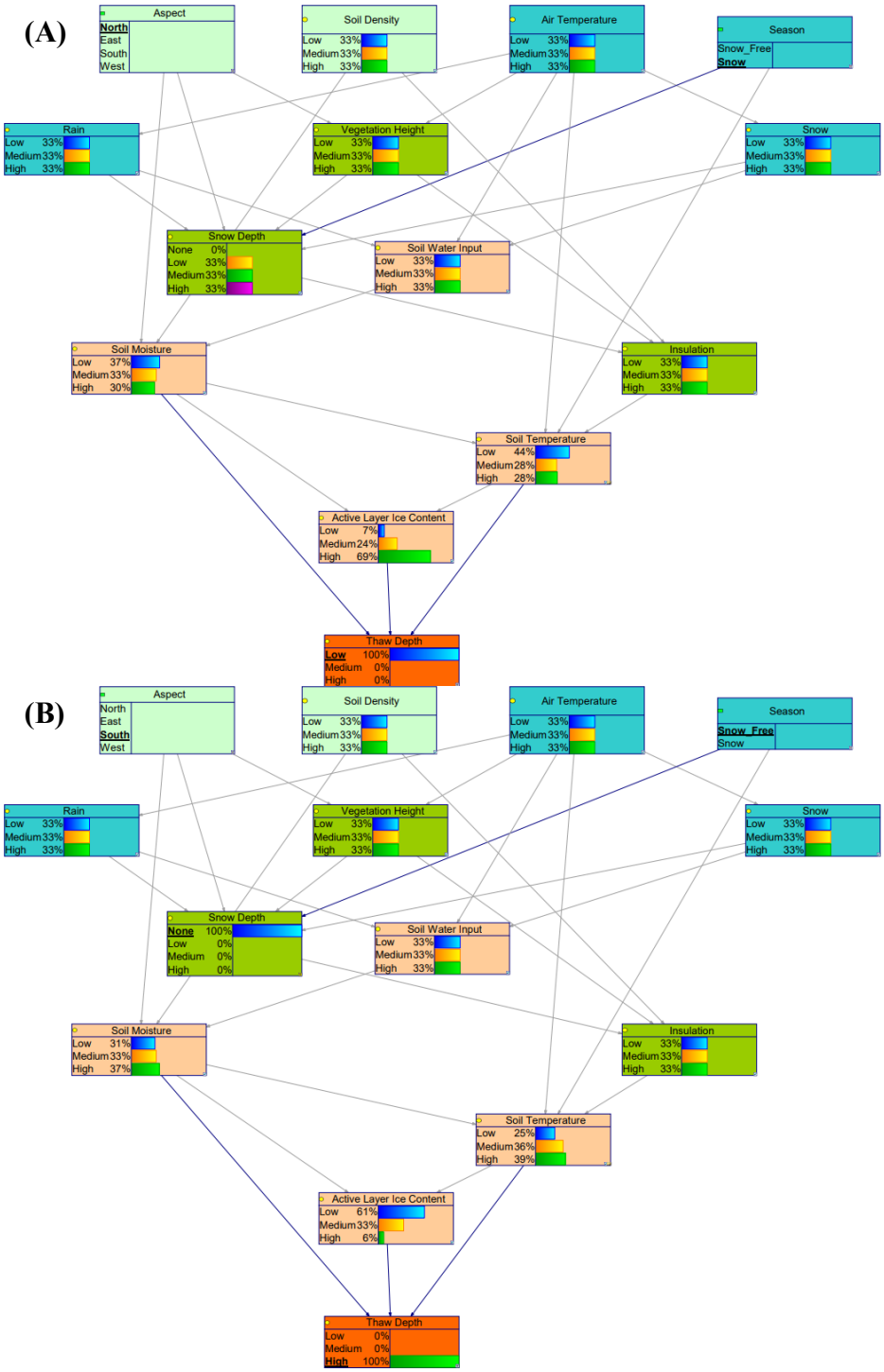

Figure 4.14 Diagnosis experiments with thaw depth as the only informed node for (A) low thaw depth, north aspect, and snow season and (B) high thaw depth, south aspect, and snow free season.

Experiments setting air temperature to a uniform distribution (Figures 4.15 and 4.16) show that air temperature is skewed slightly lower for low thaw depth and still favor a medium state for high thaw depth in the north aspect/snow season scenario. A slightly higher probability for low air temperature under low thaw depth conditions is also seen for the south aspect/snow free season scenario, though the same scenario yielded almost equal probabilities for low and high air temperature under high thaw depth.

Experiments setting the state of soil temperature to low (or high) under the various aspect, season, and thaw depth scenarios (Figure 4.17) show that soil moisture and insulation probabilities are appropriately higher in the snow season for both low and high soil temperatures while soil moisture is lower for high soil temperatures and higher for low soil temperatures in the snow free season. Insulation is high in the snow free, low soil temperature, low thaw depth scenario and low in the snow free, high soil temperature, low thaw depth scenario, but in the corresponding high thaw depth scenarios, insulation is split between low and high.

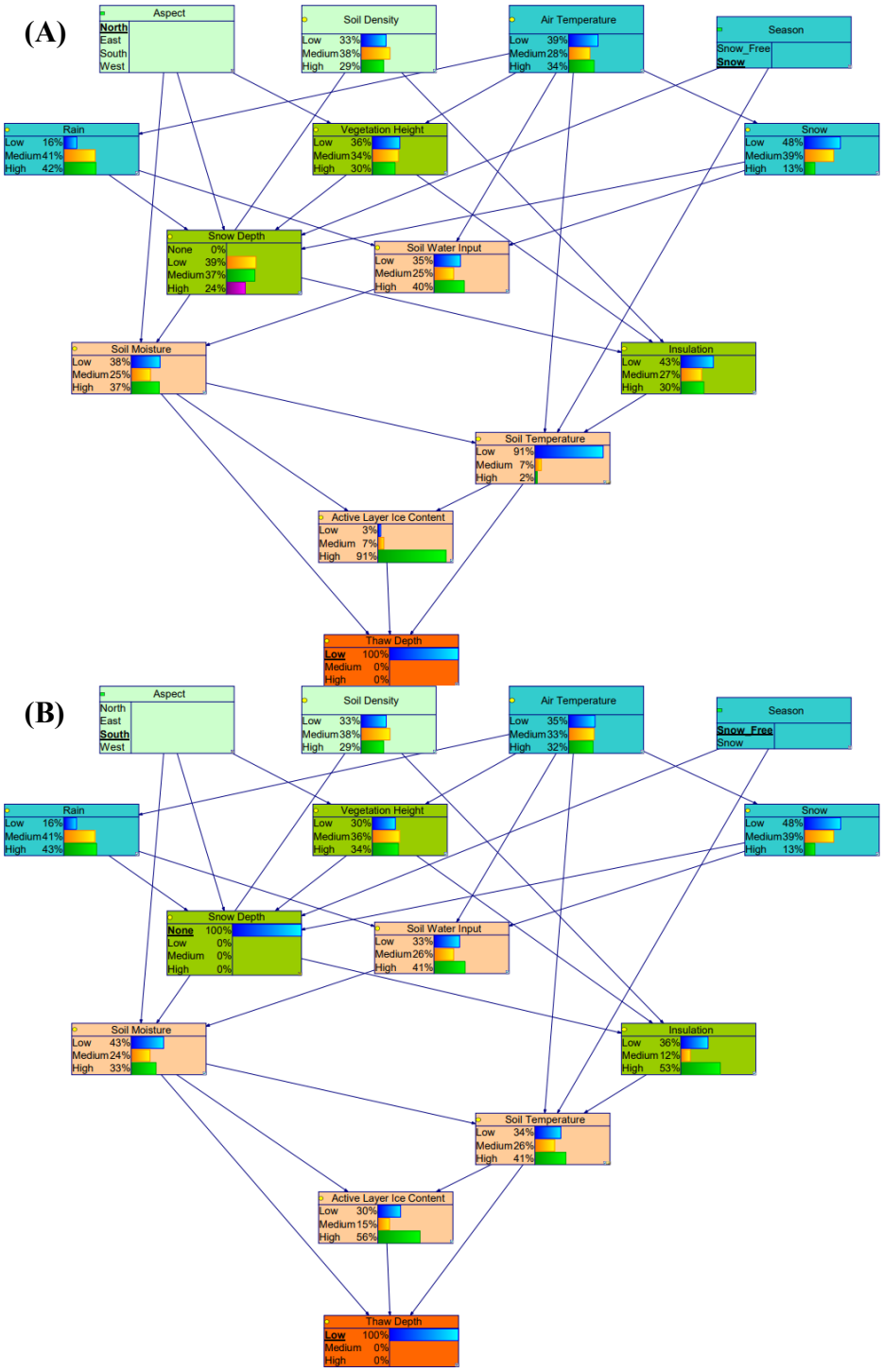

Figure 4.15 Diagnosis experiments with all nodes informed except for air temperature for (A) low thaw depth, north aspect, and snow season and (B) low thaw depth, south aspect, and snow free season.

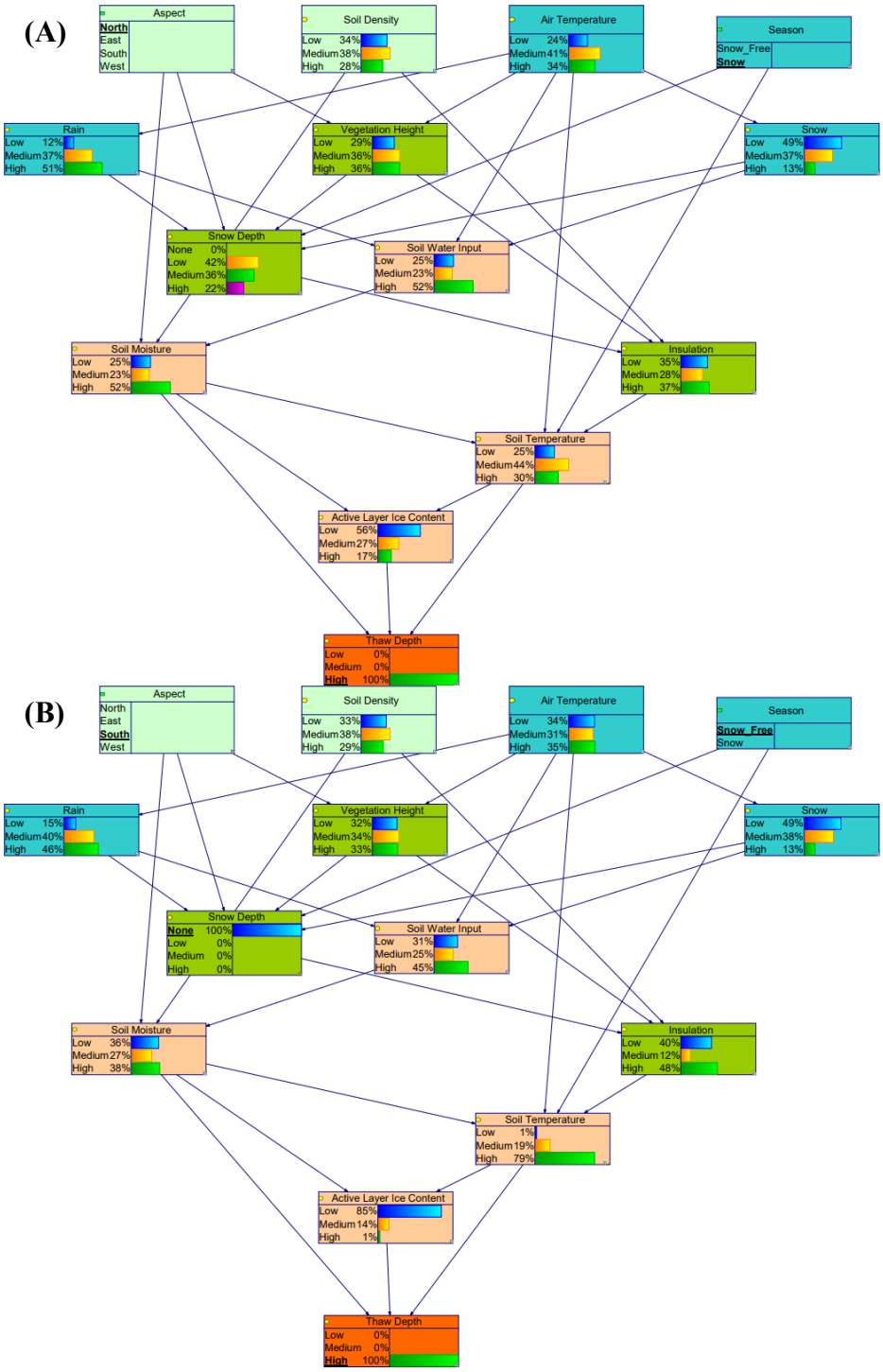

Figure 4.16 Diagnosis experiments with all nodes informed except for air temperature for (A) high thaw depth, north aspect, and snow season and (B) high thaw depth, south aspect, and snow free season.

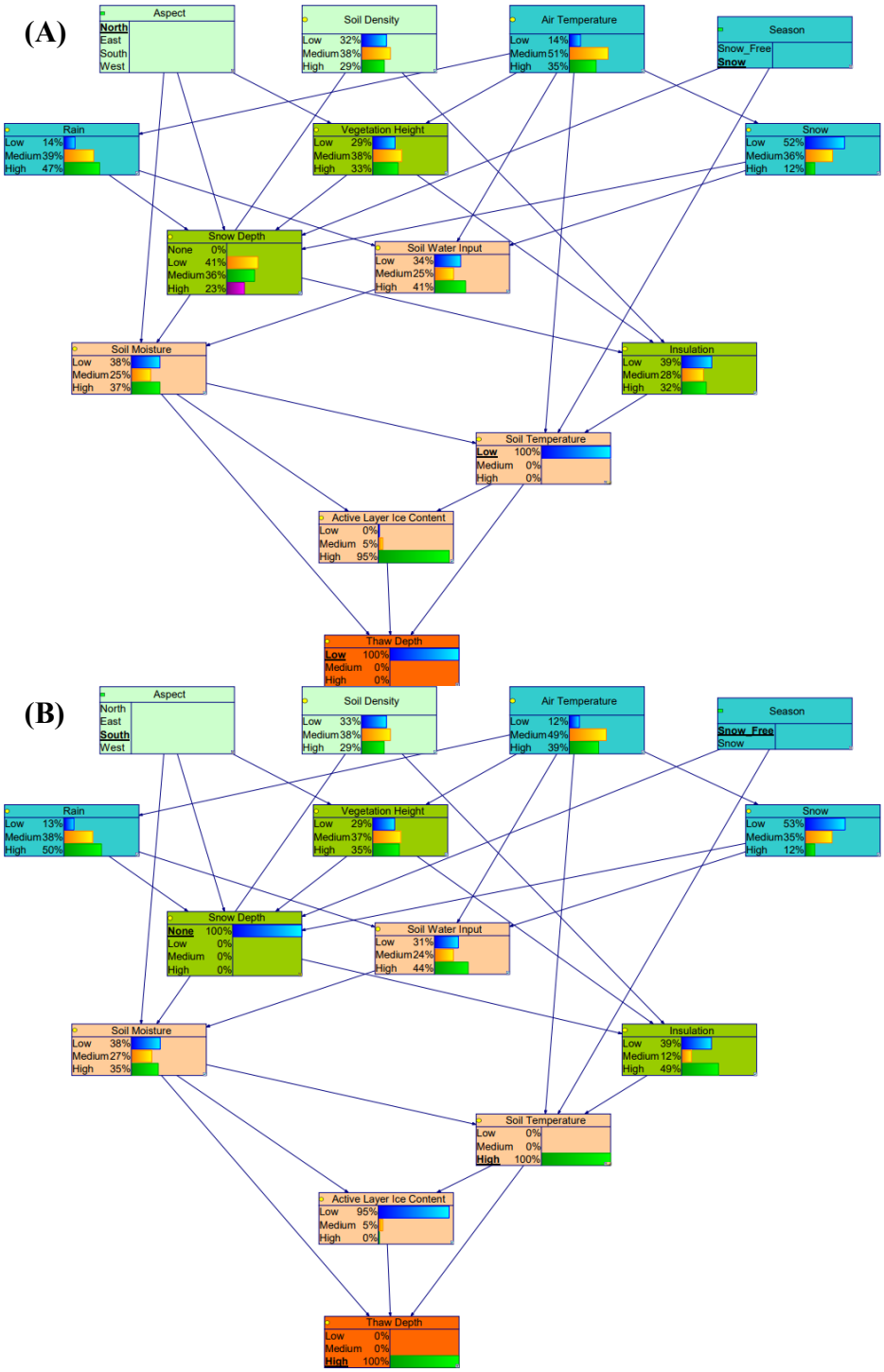

Figure 4.17 Diagnosis experiments with all nodes informed and setting soil temperature states for (A) low thaw depth, north aspect, snow season, and low soil temperature and (B) high thaw depth, south aspect, snow free season, and high soil temperature.

The final set of experiments set the state of snow depth along with various aspect, season, and thaw depth state combinations (Figure 4.18). In the case for north aspect, snow season, low thaw depth, and low snow depth, there was high soil water input, high rain, low/medium snow, low insulation, high soil moisture, low soil temperature, and high active layer ice content; for high snow depth, this changed to low soil water input, low rain, low/medium snow, fairly uniform insulation, low soil moisture, low soil temperature, and high active layer ice content. In the case for south aspect, snow free season, and high thaw depth, there was lower soil water input, lower rain, low or high insulation, lower soil moisture, high soil temperature, and low active layer ice content; snow depth was not set for the snow free season, as by definition there is a 100% chance of no snow for this season.

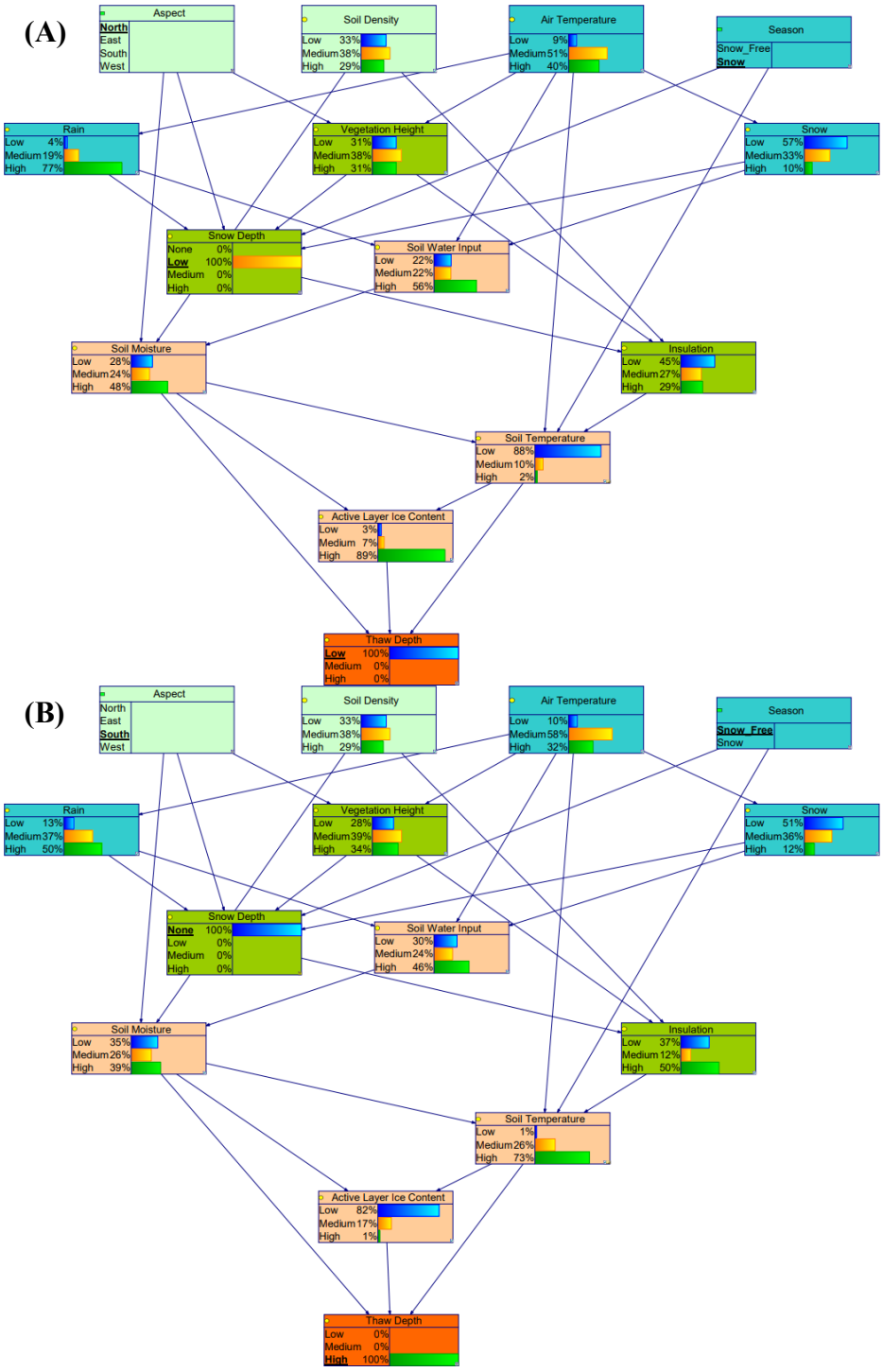

Figure 4.18 Diagnosis experiments with all nodes informed and setting snow depth states for (A) low thaw depth, north aspect, snow season, and low snow depth and (B) high thaw depth, south aspect, snow free season, and no snow depth.

In order for the model to be considered validated, 9 out of the 12 chance nodes for the extreme low and high scenarios had to perform as expected before moving onto evaluation. Using Figures 4.12 and 4.15 as guides, the 75% majority is met when both prognosis and diagnosis scenarios are considered. Overall, there is more rain and soil water input and taller vegetation under warmer temperatures. The snow depth node performs as expected, where there is no snow in the snow free season and probabilities add up to 100% for the snow season. While it would be expected that snow would be lower or non-existent for the snow free season, it cannot be controlled for without an arc to the season node or two separate CPTs that are dependent on season. Soil moisture is higher for north aspects, as expected, and soil temperature responds to low and high forcing factors such as air temperature and season appropriately (e.g., low soil temperature with low air temperature and snow season and high soil temperature with high air temperature and snow free season). Similarly, active layer ice content responds with less ice under warmer air and soil temperature conditions and more ice under cooler air and soil temperature conditions. Finally, thaw depth is sensitive to soil temperature and ice content by being low under high ice, low temperature conditions and being high under low ice, high temperature conditions. The fairly uniform distribution of soil moisture obscures its influence on thaw depth, but low soil moisture contributes to higher soil temperatures in the snow season and low temperatures in the snow season. While insulation does not vary much between experiments, it is generally lower when there is low vegetation and low snow depth and higher when there is higher snow depth and vegetation.

4.3. Evaluation – Case Study with Physical Observations

Evaluation was conducted using the validated conceptual model in Figure 4.9 and corresponding CPTs. The vegetation height node was informed with the probabilities determined from the physical observations. This resulted in a 100% probability of low vegetation on north and west aspects, 86%/10%/3% probability of low/medium/high vegetation on east aspects, and 83%/17%/0% probability of low/medium/high vegetation on south aspects, regardless of air temperature. Since observations are only available for the snow free season, the soil temperature CPT was modified to reflect that the snow and snow free seasons can have independent low, medium, and high probabilities, or in other words, that the boundaries for low, medium, and high soil temperature can differ depending on the season. A set of 20 prognosis experiments (Appendix B) were conducted to evaluate the ability of PermaBN to accurately predict the expected thaw depth distribution of 87% low thaw depth, 13% medium thaw depth, and 0% high thaw depth. The following paragraphs describe the key evaluation experiments.

Figure 4.19 shows the thaw depth predictions for the snow free season for all aspects. For this season, PermaBN predicts a 48% chance of low thaw depth, 22% of medium thaw depth, and 29% thaw depth, for a margin of error of 39%, 5%, and 29%, respectively. Setting the aspect state only causes a slight shift in the thaw depth probabilities, with only a 1% increase in high thaw depth for north aspects, and 1% increase in low thaw depth for east and south aspects; west aspects retain the same overall distribution.

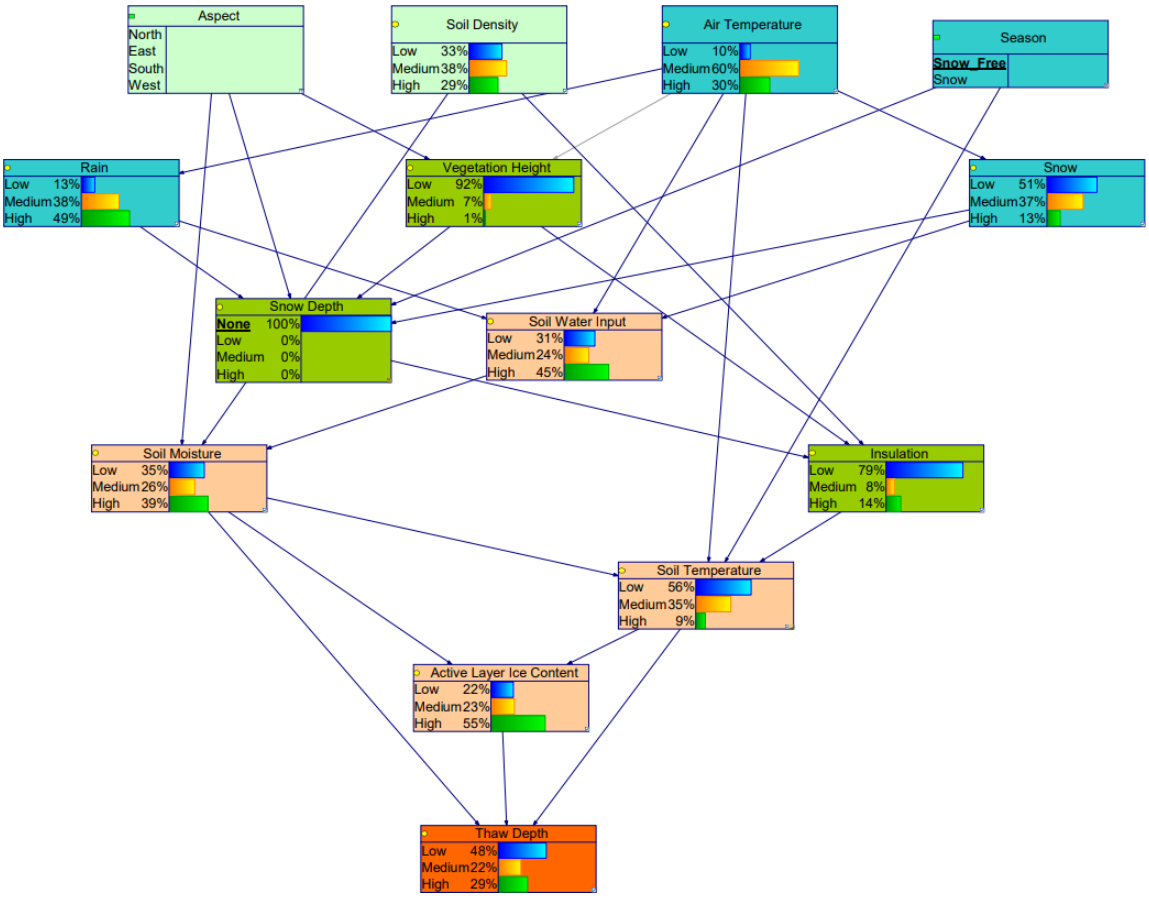

Figure 4.19 PermaBN with informed vegetation height node prognosis predictions for snow free season.

For the extreme low and high scenarios (Figure 4.20), a north aspect, low soil density, low air temperature, and snow free season results in a 60% chance of low thaw depth, 19% chance of medium thaw depth, and 21% chance of high thaw depth, for a margin of error of 27%, 2%, and 21%, respectively. A south aspect, high soil density, high air temperature, and snow free season results in a 54% chance of low thaw depth, 19% chance of medium thaw depth, and 27% high thaw depth, for a margin of error of 33%, 2%, and 27%, respectively.

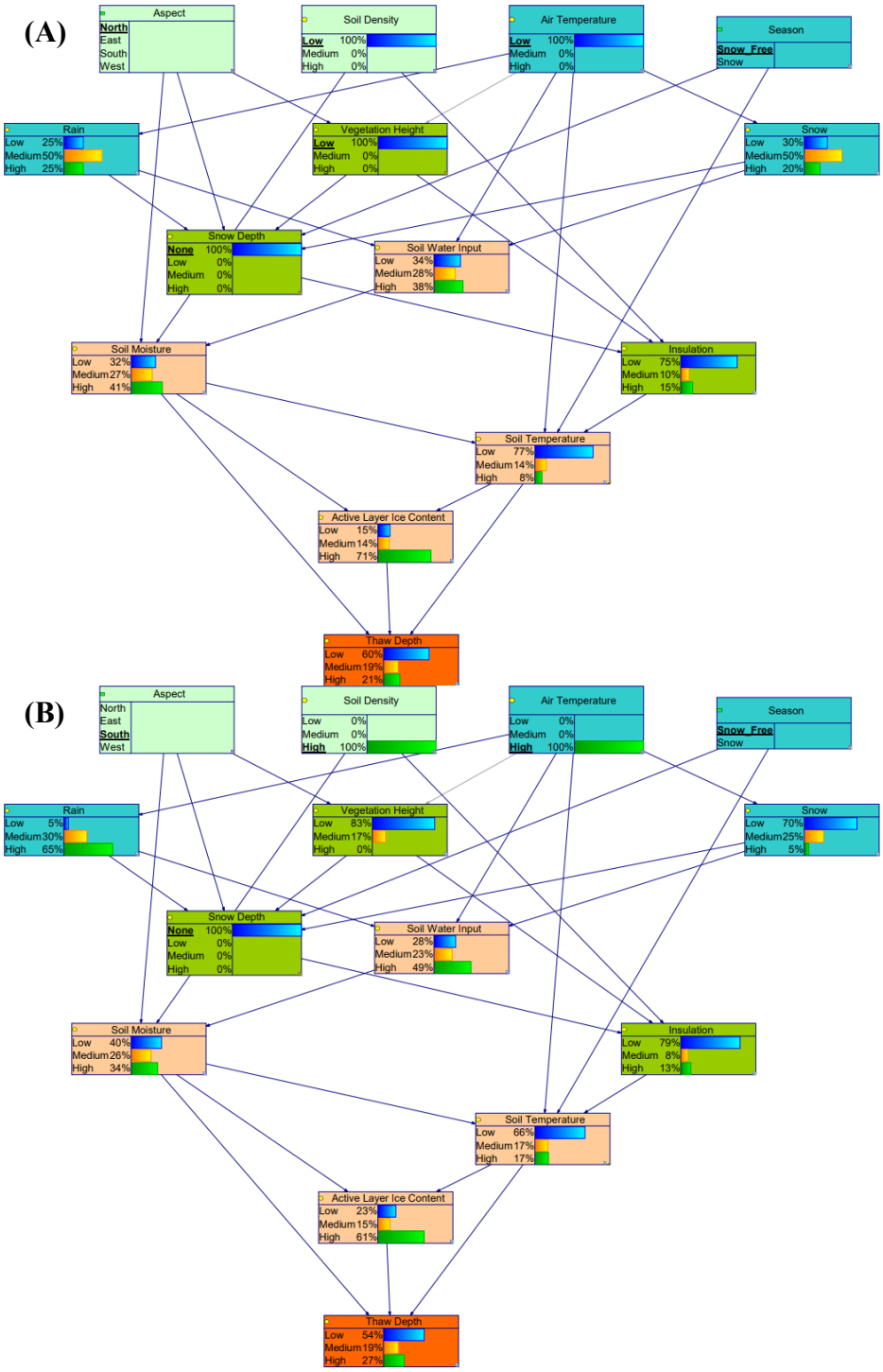

Figure 4.20 PermaBN with informed vegetation height node predictions prognosis for (A) north aspect, low soil density, low air temperature, and snow free season and (B) south aspect, high soil density, high air temperature, and snow free season.

Experiments also tested the most likely June – August conditions for the Siksik Creek Basin. A south aspect was selected based on the mean aspect for the ss1 and ss1lys transects (Appendix D), a low soil density based on site characterization by Grunberg et al. (2020) stating a ~5 cm soil organic layer and approximately equal mineral soil composition of clay, silt, and sand, and medium air temperature based on Grunberg et al. (2020)'s definition of summer as the time period with an average air temperature greater than or equal to 8°C, their 1999 – 2018 mean annual cycle plot for summer air temperatures, and 2015 air temperature data from Inuvik station (Environment and Climate Change Canada, 2015). As seen in Figure 4.21, this results in a 44% chance of low thaw depth, 24% chance of medium thaw depth, and 32% chance of high thaw depth, which is a margin of error of 43%, 7%, and 32%, respectively. However, when soil temperature is set to low in addition to the south aspect, low soil density, and medium air temperature (Figure 4.22), there is a 74% chance of low thaw depth, 16% chance of medium thaw depth, and 10% chance of high thaw depth, for a margin of error of 13%, 1%, and 10%, respectively. A final set of prognosis experiments testing the effects of a uniform soil temperature distribution were also conducted, with all tested aspect, soil density, and air temperature combinations yielding an approximately 34% chance of low thaw depth, 22% chance of medium thaw depth, and 44% chance of high thaw depth, for a margin of error of 53%, 5%, and 44%, respectively.

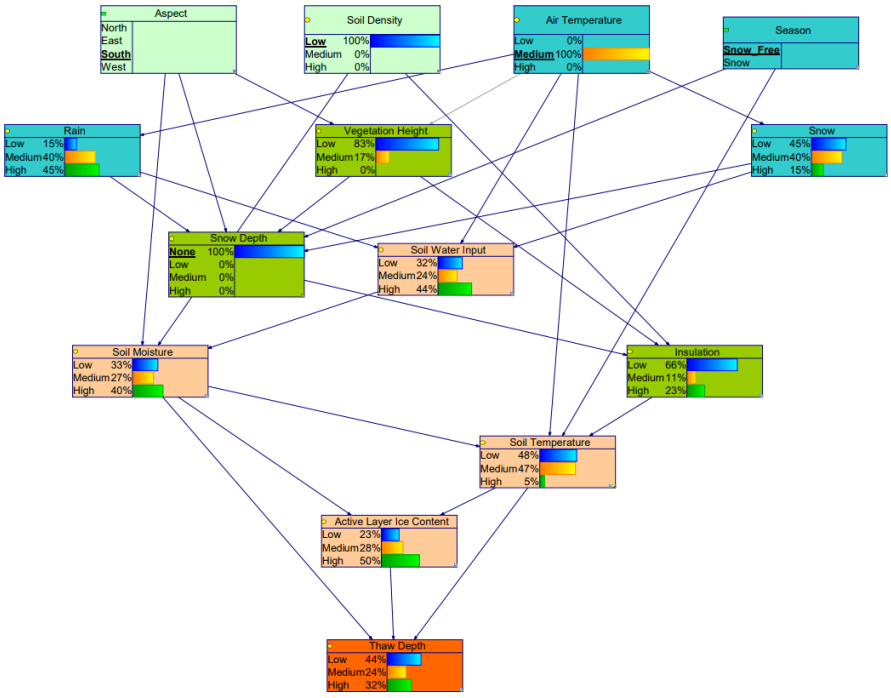

Figure 4.21 PermaBN with informed vegetation height node prognosis predictions for south aspect, low soil density, medium air temperature, and snow free season.

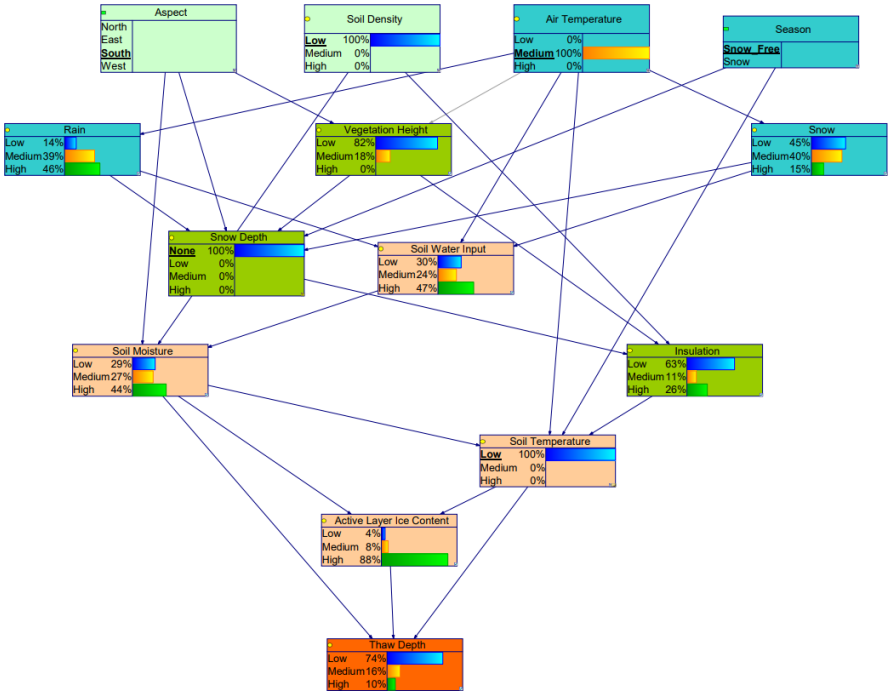

Figure 4.22 PermaBN with informed vegetation height node prognosis predictions for south aspect, low soil density, medium air temperature, low soil temperature, and snow free season.

A set of 15 diagnosis experiments (Appendix B) were also conducted. These experiments are primarily for exploratory purposes, as there is insufficient evidence within the parent nodes to properly evaluate the response of model. For all thaw depths in the snow free season (low and high thaw depth experiments shown in Figure 2.23), there is strong favoring of medium air temperature, low insulation, fairly uniform soil moisture, low or medium soil temperature, and varying active layer ice content (high for low thaw depth, medium or high for medium thaw depth, and low or medium for high thaw depth). Similarly, experiments for low and high thaw depth for all aspects yielded medium air temperature, low insulation, uniform or high skewed soil moisture, low or high soil temperature (low or high thaw depth, respectively), and high or low active layer ice content (low or high thaw depth, respectively).

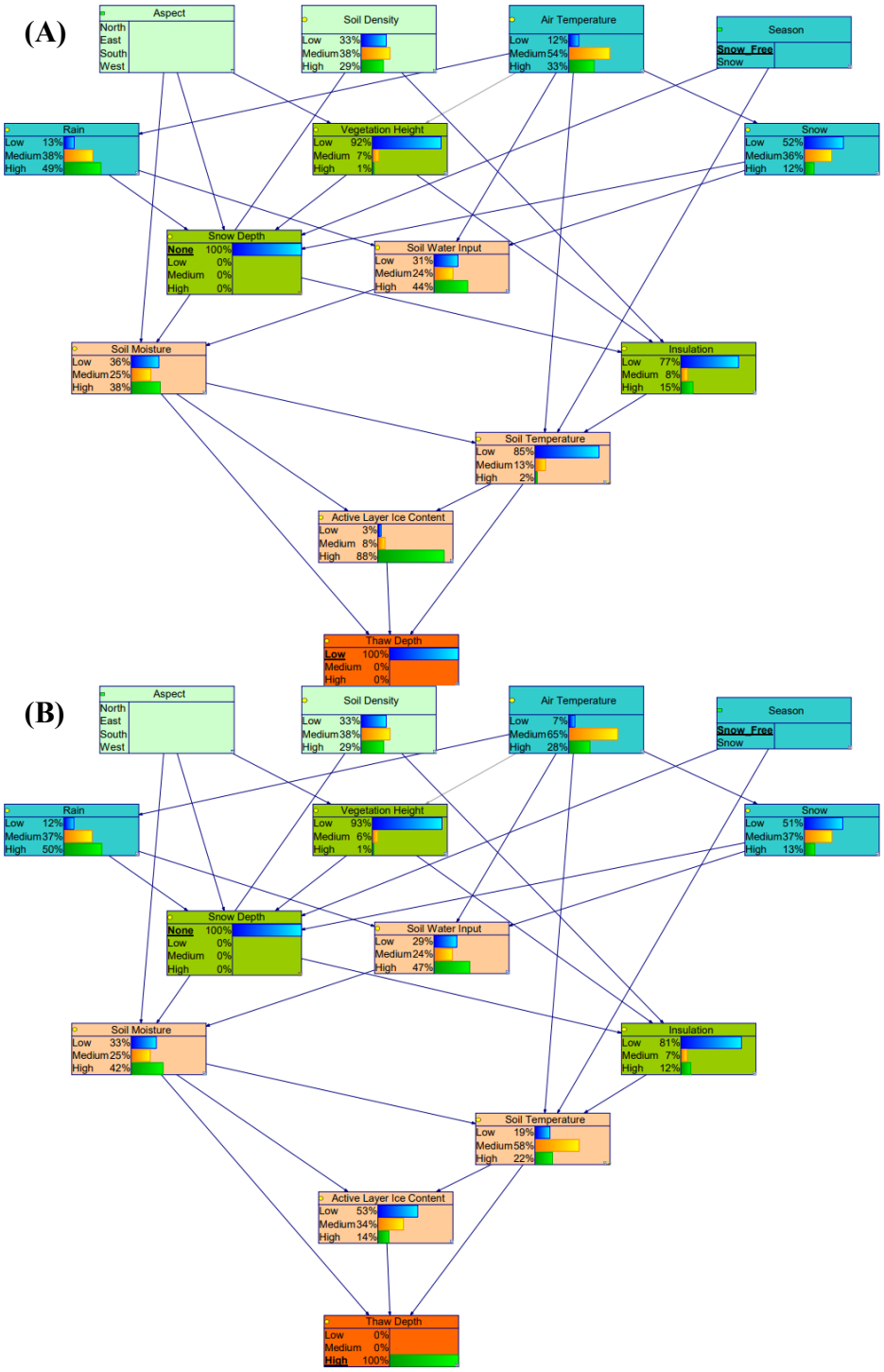

Figure 4.23 PermaBN with informed vegetation height node diagnosis analysis for (A) low thaw depth and (B) high thaw depth for the snow free season.

Remaining experiments continued to favor medium air temperatures, low insulation, and low or high active layer ice content depending on thaw depth; depending on the soil temperature scenario, soil moisture was either slightly low skewed (high soil temperature) or high skewed (low soil temperature). Finally, experiments testing likely aspect (south) and thaw depth (low or medium) conditions (Figure 4.24) showed favoring of medium air temperature, fairy uniform soil density and soil moisture, low insulation, low or medium soil temperature (low or medium thaw depth, respectively), and high or medium active layer ice content (low or medium thaw depth, respectively). It is interesting to note that the south aspect and low thaw depth scenario yields a 12% chance of low air temperature, 54% chance of medium air temperature, and 33% chance of high air temperature, which is very close to the expected 17%, 53%, and 30% chance of low, medium, and high air temperatures for 2015-06-15 (Julian day 168) to 2015-08-20 (Julian day 232) at Inuvik station.

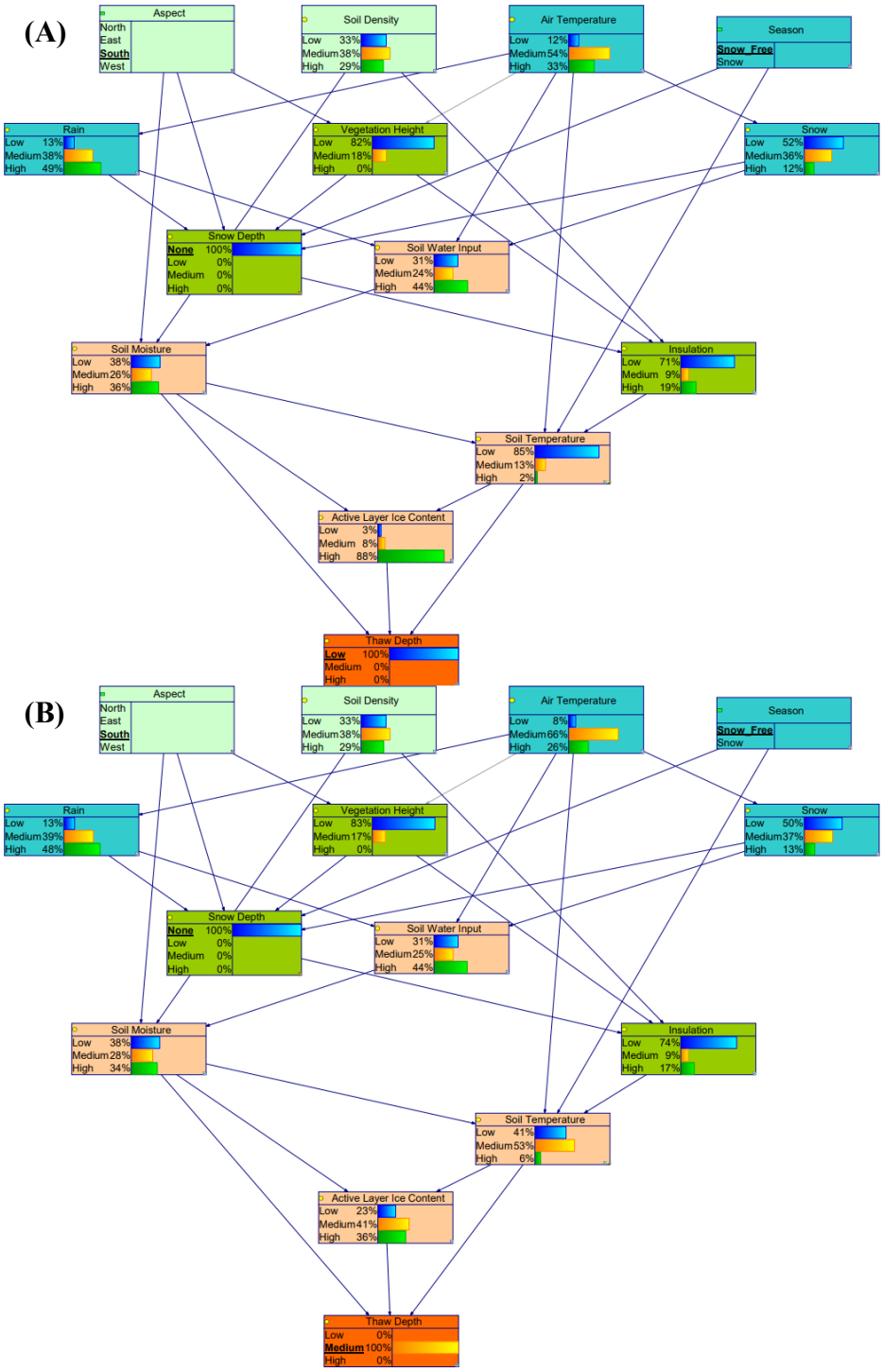

Figure 4.24 PermaBN with informed vegetation height node diagnosis analysis for (A) south aspect and low thaw depth and (B) south aspect and medium thaw depth for the snow free season.

5. DISCUSSION

5.1. Case Study

The results of the Siksik Creek Basin case study demonstrate the ability of PermaBN to integrate multiple types of evidence into a single model. Limited availability of physical observations overlapping both spatially and temporally proved to be a significant challenge in fully validating and evaluating the model, since missing parent nodes make it difficult to quantitatively define the children CPTs in a robust manner. For example, the thaw depth node could not be determined through quantitative binning like the vegetation height node. It was also not possible to evaluate the snow season predictions since the data only spanned the June – August 2015 snow free period. Manual adjustment of and expertly assessed CPTs also come with the caveat that the solutions are not unique, providing further uncertainty in the node distributions as well as the specific cases within the CPT (e.g., the probability that thaw depth is low given low soil moisture, active layer ice content, and soil temperature). Another caveat to consider with this case study is that PermaBN was initially designed with the pan-Arctic and multiyear time scales in mind, such that the case study may not accurately reflect that initial design. For example, the air temperature joint distribution was initially defined with the assumption of warming temperatures in the Arctic, hence the higher probabilities for medium and high air temperatures as compared to low air temperatures. Without physical observations to determine the probability table, however, it is uncertain

how accurate or inaccurate this assumption is for the Siksik Creek Basin for the June – August 2015 time period.

Nonetheless, the results of the most likely conditions prognosis and diagnosis experiments (i.e., those setting aspect as south, soil density as low, air temperature as medium, and/or soil temperature as low) suggest that PermaBN could perform relatively well when system conditions are known and that, in the case of the Siksik Creek Basin, air temperatures for Inuvik and soil temperatures from elsewhere in Trail Valley Creek could be used to provide more informed expert assessment in the model. For instance, combining estimated boundaries of less than 8°C for low air temperature, 8 – 15°C for medium air temperature, and greater than 15°C for high air temperature based on the work of Grunberg et al. (2020) with weather station data from Inuvik provided an estimated 17% chance of low air temperature, 53% chance of medium air temperature, and 30% chance of high air temperature. These estimations are quite similar to the original expert assessment values of a 10% chance for low, 60% chance of medium, and 30% chance of high air temperatures, as well as the diagnosis experiment with a south aspect, snow free season, and low thaw depth that yielded a 12% chance of low, 54% chance of medium, and 33% chance of high air temperatures. Further, when analyzing Trail Valley Creek soil temperature measurements made in June – August 2017 and 2018 by Boike et al. (2020) that were collected at 2, 5, 10, and 20 cm depths, the mean soil temperature over the 2 – 2 cm column was 8°C; soil temperatures varied from ~2.6°C in mid-June to nearly 11°C in July through early August. While there were no values from either Wilcox et al. (2019) or Grunberg et al. (2020) to base binning

boundaries on, it is likely that soil temperatures would be considered low or medium, especially if deeper depths are considered. Conversely, if only topsoil measurements were considered, soil temperatures would likely be high. As for soil density, Grunberg et al. (2020) and Quinton et al. (2000) state that Trail Valley Creek soil has a ~5 cm thick soil organic layer underlain by approximately equal percentages of clay, silt, and sand mineral soil; while approximately equal, silt is slightly more common than clay, and both are more common than sand. This latter finding supports the probabilities of 33% chance of low, 38% chance of medium, and 29% chance of high soil density that were defined through expert assessment.

It is important to note that the studies by Boike et al. (2020) and Grunberg et al. (2020) do not have the same spatiotemporal resolution as the physical observations by Wilcox et al. (2019), but it is interesting nonetheless that setting node states based on the estimated likely scenarios of a south aspect, low soil density, medium air temperature, and low soil temperature in one of the prognosis experiments yielded the closest prediction (74% chance of low, 16% chance of medium, and 10% chance of high thaw depth) to the expected values of 87% chance of low and 13% chance of medium thaw depth. With refinement of the thaw depth parent nodes, it is likely that PermaBN could generate more accurate predictions. However, it was unexpected that the thaw depths strongly favored less thaw. Even when applying the thaw depth boundaries of less than 50 cm, 50 – 80 cm, and greater than 80 cm to all transects in the Siksik Creek Basin dataset, only 3% of depth measurements were expected to be high (i.e., greater than 80 cm), and 78% of measurements were expected to be low (i.e., less than 50 cm). This may

indicate that permafrost in the Siksik Creek Basin has experienced less thaw than elsewhere in the broader Trail Valley Creek area or that the boundaries based on ALT for Trail Valley Creek are not as representative of the Siksik Creek Basin.

A final observation about the model evaluation stage is that aspect was not found to impact thaw depth by more than 1 – 2% between the different states. This may be due to the fact that aspect's primary contribution was to the vegetation height node and subsequently vegetation height's contribution to insulation. Since vegetation height for all aspects had an 83 – 100% chance of being low, and soil density had a fairly uniform distribution, insulation was always predominately low. The limited variability in insulation contributed to less influence on the soil temperature node, which is a key driver of thaw depth in the model. Likewise, the limited variability in the fairly uniform soil moisture node resulted in less influence on the soil temperature and thaw depths.

Despite the limitations in the validation and evaluation approaches adopted, namely the need for more thorough expert assessment and the lack of physical observations to characterize each node in the model for both seasons, PermaBN is a unique proof-of-concept of a modeling approach that combines topography, meteorological conditions, soil characteristics, and vegetation into a single model. As seen in Table 2.1, there is no one model that accounts for all of the variables present in PermaBN. While the statistical model by Wilcox et al. (2019) accounts for vegetation and aspect, it does not include air temperature, precipitation, and soil parameters. Likewise, the statistical model by Hjort et al. (2018) accounts for certain soil parameters and slope, but excludes vegetation, air temperature, and precipitation, and the one by

Aalto et al. (2018) accounts for air temperature, precipitation, SOC, and potential incoming solar radiation, but not vegetation or additional soil characteristics. Older, predominantly non-statistical models thoroughly account for soil characteristics or thermal dynamics related to snow depth and moisture conditions but largely lack the inclusion of vegetation or atmospheric components other than air temperature. The closest model match appears to be the NEST model by Zhang et al. (2006) which includes vegetation, air temperature, precipitation, solar radiation, ground ice content, mineral vs. organic soil, and other soil thermal properties (i.e., thermal conductivity and geothermal heat flux), though it omits the explicit representation of soil moisture and soil temperature. Future testing of PermaBN could be done by comparing the results of the two models.

5.2. Limitations

As outlined in Chen and Pollino (2012), uncertainties in BNs can originate from incomplete understanding of the process(es) being modeled, incomplete data, or subjective biases in the expert assessments. BNs allow for explicit representation of uncertainty, but they cannot differentiate between different types of uncertainty, such as uncertainties with input data and model structure (Chen and Pollino, 2012). While expert assessment datasets can help reduce uncertainties in model structure in particular (Chen and Pollino, 2012), they are prone to introducing bias and epistemic uncertainty and may yield results that are accurate but not necessarily precise (Kuhnert et al., 2010, Webster and McLaughlin, 2014). Following proper methods and procedures when eliciting expert assessment datasets may help reduce these uncertainties. Exploring alternative

quantitative methods for determining the CPTs could also help reduce uncertainties in the model. For instance, sensitivity analysis can allow for identification of missing or unneeded linkages, and act as an alternative evaluation method for determining which variables in the model are most influential; conditional probabilities can also be learned from algorithms, such as the Lauritzen – Spiegelhalter algorithm or Gibbs sampling (Chen and Pollino, 2012). Finally, the inclusion of decision nodes can limit the tools and algorithms available for use in the GeNIe software program. The inclusion of decision nodes results in the BN being classified as an "influence diagram," and some tools, such as the "sensitivity analysis" tool, are unavailable for use with influence diagrams within the software. The decision nodes would either need to be removed or converted to chance nodes prior to running these tools in GeNIe.

5.3. Future Work

As development of BNs is often seen as an on-going process (Chen and Pollino, 2012), there are many avenues of future work that can be undertaken with PermaBN. Foremost could be addressing the limitations previously discussed by: (1) aiming to reduce uncertainty in the expertly assessed CPTs through more robust elicitation procedures, (2) conducting sensitivity analysis, (3) exploring algorithms for determining the CPTs, (4) re-characterizing the BN to remove the decision nodes to allow for more analysis options within the BN software, and (5) improving validation by finding or creating new datasets for evaluation. Related to the point on exploring algorithms for determining CPTs is calibration of the BN. Three types of calibration could be considered: (1) manual calibration, (2) optimization, and (3) probabilistic calibration.

Manual calibration would entail manually manipulating the CPTs until the parent node yields the expected thaw depth response. Optimization would entail having an algorithm solve for the most likely scenario amongst the parent nodes given a particular state of the thaw depth node; optimization would yield a single, unique result. In contrast, probabilistic calibration would explore many different scenarios for the parent nodes and report which of the scenarios are most likely. These methods of calibration are unique to BNs and would allow for the BN to perform better the next time it is run. Since manual calibration is time consuming and does not yield unique results, the recommended next step would be conducting optimization.

Once the methodological development of PermaBN is refined, the next steps could entail: (1) integration of hydrological variables, (2) integration of PermaBN into a larger risk framework as a sub-model, and (3) application to a pan-Arctic case study. If PermaBN is only intended to function as an ecological or predictive model, hydrological variables such as sub-surface and surface water flow rates, water temperature, presence of lakes and rivers, and river discharge could be directly integrated into the model. Alternatively, PermaBN and corresponding hydrological influences could be integrated as sub-models into a larger BN framework aimed at quantifying social, economic, and environmental consequences of a warming Arctic (Loisel and Medina-Cetina, 2019). Whether as a stand-alone ecological model or integrated risk framework sub-model, PermaBN could also be applied to a multitude of pan-Arctic case studies, and its predictions could be compared to existing permafrost models for evaluation of performance. Overall, the relative simplicity of the PermaBN framework allows for the

identification and exploration of multiple science questions, as it can be cheaply and quickly run using a large number and combination of variables.

6. CONCLUSIONS

PermaBN is a Bayesian network designed to assess permafrost thaw in the continuous permafrost region of the Arctic. It provides an alternative method for assessing permafrost thaw that allows for the integration of multiple types of evidence (e.g., physical observations, model outputs, and expert assessments) into a single model. This study outlines and discusses best BN model practices while providing a proof-of-concept of this unique modeling method. The framework presented offers a transparent modeling approach that is able to represent systems in data sparse regions such as the Arctic. Further, it facilitates the quantification of uncertainty through the use of probabilities.

The case study that was selected to further evaluate PermaBN also shed light on important aspects of both the model development and field data collection. For instance, physical observations allow for reduction in uncertainty for those nodes that have data available; here, aspect and vegetation height data allowed for uncertainty in vegetation height conditions to be reduced since it was known which aspects contributed to which vegetation classes. Conversely, the model highlighted data gaps, such as long-term thaw depth measurements with concurrent meteorological and soil measurements. Filling these data gaps would certainly help validating models and furthering their development.

Aside from the benefits this modeling approach provides in data sparse regions, BNs also have the ability to engage a wider audience than traditional modeling approaches. Users without highly technical modeling skills can build BNs, and the graphical structure can easily be understood by and communicated to non-technical

stakeholders. This is valuable in the context of interdisciplinary and participatory endeavors. With future development of PermaBN to include a more robust validation procedure, hydrological variables, and/or integration with a risk assessment framework, PermaBN could be applied to carbon modeling studies, infrastructure hazard assessments, and policy decisions aimed at mitigation of and adaptation to permafrost thaw.

REFERENCES

Aalto, J., Karjalainen, O., Hjort, J. and Luoto, M. 2018. Statistical Forecasting of Current and Future Circum-Arctic Ground Temperatures and Active Layer Thickness. *Geophysical Research Letters*, 45(10), pp. 4889-4898. doi:10.1029/2018gl078007.

Aalto, J., le Roux, P. C. and Luoto, M. 2013. Vegetation Mediates Soil Temperature and Moisture in Arctic-Alpine Environments. *Arctic Antarctic and Alpine Research*, 45(4), pp. 429-439. doi:10.1657/1938-4246-45.4.429.

Abu-Hamdeh, N. H. and Reeder, R. C. 2000. Soil thermal conductivity: Effects of density, moisture, salt concentration, and organic matter. *Soil Science Society of America Journal*, 64(4), pp. 1285-1290. doi:10.2136/sssaj2000.6441285x.

Afenyo, M., Khan, F., Veitch, B. and Yang, M. 2017. Arctic shipping accident scenario analysis using Bayesian Network approach. *Ocean Engineering*, 133, pp. 224-230. doi:10.1016/j.oceaneng.2017.02.002.

Aguilera, P. A., Fernandez, A., Fernandez, R., Rumi, R. and Salmeron, A. 2011. Bayesian networks in environmental modelling. *Environmental Modelling & Software*, 26(12), pp. 1376-1388. doi:10.1016/j.envsoft.2011.06.004.

Anisimov, O. A., Shiklomanov, N. I. and Nelson, F. E. 1997. Global warming and active-layer thickness: results from transient general circulation models. *Global and Planetary Change*, 15(3-4), pp. 61-77. doi:10.1016/s0921-8181(97)00009-x.

Arya, L. M. and Paris, J. F. 1981. A PHYSICOEMPIRICAL MODEL TO PREDICT THE SOIL-MOISTURE CHARACTERISTIC FROM PARTICLE-SIZE DISTRIBUTION AND BULK-DENSITY DATA. *Soil Science Society of America Journal*, 45(6), pp. 1023-1030. doi:10.2136/sssaj1981.03615995004500060004x.

Barrio, I. C., Linden, E., Te Beest, M., Olofsson, J., Rocha, A., Soininen, E. M., Alatalo, J. M., Andersson, T., Asmus, A., Boike, J., Brathen, K. A., Bryant, J. P., Buchwal, A., Bueno, C. G., Christie, K. S., Denisova, Y. V., Egelkraut, D., Ehrich, D., Fishback, L., Forbes, B. C., Gartzia, M., Grogan, P., Hallinger, M.,

Heijmans, M. M. P. D., Hik, D. S., Hofgaard, A., Holmgren, M., Hoye, T. T., Huebner, D. C., Jonsdottir, I. S., Kaarlejarvi, E., Kumpula, T., Lange, C., Lange, J., Levesque, E., Limpens, J., Macias-Fauria, M., Myers-Smith, I., van Nieukerken, E. J., Normand, S., Post, E. S., Schmidt, N. M., Sitters, J., Skoracka, A., Sokolov, A., Sokolova, N., Speed, J. D. M., Street, L. E., Sundqvist, M. K., Suominen, O., Tananaev, N., Tremblay, J. P., Urbanowicz, C., Uvarov, S. A., Watts, D., Wilmking, M., Wookey, P. A., Zimmermann, H. H., Zverev, V. and Kozlov, M. V. 2017. Background invertebrate herbivory on dwarf birch (*Betula glandulosa-nana* complex) increases with temperature and precipitation across the tundra biome. *Polar Biology*, 40(11), pp. 2265-2278. doi:10.1007/s00300-017-2139-7.

BayesFusion. 2019. GeNIe. 2.4 ed.

Bintanja, R. and Andry, O. 2017. Towards a rain-dominated Arctic. *Nature Climate Change*, 7(4), pp. 263-+. doi:10.1038/nclimate3240.

Bintanja, R. and Selten, F. M. 2014. Future increases in Arctic precipitation linked to local evaporation and sea-ice retreat. *Nature*, 509(7501), pp. 479-+. doi:10.1038/nature13259.

Bintanja, R., van der Wiel, K., van der Linden, E. C., Reusen, J., Bogerd, L., Krikken, F. and Selten, F. M. 2020. Strong future increases in Arctic precipitation variability linked to poleward moisture transport. *Science Advances*, 6(7), pp. 6. doi:10.1126/sciadv.aax6869.

Biskaborn, B. K., Lanckman, J. P., Lantuit, H., Elger, K., Streletskiy, D. A., Cable, W. L. and Romanovsky, V. E. 2015. The new database of the Global Terrestrial Network for Permafrost (GTN-P). *Earth System Science Data*, 7(2), pp. 245-259. doi:10.5194/essd-7-245-2015.

Biskaborn, B. K., Smith, S. L., Noetzli, J., Matthes, H., Vieira, G., Streletskiy, D. A., Schoeneich, P., Romanovsky, V. E., Lewkowicz, A. G., Abramov, A., Allard, M., Boike, J., Cable, W. L., Christiansen, H. H., Delaloye, R., Diekmann, B., Drozdov, D., Etzelmuller, B., Grosse, G., Guglielmin, M., Ingeman-Nielsen, T., Isaksen, K., Ishikawa, M., Johansson, M., Johannsson, H., Joo, A., Kaverin, D., Kholodov, A., Konstantinov, P., Kroger, T., Lambiel, C., Lanckman, J. P., Luo, D. L., Malkova, G., Meiklejohn, I., Moskalenko, N., Oliva, M., Phillips, M., Ramos, M., Sannel, A. B. K., Sergeev, D., Seybold, C., Skryabin, P., Vasiliev,

A., Wu, Q. B., Yoshikawa, K., Zheleznyak, M. and Lantuit, H. 2019. Permafrost is warming at a global scale. *Nature Communications*, 10, pp. 11. doi:10.1038/s41467-018-08240-4.

Blok, D., Heijmans, M. M. P. D., Schaepman-Strub, G., Kononov, A. V., Maximov, T. C. and Berendse, F. 2010. Shrub expansion may reduce summer permafrost thaw in Siberian tundra. *Global Change Biology*, 16(4), pp. 1296-1305. doi:10.1111/j.1365-2486.2009.02110.x.

Boike, J., Cable, W. L., Bornemann, N. and Lange, S. 2020. Trail Valley Creek, NWT, Canada Soil Moisture and Temperature 2016 - 2019.

Boike, J., Roth, K. and Ippisch, O. 2003. Seasonal snow cover on frozen ground: Energy balance calculations of a permafrost site near Ny-Alesund, Spitsbergen. *Journal of Geophysical Research-Atmospheres*, 108(D1), pp. 11. doi:10.1029/2001jd000939.

Bonan, G. B. 2008. Forests and climate change: Forcings, feedbacks, and the climate benefits of forests. *Science*, 320(5882), pp. 1444-1449. doi:10.1126/science.1155121.

Box, J. E., Colgan, W. T., Christensen, T. R., Schmidt, N. M., Lund, M., Parmentier, F. J. W., Brown, R., Bhatt, U. S., Euskirchen, E. S., Romanovsky, V. E., Walsh, J. E., Overland, J. E., Wang, M. Y., Corell, R. W., Meier, W. N., Wouters, B., Mernild, S., Mard, J., Pawlak, J. and Olsen, M. S. 2019. Key indicators of Arctic climate change: 1971-2017. *Environmental Research Letters*, 14(4), pp. 18. doi:10.1088/1748-9326/aafc1b.

Brown, J., Ferrians, O., Heginbottom, J. A. and Melnikov, E. 1997. Circum-Arctic Map of Permafrost and Ground-Ice Conditions, Version 2.

Brown, J., Ferrians, O., Heginbottom, J. A. and Melnikov, E. 2002. Circum-Arctic Map of Permafrost and Ground-Ice Conditions, Version 2. *NSIDC: National Snow and Ice Data Center*.

Burn, C. R. and Kokelj, S. V. 2009. The Environment and Permafrost of the Mackenzie Delta Area. *Permafrost and Periglacial Processes*, 20(2), pp. 83-105. doi:10.1002/ppp.655.

Chen, S. H. and Pollino, C. A. 2012. Good practice in Bayesian network modelling. *Environmental Modelling & Software*, 37, pp. 134-145. doi:10.1016/j.envsoft.2012.03.012.

Comiso, J. C., Parkinson, C. L., Gersten, R. and Stock, L. 2008. Accelerated decline in the Arctic Sea ice cover. *Geophysical Research Letters*, 35(1), pp. 6. doi:10.1029/2007gl031972.

Douglas, T. A., Turetsky, M. R. and Koven, C. D. 2020. Increased rainfall stimulates permafrost thaw across a variety of Interior Alaskan boreal ecosystems. *Npj Climate and Atmospheric Science*, 3(1), pp. 7. doi:10.1038/s41612-020-0130-4.

Dutta, R. and Barnhart, W. D. 2020. InSAR Estimates of Active Layer Thickness in the Entire Continuous Permafrost Regions of Alaska. *AGU Fall Meeting 2020.*

Environment and Climate Change Canada. 2015. Historical Data - Inuvik A Station.

Evans, B. M., Walker, D. A., Benson, C. S., Nordstrand, E. A. and Petersen, G. W. 1989. SPATIAL INTERRELATIONSHIPS BETWEEN TERRAIN, SNOW DISTRIBUTION AND VEGETATION PATTERNS AT AN ARCTIC FOOTHILLS SITE IN ALASKA. *Holarctic Ecology*, 12(3), pp. 270-278.

Fahd, F., Veitch, B. and Khan, F. 2020. Risk assessment of Arctic aquatic species using ecotoxicological biomarkers and Bayesian network. *Marine Pollution Bulletin*, 156, pp. 11. doi:10.1016/j.marpolbul.2020.111212.

Feng, S., Ho, C. H., Hu, Q., Oglesby, R. J., Jeong, S. J. and Kim, B. M. 2012. Evaluating observed and projected future climate changes for the Arctic using the Koppen-Trewartha climate classification. *Climate Dynamics*, 38(7-8), pp. 1359-1373. doi:10.1007/s00382-011-1020-6.

Fisher, J. P., Estop-Aragones, C., Thierry, A., Charman, D. J., Wolfe, S. A., Hartley, I. P., Murton, J. B., Williams, M. and Phoenix, G. K. 2016. The influence of vegetation and soil characteristics on active-layer thickness of permafrost soils in boreal forest. *Global Change Biology*, 22(9), pp. 3127-3140. doi:10.1111/gcb.13248.

Flynn, M., Ford, J. D., Labbe, J., Schrott, L. and Tagalik, S. 2019. Evaluating the effectiveness of hazard mapping as climate change adaptation for community planning in degrading permafrost terrain. *Sustainability Science*, 14(4), pp. 1041-1056. doi:10.1007/s11625-018-0614-x.

Frauenfeld, O. W., Zhang, T. J., Barry, R. G. and Gilichinsky, D. 2004. Interdecadal changes in seasonal freeze and thaw depths in Russia. *Journal of Geophysical Research-Atmospheres*, 109(D5), pp. 12. doi:10.1029/2003jd004245.

Getoor, L., Rhee, J. T., Koller, D. and Small, P. 2004. Understanding tuberculosis epidemiology using structured statistical models. *Artificial Intelligence in Medicine*, 30(3), pp. 233-256. doi:10.1016/j.artmed.2003.11.003.

Gockede, M., Kwon, M. J., Kittler, F., Heimann, M., Zimov, N. and Zimov, S. 2019. Negative feedback processes following drainage slow down permafrost degradation. *Global Change Biology*, 25(10), pp. 3254-3266. doi:10.1111/gcb.14744.

Goodrich, L. E. 1978. EFFICIENT NUMERICAL TECHNIQUE FOR ONE-DIMENSIONAL THERMAL PROBLEMS WITH PHASE-CHANGE. *International Journal of Heat and Mass Transfer*, 21(5), pp. 615-621. doi:10.1016/0017-9310(78)90058-3.

Goodrich, L. E. 1982. THE INFLUENCE OF SNOW COVER ON THE GROUND THERMAL REGIME. *Canadian Geotechnical Journal*, 19(4), pp. 421-432. doi:10.1139/t82-047.

Gruber, S. 2012. Derivation and analysis of a high-resolution estimate of global permafrost zonation. *Cryosphere*, 6(1), pp. 221-233. doi:10.5194/tc-6-221-2012.

Grunberg, I., Wilcox, E. J., Zwieback, S., Marsh, P. and Boike, J. 2020. Linking tundra vegetation, snow, soil temperature, and permafrost. *Biogeosciences*, 17(16), pp. 4261-4279. doi:10.5194/bg-17-4261-2020.

Hanna, E., Cappelen, J., Fettweis, X., Mernild, S. H., Mote, T. L., Mottram, R., Steffen, K., Ballinger, T. J. and Hall, R. 2020. Greenland surface air temperature changes from 1981 to 2019 and implications for ice-sheet melt and mass-balance change. *International Journal of Climatology*, pp. 17. doi:10.1002/joc.6771.

Haynes, K. M., Connon, R. F. and Quinton, W. L. 2018. Permafrost thaw induced drying of wetlands at Scotty Creek, NWT, Canada. *Environmental Research Letters*, 13(11), pp. 13. doi:10.1088/1748-9326/aae46c.

Hjort, J., Karjalainen, O., Aalto, J., Westermann, S., Romanovsky, V. E., Nelson, F. E., Etzelmuller, B. and Luoto, M. 2018. Degrading permafrost puts Arctic infrastructure at risk by mid-century. *Nature Communications*, 9, pp. 9. doi:10.1038/s41467-018-07557-4.

Holland, P. G. and Steyn, D. G. 1975. Vegetational Responses to Latitudinal Variations in Slope Angle and Aspect. *Journal of Biography*, 2(3), pp. 179-183. doi:10.2307/3037989.

Hu, F. S., Higuera, P. E., Duffy, P., Chipman, M. L., Rocha, A. V., Young, A. M., Kelly, R. and Dietze, M. C. 2015. Arctic tundra fires: natural variability and responses to climate change. *Frontiers in Ecology and the Environment*, 13(7), pp. 369-377. doi:10.1890/150063.

Hugelius, G., Loisel, J., Chadburn, S., Jackson, R. B., Jones, M., MacDonald, G., Marushchak, M., Olefeldt, D., Packalen, M., Siewert, M. B., Treat, C., Turetsky, M., Voigt, C. and Yu, Z. C. 2020. Large stocks of peatland carbon and nitrogen are vulnerable to permafrost thaw. *Proceedings of the National Academy of Sciences of the United States of America*, 117(34), pp. 20438-20446. doi:10.1073/pnas.1916387117.

Hugelius, G., Strauss, J., Zubrzycki, S., Harden, J. W., Schuur, E. A. G., Ping, C. L., Schirrmeister, L., Grosse, G., Michaelson, G. J., Koven, C. D., O'Donnell, J. A., Elberling, B., Mishra, U., Camill, P., Yu, Z., Palmtag, J. and Kuhry, P. 2014. Estimated stocks of circumpolar permafrost carbon with quantified uncertainty ranges and identified data gaps. *Biogeosciences*, 11(23), pp. 6573-6593. doi:10.5194/bg-11-6573-2014.

IPCC. 2013. Climate Change 2013: The Physical Science Basis. Contribution of Working Group I to the Fifth Assessment Report of the Intergovernmental Panel on Climate Change. Cambridge, United Kingdom and New York, NY, USA: Cambridge University Press.

Jafarov, E. E., Marchenko, S. S. and Romanovsky, V. E. 2012. Numerical modeling of permafrost dynamics in Alaska using a high spatial resolution dataset. *Cryosphere*, 6(3), pp. 613-624. doi:10.5194/tc-6-613-2012.

Jan, A. and Painter, S. L. 2020. Permafrost thermal conditions are sensitive to shifts in snow timing. *Environmental Research Letters*, 15(8), pp. 12. doi:10.1088/1748-9326/ab8ec4.

Jorgenson, M. T., Kanevskiy, M., Shur, Y., Moskalenko, N., Brown, D. R. N., Wickland, K., Striegl, R. and Koch, J. 2015. Role of ground ice dynamics and ecological feedbacks in recent ice wedge degradation and stabilization. *Journal of Geophysical Research-Earth Surface*, 120(11), pp. 2280-2297. doi:10.1002/2015jf003602.

Jorgenson, M. T. and Osterkamp, T. E. 2005. Response of boreal ecosystems to varying modes of permafrost degradation. *Canadian Journal of Forest Research*, 35(9), pp. 2100-2111. doi:10.1139/x05-153.

Jorgenson, M. T., Romanovsky, V., Harden, J., Shur, Y., O'Donnell, J., Schuur, E. A. G., Kanevskiy, M. and Marchenko, S. 2010. Resilience and vulnerability of permafrost to climate change. *Canadian Journal of Forest Research*, 40(7), pp. 1219-1236. doi:10.1139/x10-060.

Kaikkonen, L., Parviainen, T., Rahikainen, M., Uusitalo, L. and Lehikoinen, A. 2021. Bayesian Networks in Environmental Risk Assessment: A Review. *Integrated Environmental Assessment and Management*, 17(1), pp. 62-78. doi:10.1002/ieam.4332.

Karjalainen, O., Aalto, J., Luoto, M., Westermann, S., Romanovsky, V. E., Nelson, F. E., Etzelmuller, B. and Hjort, J. 2019. Circumpolar permafrost maps and geohazard indices for near-future infrastructure risk assessments. *Scientific Data*, 6, pp. 16. doi:10.1038/sdata.2019.37.

Keller, F. 1992. AUTOMATED MAPPING OF MOUNTAIN PERMAFROST USING THE PROGRAM PERMAKART WITHIN THE GEOGRAPHICAL INFORMATION-SYSTEM ARC INFO. *Permafrost and Periglacial Processes, Vol 3, No 2, Apr-Jun 1992: Permafrost and Periglacial Environments in Mountain Areas*, pp. 133-138.

Kjaerulff, U. 1995. DHUGIN - A COMPUTATIONAL SYSTEM FOR DYNAMIC TIME-SLICED BAYESIAN NETWORKS. *International Journal of Forecasting*, 11(1), pp. 89-111. doi:10.1016/0169-2070(94)02003-8.

Kokelj, S. V. and Jorgenson, M. T. 2013. Advances in Thermokarst Research. *Permafrost and Periglacial Processes*, 24(2), pp. 108-119. doi:10.1002/ppp.1779.

Korb, K. B. and Nicholson, A. E. 2004. *Bayesian Artificial Intelligence,* London, UK, Chapman & Hall/CRC.

Koven, C. D., Riley, W. J. and Stern, A. 2013. Analysis of Permafrost Thermal Dynamics and Response to Climate Change in the CMIP5 Earth System Models. *Journal of Climate*, 26(6), pp. 1877-1900. doi:10.1175/jcli-d-12-00228.1.

Kudryavtsev, V. A., Garagulya, L. S., Kondrat'yeva, K. A. and Melamed, V. G. 1974. *Fundamentals of Frost Forecasting in Geological Engineering Investigations,* Cold Regions Research and Engineering Laboratory: Hanover, NH.

Kuhnert, P. M., Martin, T. G. and Griffiths, S. P. 2010. A guide to eliciting and using expert knowledge in Bayesian ecological models. *Ecology Letters*, 13(7), pp. 900-914. doi:10.1111/j.1461-0248.2010.01477.x.

Kwok, R., Cunningham, G. F., Wensnahan, M., Rigor, I., Zwally, H. J. and Yi, D. 2009. Thinning and volume loss of the Arctic Ocean sea ice cover: 2003-2008. *Journal of Geophysical Research-Oceans*, 114, pp. 16. doi:10.1029/2009jc005312.

Laidre, K. L., Stirling, I., Lowry, L. F., Wiig, O., Heide-Jorgensen, M. P. and Ferguson, S. H. 2008. Quantifying the sensitivity of arctic marine mammals to climate-induced habitat change. *Ecological Applications*, 18(2), pp. S97-S125. doi:10.1890/06-0546.1.

Lawrence, D. M., Slater, A. G., Romanovsky, V. E. and Nicolsky, D. J. 2008. Sensitivity of a model projection of near-surface permafrost degradation to soil column depth and representation of soil organic matter. *Journal of Geophysical Research-Earth Surface*, 113(F2), pp. 14. doi:10.1029/2007jf000883.

Lawrence, D. M. and Swenson, S. C. 2011. Permafrost response to increasing Arctic shrub abundance depends on the relative influence of shrubs on local soil cooling versus large-scale climate warming. *Environmental Research Letters*, 6(4), pp. 8. doi:10.1088/1748-9326/6/4/045504.

Lee, H., Swenson, S. C., Slater, A. G. and Lawrence, D. M. 2014. Effects of excess ground ice on projections of permafrost in a warming climate. *Environmental Research Letters*, 9(12), pp. 8. doi:10.1088/1748-9326/9/12/124006.

Liljedahl, A. K., Boike, J., Daanen, R. P., Fedorov, A. N., Frost, G. V., Grosse, G., Hinzman, L. D., Iijma, Y., Jorgenson, J. C., Matveyeva, N., Necsoiu, M., Raynolds, M. K., Romanovsky, V. E., Schulla, J., Tape, K. D., Walker, D. A., Wilson, C. J., Yabuki, H. and Zona, D. 2016. Pan-Arctic ice-wedge degradation in warming permafrost and its influence on tundra hydrology. *Nature Geoscience*, 9(4), pp. 312-+. doi:10.1038/ngeo2674.

Liu, L., Zhang, T. J. and Wahr, J. 2010. InSAR measurements of surface deformation over permafrost on the North Slope of Alaska. *Journal of Geophysical Research-Earth Surface*, 115, pp. 14. doi:10.1029/2009jf001547.

Loisel, J. and Medina-Cetina, Z. 2019. Modeling Risks in the Arctic System. *Arctic Futures 2050 Conference.* Washington, D.C.

Loisel, J., van Bellen, S., Pelletier, L., Talbot, J., Hugelius, G., Karran, D., Yu, Z. C., Nichols, J. and Holmquist, J. 2017. Insights and issues with estimating northern peatland carbon stocks and fluxes since the Last Glacial Maximum. *Earth-Science Reviews*, 165, pp. 59-80. doi:10.1016/j.earscirev.2016.12.001.

Loranty, M. M., Abbott, B. W., Blok, D., Douglas, T. A., Epstein, H. E., Forbes, B. C., Jones, B. M., Kholodov, A. L., Kropp, H., Malhotra, A., Mamet, S. D., Myers-Smith, I. H., Natali, S. M., O'Donnell, J. A., Phoenix, G. K., Rocha, A. V., Sonnentag, O., Tape, K. D. and Walker, D. A. 2018. Reviews and syntheses: Changing ecosystem influences on soil thermal regimes in northern high-latitude permafrost regions. *Biogeosciences*, 15(17), pp. 5287-5313. doi:10.5194/bg-15-5287-2018.

Lunardini, V. J. 1978. *Theory of n-factors and correlation of data,* Proceedings of the Third International Conference on Permafrost, National Research Council of Canada Ottawa, Edmonton, Alberta, Canada.

Lunardini, V. J. 1981. *Heat transfer in cold climates*, Van Nostrand Reinhold Co.

Marcot, B. G., Steventon, J. D., Sutherland, G. D. and McCann, R. K. 2006. Guidelines for developing and updating Bayesian belief networks applied to ecological modeling and conservation. *Canadian Journal of Forest Research*, 36(12), pp. 3063-3074. doi:10.1139/x06-135.

McGuire, A. D., Chapin, F. S., Walsh, J. E. and Wirth, C. 2006. Integrated regional changes in arctic climate feedbacks: Implications for the global climate system. *Annual Review of Environment and Resources.* Palo Alto: Annual Reviews.

McLaughlin, J. W. and Packalen, M. In Review. Peat carbon vulnerability to projected climate warming in the Hudson Bay Lowlands, Canada: A decision support tool for land use planning in peatland dominated landscapes. *Frontiers in Earth Science*.

Medina-Cetina, Z. and Nadim, F. 2008. Stochastic design of an early warning system. *Georisk-Assessment and Management of Risk for Engineered Systems and Geohazards*, 2(4), pp. 223-236. doi:10.1080/17499510802086777.

Meentemeyer, V. and Zippin, J. 1981. SOIL-MOISTURE AND TEXTURE CONTROLS OF SELECTED PARAMETERS OF NEEDLE ICE GROWTH. *Earth Surface Processes and Landforms*, 6(2), pp. 113-125. doi:10.1002/esp.3290060205.

Meredith, M., Sommerkorn, M., Cassotta, S., Derksen, C., Ekaykin, A., Hollowed, A., Kofinas, G., Mackintosh, A., Melbourne-Thomas, J., Muelbert, M. M. C., Ottersen, G., Pritchard, H. and Schuur, E. A. G. 2019. IPCC Special Report on the Ocean and Cryosphere in a Changing Climate. *In:* PÖRTNER, H.-O., ROBERTS, D. C., MASSON-DELMOTTE, V., ZHAI, P., TIGNOR, M., POLOCZANSKA, E., MINTENBECK, K., ALEGRÍA, A., NICOLAI, M., OKEM, A., PETZOLD, J., RAMA, B. & WEYER, N. M. (eds.) *Polar Regions.*

Myers-Smith, I. H., Forbes, B. C., Wilmking, M., Hallinger, M., Lantz, T., Blok, D., Tape, K. D., Macias-Fauria, M., Sass-Klaassen, U., Levesque, E., Boudreau, S., Ropars, P., Hermanutz, L., Trant, A., Collier, L. S., Weijers, S., Rozema, J., Rayback, S. A., Schmidt, N. M., Schaepman-Strub, G., Wipf, S., Rixen, C., Menard, C. B., Venn, S., Goetz, S., Andreu-Hayles, L., Elmendorf, S., Ravolainen, V., Welker, J., Grogan, P., Epstein, H. E. and Hik, D. S. 2011. Shrub

expansion in tundra ecosystems: dynamics, impacts and research priorities. *Environmental Research Letters*, 6(4), pp. 15. doi:10.1088/1748-9326/6/4/045509.

Myers-Smith, I. H., Kerby, J. T., Phoenix, G. K., Bjerke, J. W., Epstein, H. E., Assmann, J. J., John, C., Andreu-Hayles, L., Angers-Blondin, S., Beck, P. S. A., Berner, L. T., Bhatt, U. S., Bjorkman, A. D., Blok, D., Bryn, A., Christiansen, C. T., Cornelissen, J. H. C., Cunliffe, A. M., Elmendorf, S. C., Forbes, B. C., Goetz, S. J., Hollister, R. D., de Jong, R., Loranty, M. M., Macias-Fauria, M., Maseyk, K., Normand, S., Olofsson, J., Parker, T. C., Parmentier, F. J. W., Post, E., Schaepman-Strub, G., Stordal, F., Sullivan, P. F., Thomas, H. J. D., Tommervik, H., Treharne, R., Tweedie, C. E., Walker, D. A., Wilmking, M. and Wipf, S. 2020. Complexity revealed in the greening of the Arctic. *Nature Climate Change*, 10(2), pp. 106-117. doi:10.1038/s41558-019-0688-1.

Myhre, G., Shindell, D., Bréon, F.-M., Collins, W., Fuglestvedt, J., Huang, J., Koch, D., Lamarque, J.-F., Lee, D., Mendoza, B., Nakajima, T., Robock, A., Stephens, G., Takemura, T. and Zhang, H. 2013. Anthropogenic and Natural Radiative Forcing. *In:* STOCKER, T. F., QIN, D., PLATTNER, G.-K., TIGNOR, M., ALLEN, S. K., BOSCHUNG, J., NAUELS, A., XIA, Y., BEX, V. & MIDGLEY, P. M. (eds.) *Climate Change 2013: The Physical Science Basis. Contribution of Working Group I to the Fifth Assessment Report of the Intergovernmental Panel on Climate Change.* Cambridge, United Kingdom and New York, NY, USA.

Nelson, F. E. 1986. PERMAFROST DISTRIBUTION IN CENTRAL CANADA - APPLICATIONS OF A CLIMATE-BASED PREDICTIVE MODEL. *Annals of the Association of American Geographers*, 76(4), pp. 550-569. doi:10.1111/j.1467-8306.1986.tb00136.x.

Nelson, F. E. and Outcalt, S. I. 1987. A COMPUTATIONAL METHOD FOR PREDICTION AND REGIONALIZATION OF PERMAFROST. *Arctic and Alpine Research*, 19(3), pp. 279-288. doi:10.2307/1551363.

Nicolsky, D. J. and Romanovsky, V. E. 2018. Modeling Long-Term Permafrost Degradation. *Journal of Geophysical Research-Earth Surface*, 123(8), pp. 1756-1771. doi:10.1029/2018jf004655.

Nitze, I., Grosse, G., Jones, B. M., Romanovsky, V. E. and Boike, J. 2018. Remote sensing quantifies widespread abundance of permafrost region disturbances across the Arctic and Subarctic. *Nature Communications*, 9, pp. 11. doi:10.1038/s41467-018-07663-3.

O'Neill, H. B. and Burn, C. R. 2012. Physical and temporal factors controlling the development of near-surface ground ice at Illisarvik, western Arctic coast, Canada. *Canadian Journal of Earth Sciences*, 49(9), pp. 1096-1110. doi:10.1139/e2012-043.

Oelke, C. and Zhang, T. J. 2004. A model study of circum-arctic soil temperatures. *Permafrost and Periglacial Processes*, 15(2), pp. 103-121. doi:10.1002/ppp.485.

Olefeldt, D., Goswami, S., Grosse, G., Hayes, D., Hugelius, G., Kuhry, P., McGuire, A. D., Romanovsky, V. E., Sannel, A. B. K., Schuur, E. A. G. and Turetsky, M. R. 2016. Circumpolar distribution and carbon storage of thermokarst landscapes. *Nature Communications*, 7, pp. 11. doi:10.1038/ncomms13043.

Oleson, K. W., Lawrence, D. M., Bonan, G. B., Flanner, M. G., Kluzek, E., Lawrence, P. J., Levis, S., Swenson, S. C., Thornton, P. E., Dai, A., Decker, M., DIckinson, R., Feddema, J., Heald, C. L., Hoffman, F., Lamarque, J. F., Mahowald, N., Niu, G.-Y., Qian, T., Randerson, J., Running, S., Sakaguchi, K., Slater, A. G., Stockli, R., Wang, A., Yang, Z.-L., Zeng, X. and Zeng, X. 2010. Technical Description of version 4.0 of the Community Land Model. Boulder, CO: National Center for Atmospheric Research.

Overeem, I., Jafarov, E., Wang, K., Schaefer, K., Stewart, S., Clow, G., Piper, M. and Elshorbany, Y. 2018. A modeling toolbox for permafrost landscapes Eos.

Park, H., Sherstiukov, A. B., Fedorov, A. N., Polyakov, I. V. and Walsh, J. E. 2014. An observation-based assessment of the influences of air temperature and snow depth on soil temperature in Russia. *Environmental Research Letters*, 9(6), pp. 7. doi:10.1088/1748-9326/9/6/064026.

Parmentier, F. J. W., Christensen, T. R., Rysgaard, S., Bendtsen, J., Glud, R. N., Else, B., van Huissteden, J., Sachs, T., Vonk, J. E. and Sejr, M. K. 2017. A synthesis of the arctic terrestrial and marine carbon cycles under pressure from a dwindling cryosphere. *Ambio*, 46, pp. S53-S69. doi:10.1007/s13280-016-0872-8.

Permafrost Subcommittee. 1988. Glossary of Permafrost and Related Ground-Ice Terms. National Research Council of Canada.

Petzold, D. E. and Mulhern, T. 1987. VEGETATION DISTRIBUTIONS ALONG LICHEN-DOMINATED SLOPES OF OPPOSING ASPECT IN THE EASTERN CANADIAN SUB-ARCTIC. *Arctic*, 40(3), pp. 221-224.

Pistone, K., Eisenman, I. and Ramanathan, V. 2014. Observational determination of albedo decrease caused by vanishing Arctic sea ice. *Proceedings of the National Academy of Sciences of the United States of America*, 111(9), pp. 3322-3326. doi:10.1073/pnas.1318201111.

Qin, Y., Chen, J. S., Yang, D. W. and Wang, T. H. 2018. Estimating Seasonally Frozen Ground Depth From Historical Climate Data and Site Measurements Using a Bayesian Model. *Water Resources Research*, 54(7), pp. 4361-4375. doi:10.1029/2017wr022185.

Quinton, W. L., Gray, D. M. and Marsh, P. 2000. Subsurface drainage from hummock-covered hillslopes in the Arctic tundra. *Journal of Hydrology*, 237(1-2), pp. 113-125. doi:10.1016/s0022-1694(00)00304-8.

Rekacewicz, P. 2005. *Circumpolar Active-Layer Permafrost System (CAPS), version 1.0. Data from International Permafrost Associate 1998*.

Riseborough, D. 2007. The effect of transient conditions on an equilibrium permafrost-climate model. *Permafrost and Periglacial Processes*, 18(1), pp. 21-32. doi:10.1002/ppp.579.

Riseborough, D., Shiklomanov, N., Etzelmuller, B., Gruber, S. and Marchenko, S. 2008. Recent advances in permafrost modelling. *Permafrost and Periglacial Processes*, 19(2), pp. 137-156. doi:10.1002/ppp.615.

Rouse, W. R., Douglas, M. S. V., Hecky, R. E., Hershey, A. E., Kling, G. W., Lesack, L., Marsh, P., McDonald, M., Nicholson, B. J., Roulet, N. T. and Smol, J. P. 1997. Effects of climate change on the freshwaters of arctic and subarctic North America. *Hydrological Processes*, 11(8), pp. 873-902. doi:10.1002/(sici)1099-1085(19970630)11:8<873::aid-hyp510>3.0.co;2-6.

Rykiel, E. J. 1996. Testing ecological models: The meaning of validation. *Ecological Modelling*, 90(3), pp. 229-244. doi:10.1016/0304-3800(95)00152-2.

Schuur, E. A. G. and Mack, M. C. 2018. Ecological Response to Permafrost Thaw and Consequences for Local and Global Ecosystem Services. *Annual Review of Ecology, Evolution, and Systematics, Vol 49*, 49, pp. 279-301. doi:10.1146/annurev-ecolsys-121415-032349.

Schuur, E. A. G., McGuire, A. D., Schadel, C., Grosse, G., Harden, J. W., Hayes, D. J., Hugelius, G., Koven, C. D., Kuhry, P., Lawrence, D. M., Natali, S. M., Olefeldt, D., Romanovsky, V. E., Schaefer, K., Turetsky, M. R., Treat, C. C. and Vonk, J. E. 2015. Climate change and the permafrost carbon feedback. *Nature*, 520(7546), pp. 171-179. doi:10.1038/nature14338.

Schuur, E. A. G., Vogel, J. G., Crummer, K. G., Lee, H., Sickman, J. O. and Osterkamp, T. E. 2009. The effect of permafrost thaw on old carbon release and net carbon exchange from tundra. *Nature*, 459(7246), pp. 556-559. doi:10.1038/nature08031.

Screen, J. A. and Simmonds, I. 2010. The central role of diminishing sea ice in recent Arctic temperature amplification. *Nature*, 464(7293), pp. 1334-1337. doi:10.1038/nature09051.

Screen, J. A. and Simmonds, I. 2012. Declining summer snowfall in the Arctic: causes, impacts and feedbacks. *Climate Dynamics*, 38(11-12), pp. 2243-2256. doi:10.1007/s00382-011-1105-2.

Serreze, M. C., Barrett, A. P., Stroeve, J. C., Kindig, D. N. and Holland, M. M. 2009. The emergence of surface-based Arctic amplification. *Cryosphere*, 3(1), pp. 11-19. doi:10.5194/tc-3-11-2009.

Serreze, M. C. and Barry, R. G. 2014. *The Arctic Climate System,* New York, NY, Cambridge University Press.

Serreze, M. C., Holland, M. M. and Stroeve, J. 2007. Perspectives on the Arctic's shrinking sea-ice cover. *Science*, 315(5818), pp. 1533-1536. doi:10.1126/science.1139426.

Serreze, M. C. and Meier, W. N. 2019. The Arctic's sea ice cover: trends, variability, predictability, and comparisons to the Antarctic. *Annals of the New York Academy of Sciences*, 1436(1), pp. 36-53. doi:10.1111/nyas.13856.

Smith, M. W. and Riseborough, D. W. 1996. Permafrost monitoring and detection of climate change. *Permafrost and Periglacial Processes*, 7(4), pp. 301-309. doi:10.1002/(sici)1099-1530(199610)7:4<301::aid-ppp231>3.0.co;2-r.

Stiegler, C., Johansson, M., Christensen, T. R., Mastepanov, M. and Lindroth, A. 2016. Tundra permafrost thaw causes significant shifts in energy partitioning. *Tellus Series B-Chemical and Physical Meteorology*, 68, pp. 11. doi:10.3402/tellusb.v68.30467.

Stroeve, J. C., Markus, T., Boisvert, L., Miller, J. and Barrett, A. 2014. Changes in Arctic melt season and implications for sea ice loss. *Geophysical Research Letters*, 41(4), pp. 1216-1225. doi:10.1002/2013gl058951.

Sweet, S. K., Griffin, K. L., Steltzer, H., Gough, L. and Boelman, N. T. 2015. Greater deciduous shrub abundance extends tundra peak season and increases modeled net CO2 uptake. *Global Change Biology*, 21(6), pp. 2394-2409. doi:10.1111/gcb.12852.

Tao, J., Reichle, R. H., Koster, R. D., Forman, B. A. and Xue, Y. 2017. Evaluation and Enhancement of Permafrost Modeling With the NASA Catchment Land Surface Model. *Journal of Advances in Modeling Earth Systems*, 9(7), pp. 2771-2795. doi:10.1002/2017ms001019.

Tarnocai, C., Canadell, J. G., Schuur, E. A. G., Kuhry, P., Mazhitova, G. and Zimov, S. 2009. Soil organic carbon pools in the northern circumpolar permafrost region. *Global Biogeochemical Cycles*, 23. doi:10.1029/2008gb003327.

The Nature Conservancy. 2009. Terrestrial Ecoregions. *The Nature Conservancy*.

Tian, H. Q., Lu, C. Q., Yang, J., Banger, K., Huntzinger, D. N., Schwalm, C. R., Michalak, A. M., Cook, R., Ciais, P., Hayes, D., Huang, M. Y., Ito, A., Jain, A. K., Lei, H. M., Mao, J. F., Pan, S. F., Post, W. M., Peng, S. S., Poulter, B., Ren, W., Ricciuto, D., Schaefer, K., Shi, X. Y., Tao, B., Wang, W. L., Wei, Y. X., Yang, Q. C., Zhang, B. W. and Zeng, N. 2015. Global patterns and controls of

soil organic carbon dynamics as simulated by multiple terrestrial biosphere models: Current status and future directions. *Global Biogeochemical Cycles*, 29(6), pp. 775-792. doi:10.1002/2014gb005021.

Uusitalo, L. 2007. Advantages and challenges of Bayesian networks in environmental modelling. *Ecological Modelling*, 203(3-4), pp. 312-318. doi:10.1016/j.ecolmodel.2006.11.033.

Varela Gonzalez, P. Y. 2017. *Probabilistic Risk Mapping Coupling Bayesian Networks and GIS, and Bayesian Model Calibration of Submarine Landslides.* Doctor of Philosophy, Texas A&M University.

Wainwright, H. M., Liljedahl, A. K., Dafflon, B., Ulrich, C., Peterson, J. E., Gusmeroli, A. and Hubbard, S. S. 2017. Mapping snow depth within a tundra ecosystem using multiscale observations and Bayesian methods. *Cryosphere*, 11(2), pp. 857-875. doi:10.5194/tc-11-857-2017.

Weber, P., Medina-Oliva, G., Simon, C. and Iung, B. 2012. Overview on Bayesian networks applications for dependability, risk analysis and maintenance areas. *Engineering Applications of Artificial Intelligence*, 25(4), pp. 671-682. doi:10.1016/j.engappai.2010.06.002.

Webster, K. L. and McLaughlin, J. W. 2014. Application of a Bayesian belief network for assessing the vulnerability of permafrost to thaw and implications for greenhouse gas production and climate feedback. *Environmental Science & Policy*, 38, pp. 28-44. doi:10.1016/j.envsci.2013.10.008.

Westermann, S., Boike, J., Langer, M., Schuler, T. V. and Etzelmuller, B. 2011. Modeling the impact of wintertime rain events on the thermal regime of permafrost. *Cryosphere*, 5(4), pp. 945-959. doi:10.5194/tc-5-945-2011.

Westermann, S., Langer, M., Boike, J., Heikenfeld, M., Peter, M., Etzelmuller, B. and Krinner, G. 2016. Simulating the thermal regime and thaw processes of ice-rich permafrost ground with the land-surface model CryoGrid 3. *Geoscientific Model Development*, 9(2), pp. 523-546. doi:10.5194/gmd-9-523-2016.

Wilcox, E. J., Keim, D., de Jong, T., Walker, B., Sonnentag, O., Sniderhan, A. E., Mann, P. and Marsh, P. 2019. Tundra shrub expansion may amplify permafrost thaw by

advancing snowmelt timing. *Arctic Science*, 5(4), pp. 202-217. doi:10.1139/as-2018-0028.

Woodard, D. L., Shiklomanov, A. N., Kravitz, B., Hartin, C. and Bond-Lamberty, B. 2021. A Permafrost Implementation in the Simple Carbon-Climate Model Hector. *Geosci. Model Dev. Discuss.*, 2021, pp. 1-21. doi:10.5194/gmd-2020-377.

Xu, X. T., Zhang, W. D., Fan, C. X. and Li, G. S. 2020. Effects of temperature, dry density and water content on the thermal conductivity of Genhe silty clay. *Results in Physics*, 16, pp. 10. doi:10.1016/j.rinp.2019.102830.

Young, K. L., Woo, M. K. and Edlund, S. A. 1997. Influence of local topography, soils, and vegetation on microclimate and hydrology at a high Arctic site, Ellesmere Island, Canada. *Arctic and Alpine Research*, 29(3), pp. 270-284. doi:10.2307/1552141.

Zhang, C., Zhang, D., Zhang, M. Y., Lang, X. and Mao, W. G. 2020. An integrated risk assessment model for safe Arctic navigation. *Transportation Research Part a-Policy and Practice*, 142, pp. 101-114. doi:10.1016/j.tra.2020.10.017.

Zhang, T., Barry, R. G., Knowles, K., Ling, F. and Armstrong, R. L. 2003. Distribution of seasonally and perennially frozen ground in the Northern Hemisphere. *Permafrost, Vols 1 and 2*, pp. 1289-1294.

Zhang, T., Osterkamp, T. E. and Stamnes, K. 1996. Influence of the depth hoar layer of the seasonal snow cover on the ground thermal regime. *Water Resources Research*, 32(7), pp. 2075-2086. doi:10.1029/96wr00996.

Zhang, Y., Chen, W. J. and Riseborough, D. W. 2006. Temporal and spatial changes of permafrost in Canada since the end of the Little Ice Age. *Journal of Geophysical Research-Atmospheres*, 111(D22), pp. 14. doi:10.1029/2006jd007284.

Zhang, Y., Sherstiukov, A. B., Qian, B. D., Kokelj, S. V. and Lantz, T. C. 2018. Impacts of snow on soil temperature observed across the circumpolar north. *Environmental Research Letters*, 13(4), pp. 10. doi:10.1088/1748-9326/aab1e7.

Zhao, R., Li, Z. W., Feng, G. C., Wang, Q. J. and Hu, J. 2016. Monitoring surface deformation over permafrost with an improved SBAS-InSAR algorithm: With emphasis on climatic factors modeling. *Remote Sensing of Environment*, 184, pp. 276-287. doi:10.1016/j.rse.2016.07.019.

Zheng, L., Overeem, I., Wang, K. and Clow, G. D. 2019. Changing Arctic River Dynamics Cause Localized Permafrost Thaw. *Journal of Geophysical Research-Earth Surface*, 124(9), pp. 2324-2344. doi:10.1029/2019jf005060.

Zwieback, S., Westermann, S., Langer, M., Boike, J., Marsh, P. and Berg, A. 2019. Improving Permafrost Modeling by Assimilating Remotely Sensed Soil Moisture. *Water Resources Research*, 55(3), pp. 1814-1832. doi:10.1029/2018wr023247.

APPENDIX A

CONDITIONAL PROBABILITY TABLES USED IN PERMABN

The conditional probability tables (CPTs) used in the pre-validation, expert assessment validation, and evaluation stages of the PermaBN model development process can be found in an external file accompanying this document.

APPENDIX B

PROGNOSIS AND DIAGNOSIS EXPERIMENTS

A full list of the prognosis and diagnosis experiments and their results can be found in an external file accompanying this document.

APPENDIX C

ANALYSIS OF SOIL MOISTURE AND SOIL TEMPERATURE CONDITIONS IN TRAIL VALLEY CREEK, NORTHWEST TERRITORIES, CANADA

Summary

Soil moisture and soil temperature are key drivers of ecosystem functioning in the Arctic, as changes in these variables can initiate secondary impacts in vegetation, permafrost, and more. While soil moisture is known to alter soil thermal dynamics, it is uncertain whether the influence of soil moisture on thermal conductivity or evaporative processes, which would increase and decrease soil temperatures, respectively, is dominant. It is also uncertain whether the influences of soil moisture on soil temperature are consistent across space (i.e., depth and site location) and time (i.e., season). Regression analyses were conducted for two sites in the continuous permafrost region of the Arctic to assess the sign and significance of correlations between soil moisture and soil temperature by depth, season, and location. Results showed that there is an overall positive, significant correlation between soil moisture and soil temperature at both Trail Valley Creek, Northwest Territories, and Prudhoe Bay, Alaska, indicating the dominance of thermal conductivity over evaporative processes at both sites. Seasonal correlations vary in sign and significant, but there are suggestions that evaporative processes may be dominant in the summer, particularly at Trail Valley Creek. Comparisons between the two sites also revealed that the soil conditions are statistically different throughout the year at each site, which in combination with the regression

analyses suggest the importance of local conditions on soil properties. This has implications for the inclusion of soil dynamics in Arctic ecosystem modeling efforts and underscores the need for thoroughly characterizing the conditions of the application domain when developing those models. The methods and results for Trail Valley Creek are detailed below.

Methods

Study Area: The relationship between soil moisture and soil temperature is analyzed at the continuous permafrost region site of Trail Valley Creek, Northwest Territories, Canada (Figure C-1). For a general description of the Trail Valley Creek area, please refer to Section 3.3.

Figure C-1 Google Earth imagery showing the position of the Trail Valley Creek measurements.

Datasets: Boike et al. (2020) collected hourly single-point volumetric soil moisture content and soil temperature observations from 27 August 2016 – 2 August 2019 at 2, 5, 10, and 20 cm depths at the Trail Valley Creek site. The dataset was aggregated to a mean weekly temporal scale in order to smooth out the data, which occasionally had missing hourly values. The weekly data were also assigned a season (e.g., winter, spring, summer, or autumn) based on the solstices and equinoxes. For instance, winter is defined as those weeks including the winter solstice (i.e., December 21 or 22) through the spring equinox (i.e., March 20). This division allows for both an annual weekly analysis as well as an additional seasonal analysis that aims to roughly capture the snow versus snow-free seasons. For analysis, the annual time scales considered are Winter 2016 – Autumn 2017, Winter 2017 – Autumn 2018, and Winter 2018 – Summer 2019. The final year is shorter due to the early end of the Trail Valley Creek observations.

Regression Analyses and Comparison of Trends: Prior to regression analysis, the data were checked for normality and homoscedasticity. Residual analysis in combination with the results of Shapiro and Levene's tests showed that the dataset was both non-normal and heteroscedastic. It should be noted that the appearance of a pattern in the residual analysis indicates that additional predictor variables may be missing; while adding additional predictor variables, such as air temperature or precipitation, may enhance the regression analyses ability to predict soil temperatures, that was outside the scope of this analysis. Since the basic assumptions of linear regression analysis were violated, a non-linear regression using a 3rd order polynomial fit, which was determined

through an AIC analysis, and Spearman correlations were used to assess soil temperature as a function of soil moisture for each depth at both annual and seasonal time scales. Trends between the two Trail Valley Creek and Prudhoe Bay sites (latter not shown or detailed) were compared by assessing the correlation coefficients and p-values from each plot and conducting Friedman tests between variables and sites. Here, a p-value less than 0.05 was considered significant. In the Friedman test to assess differences in the variables by season at each site, groups were defined by week and blocks were defined by year. Similarly, to assess differences in the variables by location for each year, groups were defined by location and blocks were defined by week.

Results

Soil Observations: Trail Valley Creek yearly soil temperature and soil moisture trends for 5 cm and 20 cm depths are seen in Figure C-2. Values are plotted for 2016 – 2019, and the dotted lines represent the weekly seasonal divisions where weeks 51 – 52/1 – 12 are winter, 13 – 24 are spring, 25 – 38 are summer, and 39 – 50 are autumn. While the 2016 and 2019 time series are incomplete, they appear to be within a similar range as the other years. Winter/autumn temperatures also appear to vary more from year to year than summer/spring temperatures.

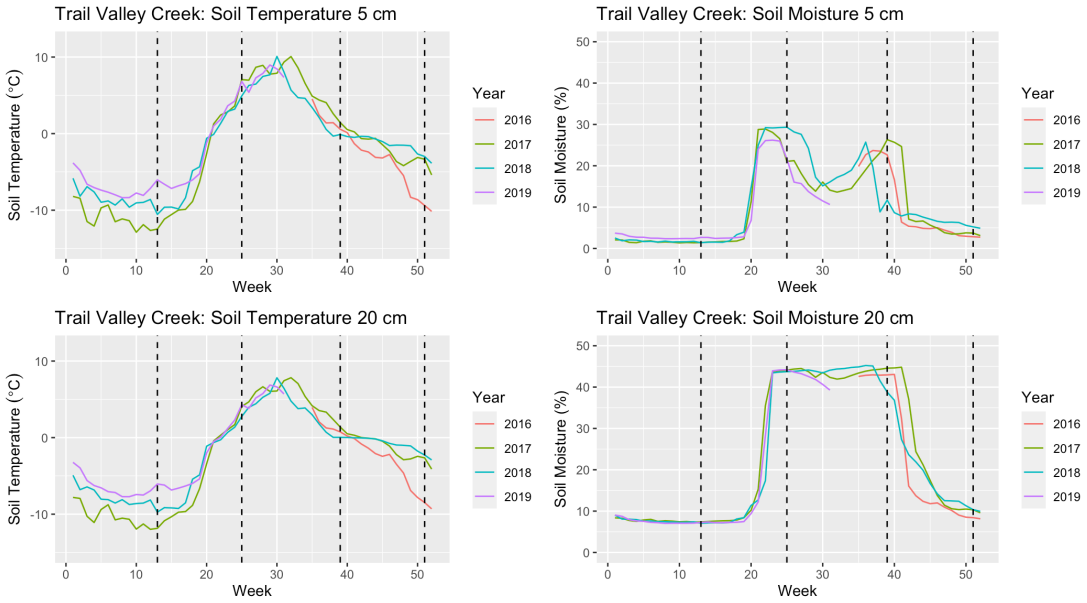

Figure C-2 Weekly soil temperature and soil moisture plots for Trail Valley Creek. Dotted black lines indicate seasonal divisions. The soil records for 2016 and 2019 are incomplete at Trail Valley Creek.

Soil temperatures steadily increase through the spring before peaking in early to mid-summer. Temperatures steadily decrease through autumn before reaching their minimum in winter. At Trail Valley Creek, the soil temperature generally decreases with depth, from -1.72°C near the surface (2 cm) to -2.35°C further beneath the surface (20 cm). Soil moisture rapidly increases beginning in mid-spring and rapidly decreases at the beginning of autumn. The 5 cm trend is more variable than that of the 20 cm, as two peaks in soil moisture are seen – one in late spring and a smaller one in late summer/early autumn. Soil moisture values closer to the surface are also not as constant through the summer as they are farther down the soil column. At Trail Valley Creek, the soil moisture content generally increases with depth, from 7.96% at 2 cm to 22.05% at 20 cm.

Annual Regressions: The annual non-linear regressions for the 5 cm and 20 cm depths are shown in Figure C-3. For each year, seasonal correlations and p-values are given. Overall, negative correlations are seen in the summer, and positive correlations are seen in autumn, winter, and spring. While the correlations and p-values need to be regarded with caution as a result of the non-normal and non-homoscedastic nature of the data, it appears that the only year where summer correlations are significant was Winter 2016 – Autumn 2017. Correlations for all other seasons are significant for each of the three years. When the observations are considered collectively (i.e., not divided by season), the correlations between soil moisture and soil temperature are positive and significant for all years.

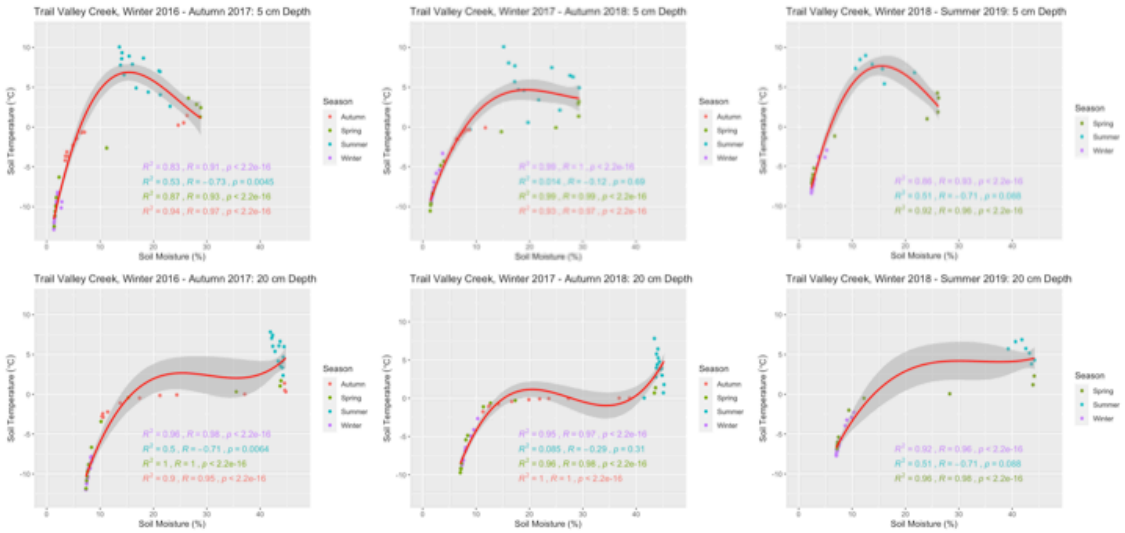

Figure C-3 Annual non-linear regressions for 5 cm and 20 cm soil observations at Trail Valley Creek. Correlations and significance values for each season are included.

Seasonal Regressions for Entire Record: Non-linear regressions combining all years for each available depth are shown in Figure C-4. Summer trends are negative and significant for all depths while the autumn, winter, and spring trends are positive and significant for all depths. However, the strength of the correlations is generally quite low for the summer. In addition, correlation strength is moderately low for winter, with the exception of the 20 cm depth where the winter correlation is very low. Similar to the winter correlations, the 20 cm spring correlations are also low. The most consistent trends are in autumn, the R^2 and R values of which vary by at most 0.02 or 0.03 across the soil column.

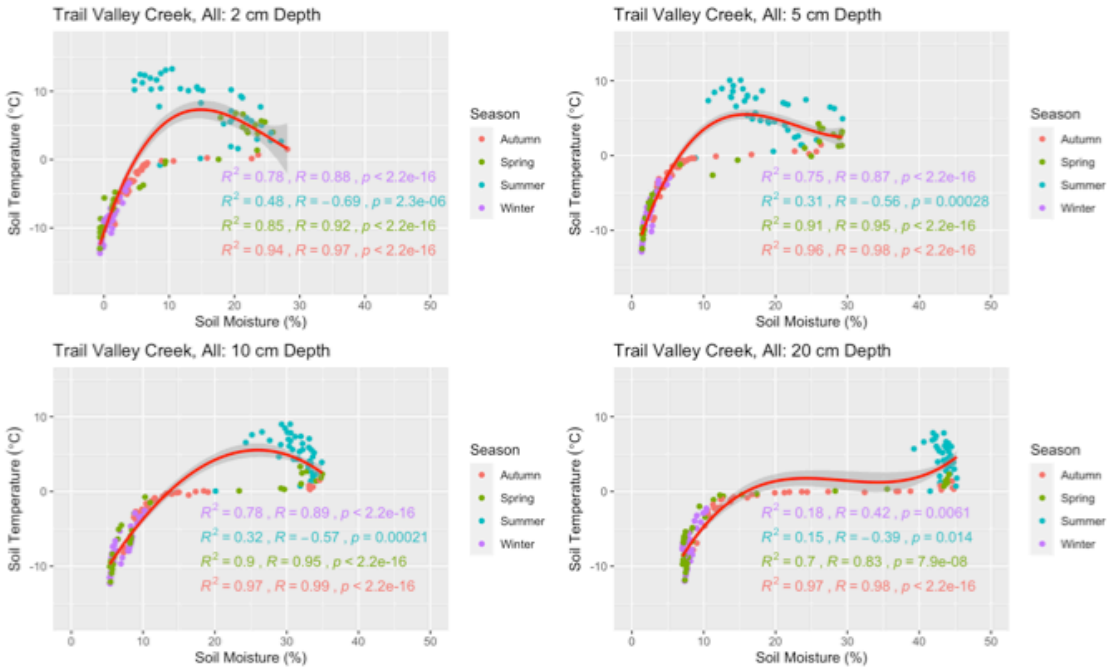

Figure C-4 Seasonal non-linear regressions for Trail Valley Creek for the period 27 August 2016 to 2 August 2019. Correlations and significance values for each season are included.

Limitations

Limitations of this study include the limited (annual) time series, single point observations, general lack of Arctic soil observations, and data distributions. The study of Arctic soil characteristics in particular is especially hindered by spare observational data in the region. Limited annual time series hinder the ability to clearly see whether there is interannual variability in soil moisture and/or soil temperature trends, but annual time series of soil moisture and soil temperature are uncommon, as most observations are only collected for individual years and/or in the summer months. Comprehensive soil datasets that overlap temporally with field observations in other locations are also uncommon. Limited spatial coverage is also a problem, as the heterogeneity in soil moisture and temperature conditions for a particular location cannot be as accurately characterized. Observational data sparsity also extends to meteorological data, though to a lesser extent. At Trail Valley Creek, for instance, there are no publicly available local air temperature and precipitation datasets. Instead, some studies use air temperature and precipitation data from the Inuvik and/or Tuktoyaktuk weather stations, which are approximately 45 km south and 80 km north of Trail Valley Creek, respectively (Wilcox et al., 2019). This lack of meteorological data hinders the ability to compare soil conditions to weather conditions that may have influenced the soil properties, such as unusually high air temperatures or amounts of precipitation. Finally, the non-normal and heteroskedastic data violates the assumptions of many statistical methods, namely, common parametric tests such as linear regression and ANOVA.

Conclusions

The results of this study show that there is a positive correlation between soil temperature and soil moisture at Trail Valley Creek, though the sign and significance of the correlation can vary by depth and/or season. This suggests that the influence of thermal conductivity dominates in most or all seasons, though the dominance of evaporative processes in the summer cannot be conclusively ruled out despite the mostly insignificant summer correlations. Ultimately, this study highlights the complicated, non-linear relationship between soil moisture and soil temperature and the importance of understanding the local conditions of a study site or region in order to fully understand how soil conditions may change in a warming Arctic. Further research is needed to conclusively determine the correlation(s) between soil moisture and soil temperature. This may be aided by assessing the influence of additional variables, such as air temperature, precipitation, and vegetation along with the soil conditions. Nonetheless, the results here were used to update the relationships between the soil moisture and soil temperature nodes in the PermaBN model given the relative proximity between these measurements and those taken in the Siksik Creek Basin.

APPENDIX D

DESCRIPTIVE STATISTICS FOR SIKSIK CREEK BASIN PHYISICAL OBSERVATIONS

As stated in the text, physical observations are available for aspect, vegetation height, and frost table depth (i.e., thaw depth) in the Siksik Creek Basin. Measures of central tendency (mean, median, and mode), variance (standard deviation), and eCDFs for the ss1 and ss1lys transects are shown here to provide justification for the decision to group the two transects together. It should again be noted that frost table depth was the only variable to change over the course of the 2015-06-11 to 2015-08-20 study period and also the only purely continuous variable. Frost table depth, which coincides with the permafrost table when the active layer is completely thawed and is the upper limit of permafrost, is calculated as the average between the hummock and interhummock frost table depth heights.

Measures of Central Tendency

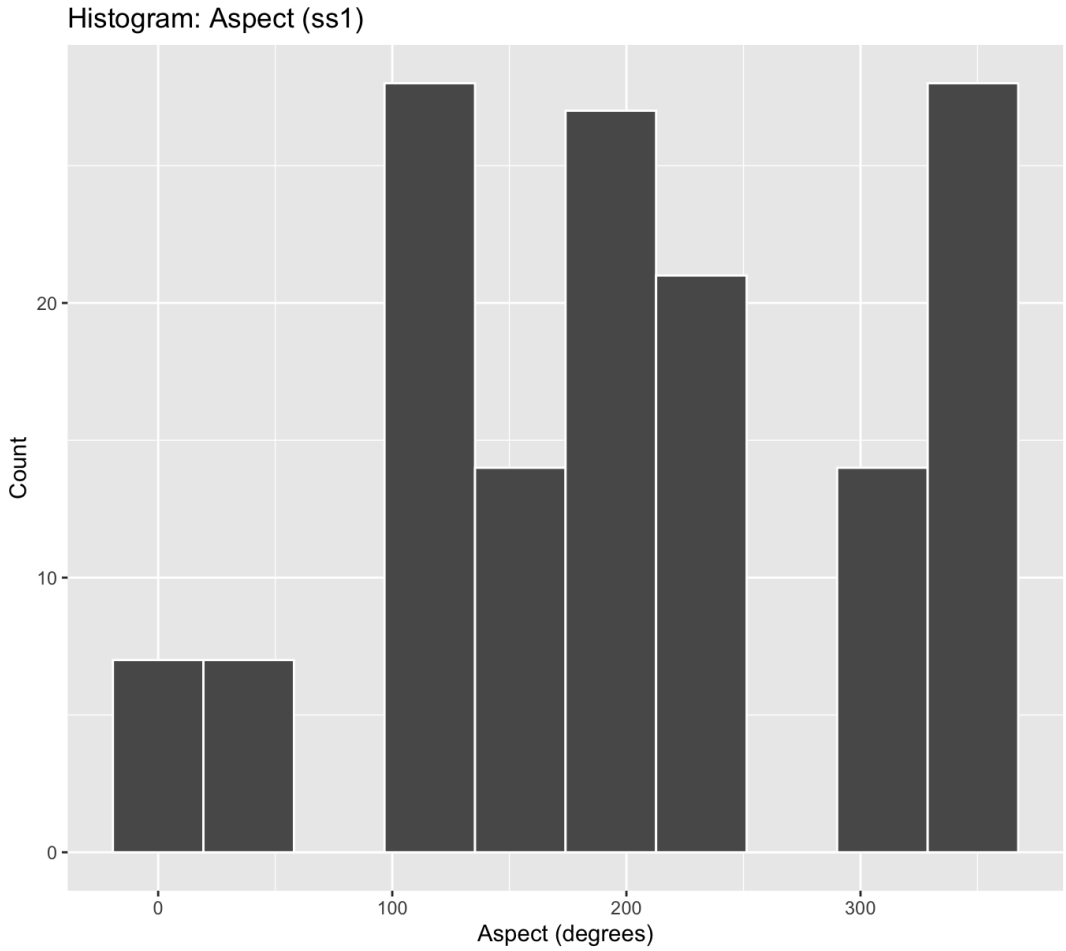

Figure D-1 Histogram (bins = 10) for aspect (degrees) along transect ss1. On average, slopes along this transect are south-facing with a high frequency of north-facing slopes.

Table D-1 Mean, median, mode, and standard deviation of aspect along transect ss1.

Mean	Median	Mode	Standard Deviation
204.9353	209.744	350.751	101.7632

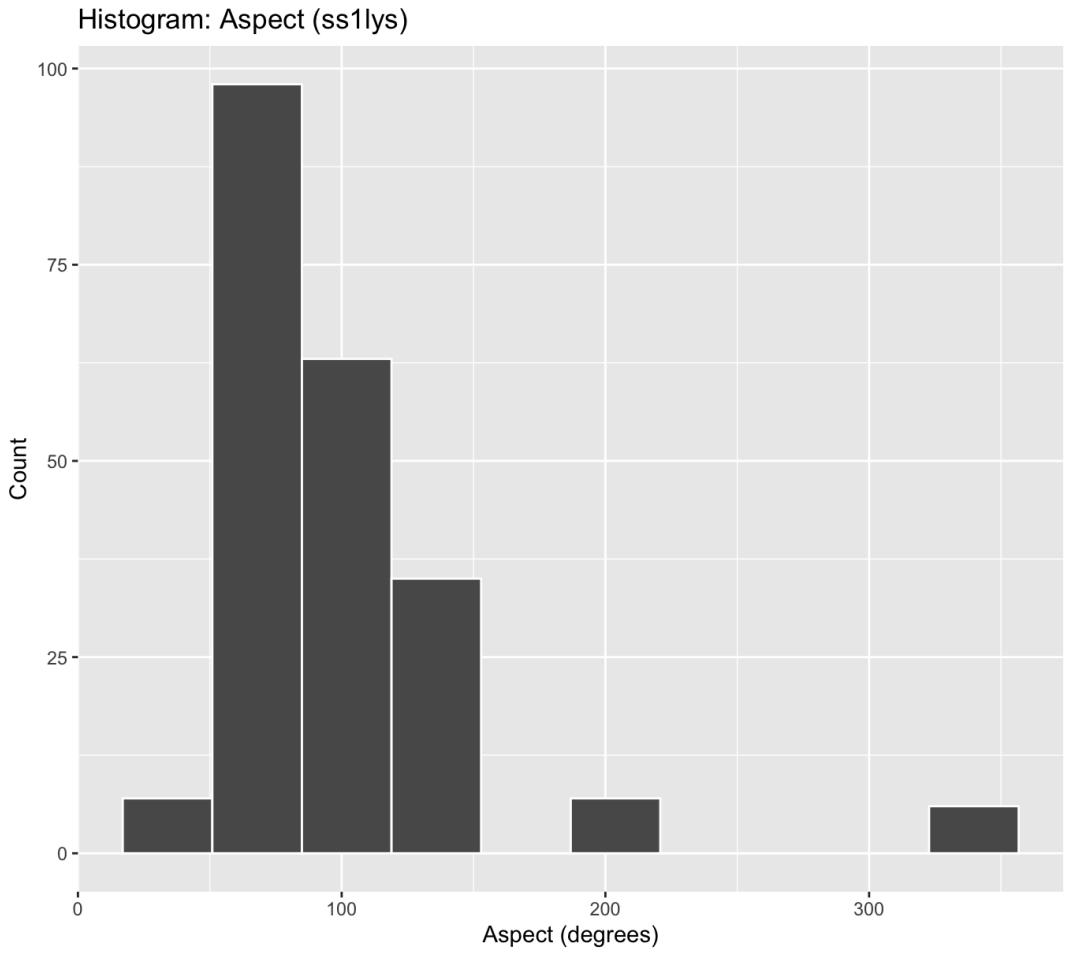

Figure D-2 Histogram (bins = 10) for aspect (degrees) along transect ss1lys. On average, slopes along this transect are east-facing with a high frequency of south-facing slopes.

Table D-2 Mean, median, mode, and standard deviation of aspect along transect ss1lys.

Mean	Median	Mode	Standard Deviation
100.7391	87.7088	150.944	54.33444

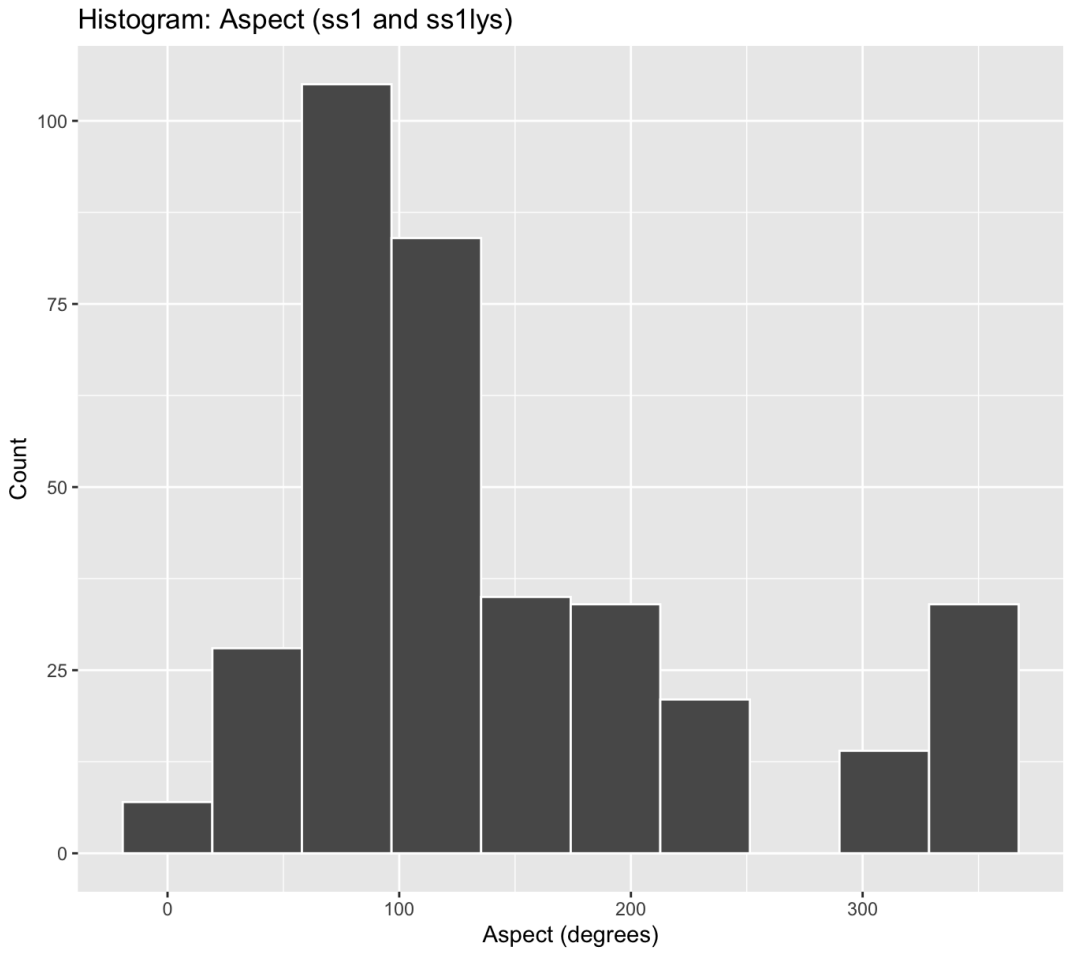

Figure D-3 Histogram (bins = 10) for aspect (degrees) along both transect ss1 and ss1lys. On average, slopes along this transect are south-facing with a high frequency of north-facing slopes; the median aspect is east-facing.

Table D-3 Mean, median, mode, and standard deviation of aspect along transects ss1 and ss1lys.

Mean	Median	Mode	Standard Deviation
142.763	106.388	350.751	92.39982

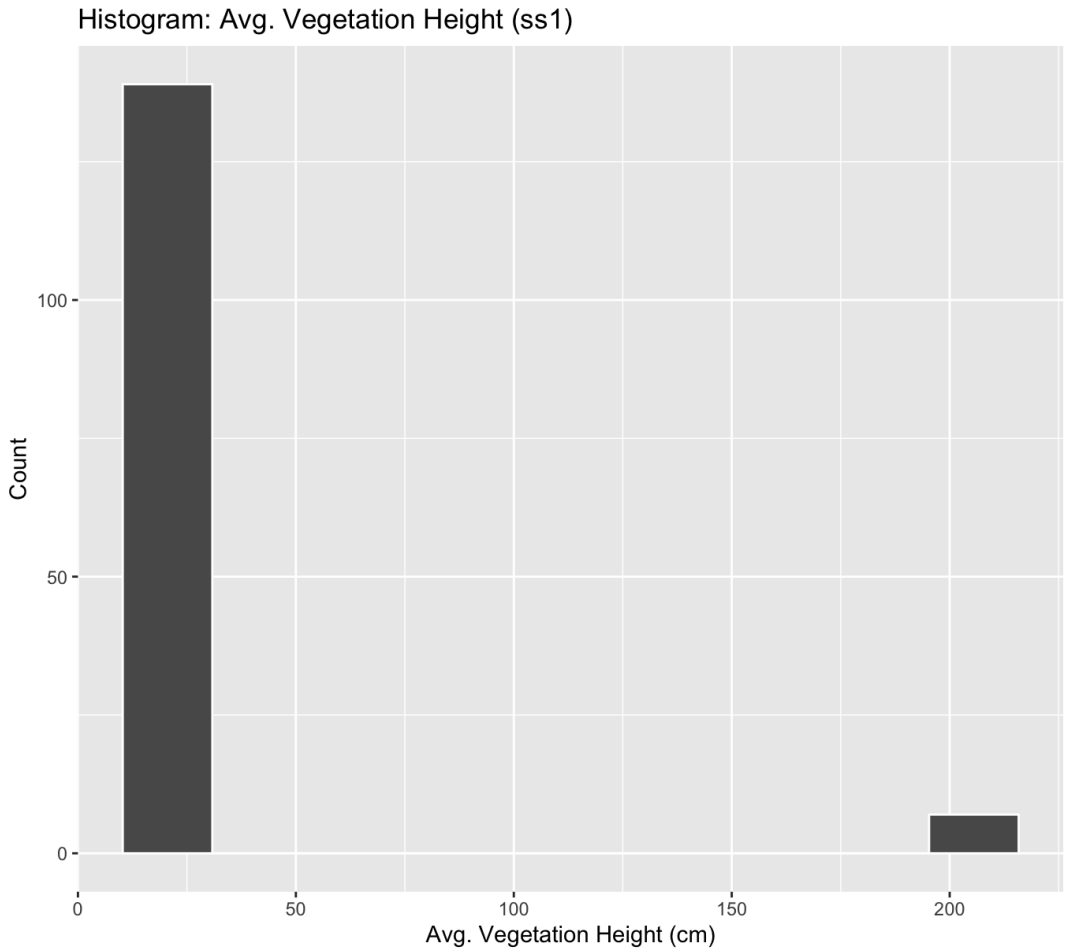

Figure D-4 Histogram (bins = 10) for average vegetation height (cm) along transect ss1. The average vegetation heights equate to predominantly tundra vegetation (average 15 cm in height) with some channel vegetation (average 200 cm in height).

Note: measures of central tendency are not provided due to the discrete nature of the vegetation height variable.

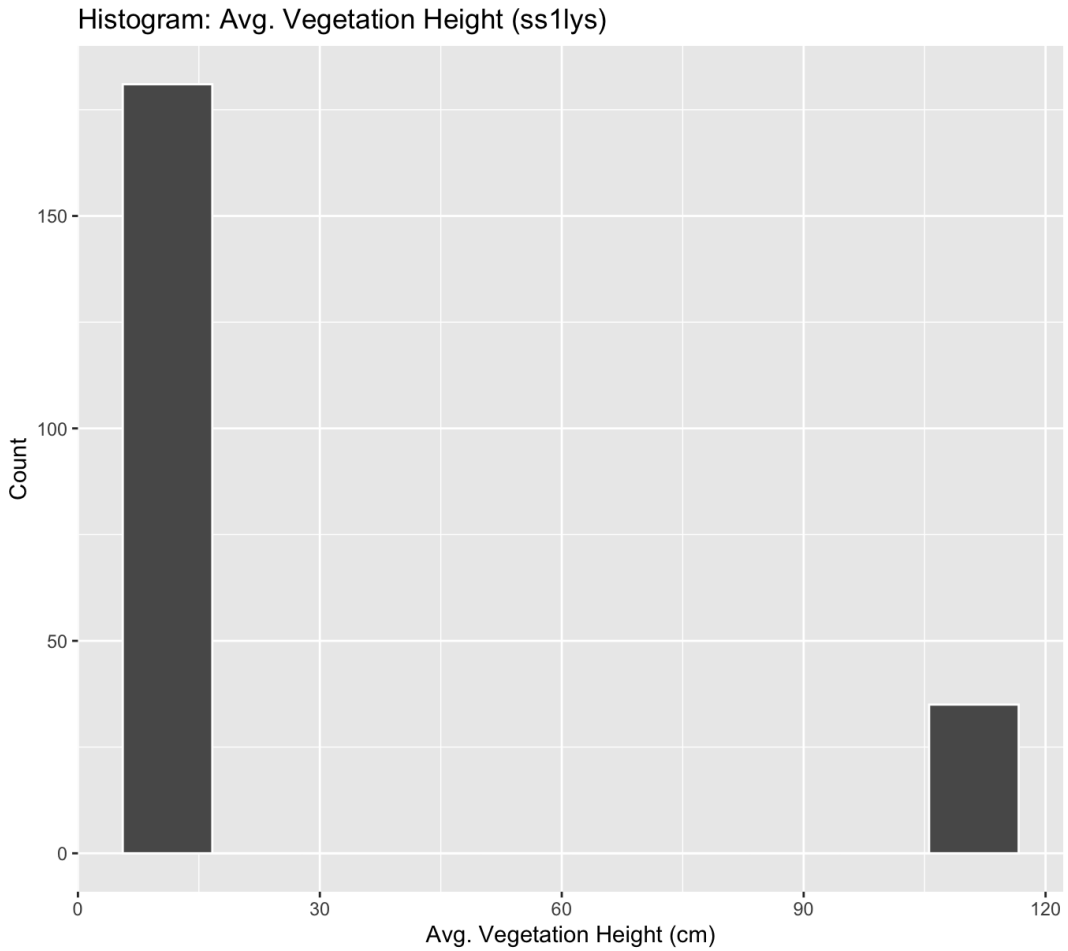

Figure D-5 Histogram (bins = 10) for average vegetation height (cm) along transect ss1lys. The average vegetation heights equate to predominantly tundra vegetation (average 15 cm in height) with some alder vegetation (average 115 cm in height).

Note: measures of central tendency are not provided due to the discrete nature of the vegetation height variable.

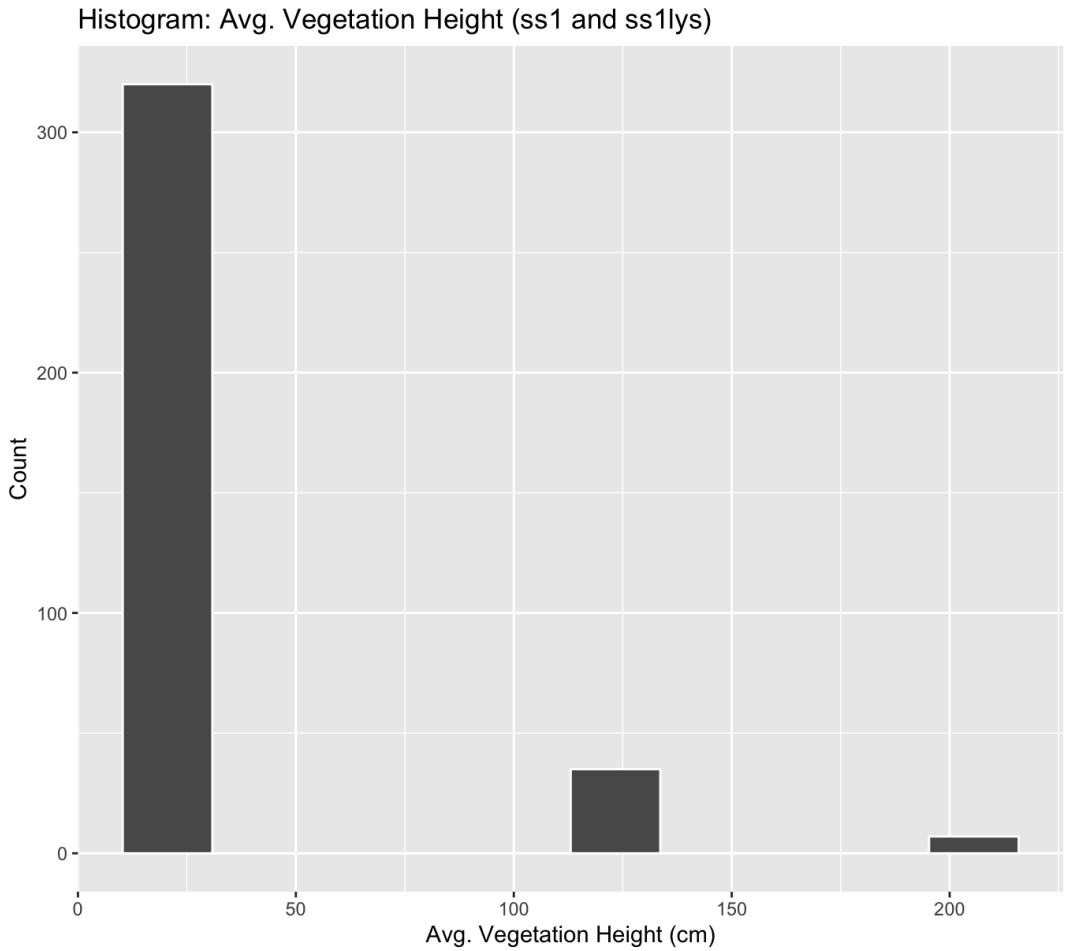

Figure D-6 Histogram (bins = 10) for average vegetation height (cm) along both transect ss1 and ss1lys. Tundra vegetation is most common, followed by alder and channel vegetation.

Note: measures of central tendency are not provided due to the discrete nature of the vegetation height variable.

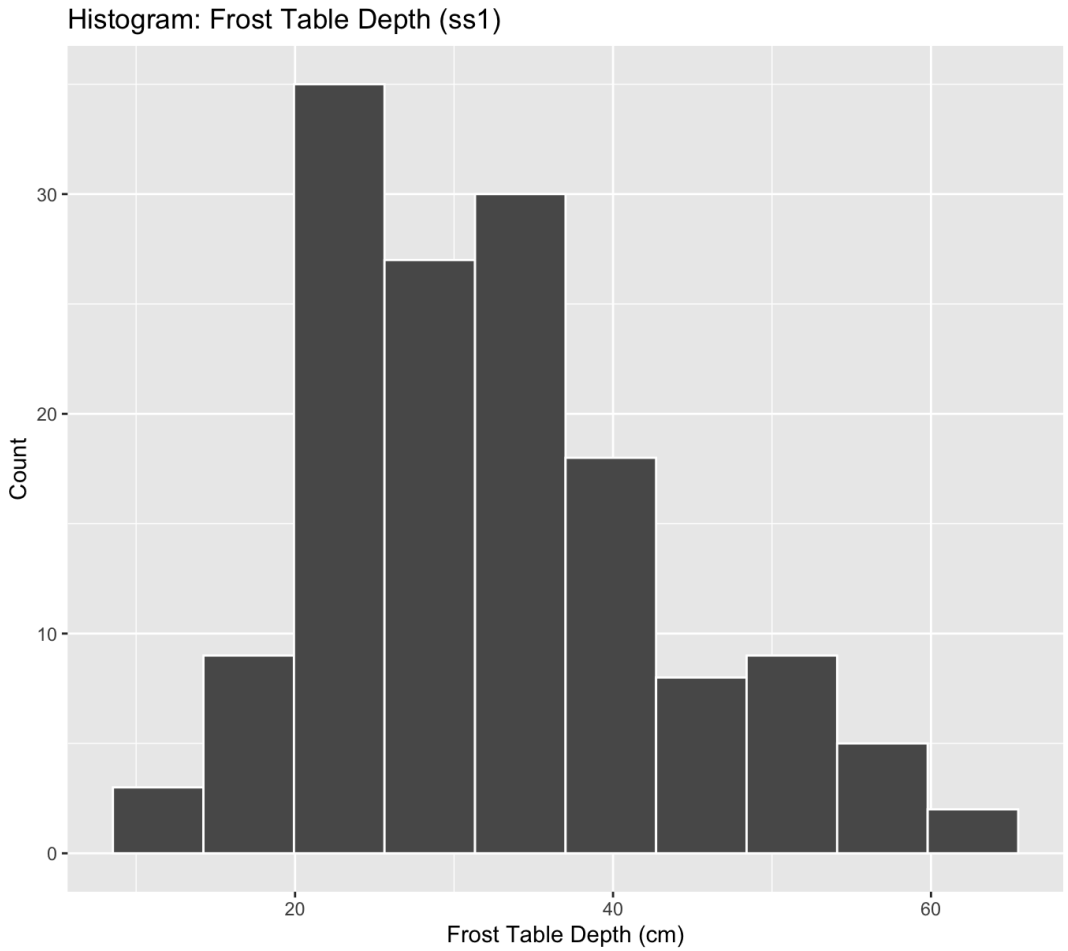

Figure D-7 Histogram (bins = 10) for frost table depth (cm) along transect ss1. The distribution of depths appears to be approximately normal with a slight right skew.

Table D-4 Mean, median, mode, and standard deviation of frost table depth along transect ss1.

Mean	Median	Mode	Standard Deviation
32.41267	31	23.5	10.83352

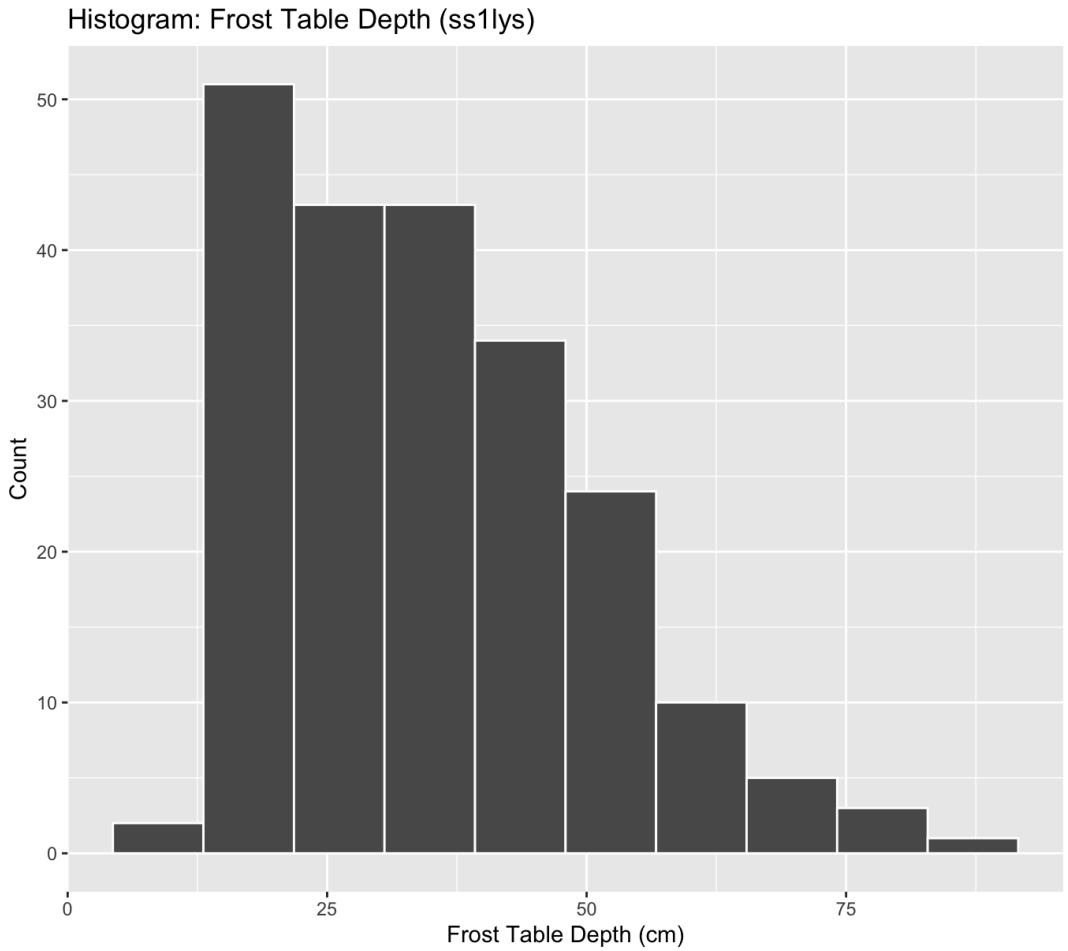

Figure D-8 Histogram (bins = 10) for frost table depth (cm) along transect ss1lys. The distribution of depths appears to be right skewed.

Table D-5 Mean, median, mode, and standard deviation of frost table depth along transect ss1lys.

Mean	Median	Mode	Standard Deviation
35.19444	32.5	18	15.53403

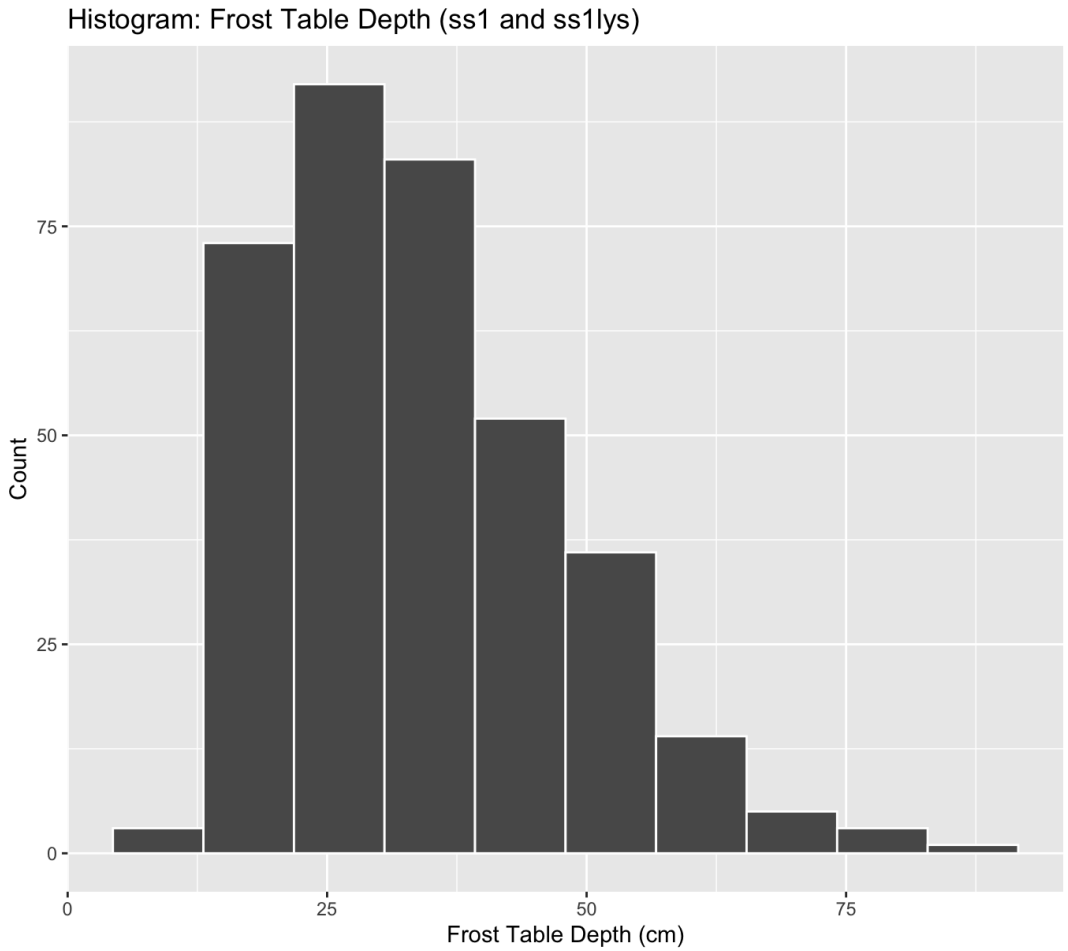

Figure D-9 Histogram (bins = 10) for frost table depth (cm) along both transect ss1 and ss1lys. The distribution of depths appears to be right skewed.

Table D-6 Mean, median, mode, and standard deviation of frost table depth along transect ss1 and ss1lys.

Mean	Median	Mode	Standard Deviation
34.07251	32	26	13.88246

eCDFs

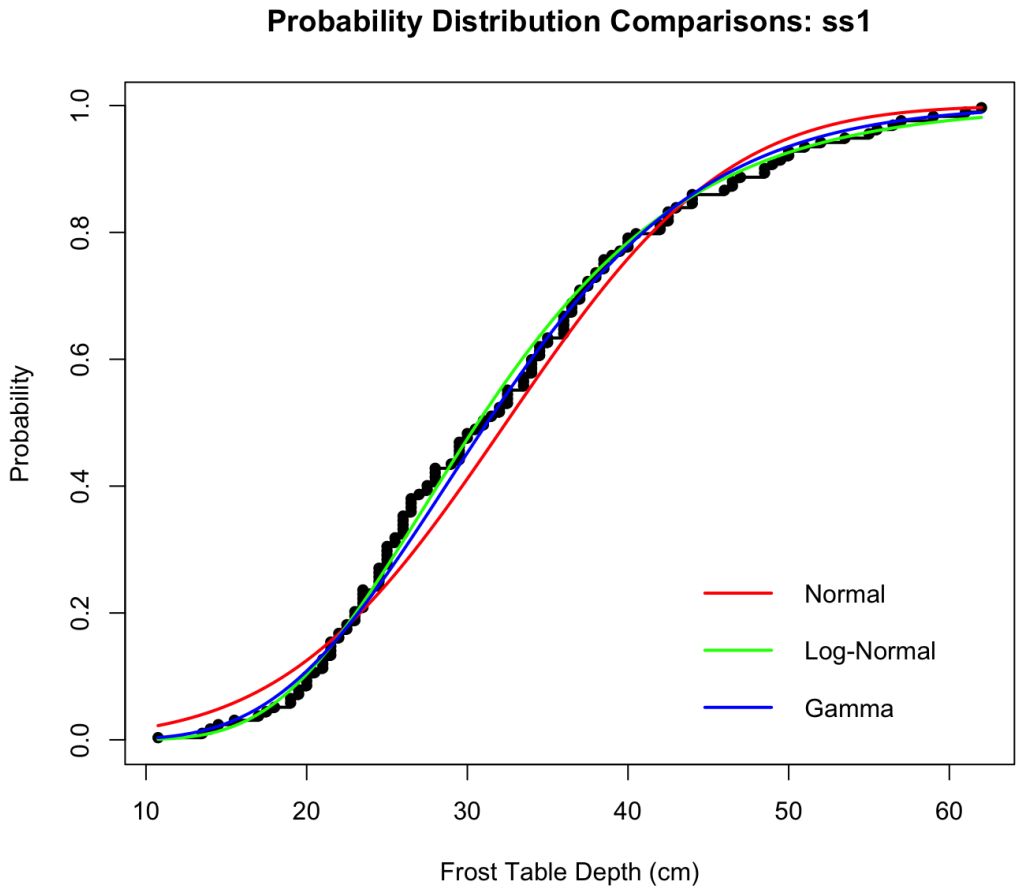

Figure D-10 eCDF for transect ss1 frost table depth (cm) from June – August 2015. Based on AIC analysis, a gamma distribution (blue line) is the best distribution fit followed closely by a log-normal distribution (green line); when analyzing the transect on a daily level (e.g., Julian day 168, 173, 190, 194, 208, 222, or 232), a log-normal distribution is the better fit, closely followed by a gamma distribution. A normal distribution (red line) is included for comparison.

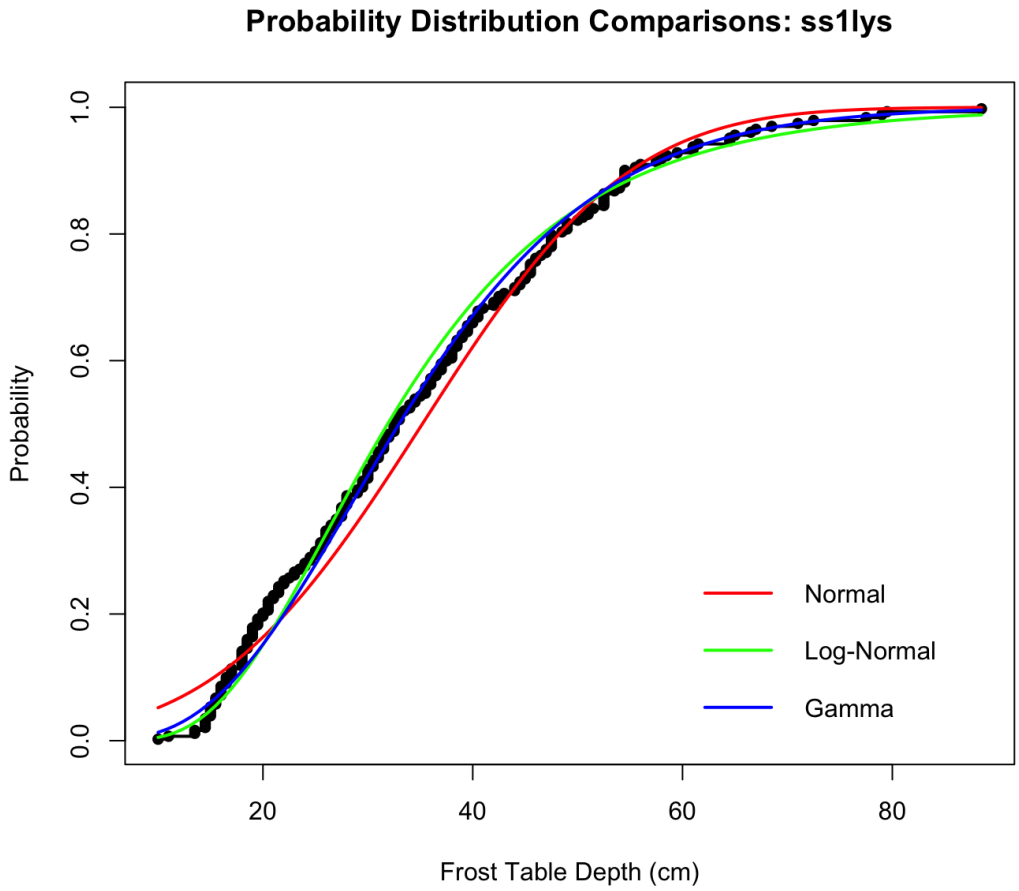

Figure D-11 eCDF for transect ss1lys frost table depth (cm) from June – August 2015. Based on AIC analysis, a gamma distribution (blue line) is the best distribution fit followed closely by a log-normal distribution (green line); when analyzing the transect on a daily level (e.g., Julian day 168, 173, 190, 194, 208, 222, or 232), a log-normal distribution is the better fit, closely followed by a gamma distribution. A normal distribution (red line) is included for comparison.